3-17-2008

The Concept Design of a Split Flow Liquid Hydrogen Turbopump

Michael A. Arguello

THE CONCEPT DESIGN OF A SPLIT FLOW LIQUID HYDROGEN TURBOPUMP

THESIS

Michael A. Arguello, Captain, USAF

AFIT/GAE/ENY/08-M01

DEPARTMENT OF THE AIR FORCE
AIR UNIVERSITY

AIR FORCE INSTITUTE OF TECHNOLOGY

Wright-Patterson Air Force Base, Ohio

The views expressed in this thesis are those of the author and do not reflect the official policy or position of the United States Air Force, Department of Defense, or the U.S. Government.

AFIT/GAE/ENY/08-M01

THE CONCEPT DESIGN OF A SPLIT FLOW LIQUID HYDROGEN TURBOPUMP

THESIS

Presented to the Faculty

Department of Aeronautical Engineering

Graduate School of Engineering and Management

Air Force Institute of Technology

Air University

Air Education and Training Command

In Partial Fulfillment of the Requirements for the

Degree of Master of Science in Aeronautical Engineering

Michael A. Arguello, BS

Captain, USAF

March 2008

AFIT/GAE/ENY1/08-M01

THE CONCEPT DESIGN OF A SPLIT FLOW LIQUID HYDROGEN TURBOPUMP

Michael A. Arguello, BS

Captain, USAF

Approved:

// SIGNED //	17Mar08
Branam, Richard D., Maj, USAF (Chairman)	Date
// SIGNED //	14Mar08
Paul I. King (Member)	Date
// SIGNED //	14Mar08
Mark F. Reeder (Member)	Date

AFIT/GAE/ENY1/08-M01

Abstract

An initial design of a split flow liquid hydrogen turbopump for the Dual Expander Aerospike Nozzle (DEAN) upper stage engine was completed. The engine nozzle is an annular aerospike. The engine cycle requires a combustion chamber pressure of 1,740 psia. The DEAN is designed to deliver 57,200 lb_f of thrust and 472 seconds of I_{sp}. The turbopump design was completed using a meanline software tool. The design consists of a single piece rotor, with a two-stage pump and radial inflow turbine. The turbopump flow rates are 15.1 and 7.55 lbm/s into the first and second stage, respectively. The first and second stage pumps use unshrouded impellers. An interstage transfer models the fluid split flow. The fluid for each stage exits through a volute. The first and second stage impeller hub-tip ratios are 0.3 and 0.35, respectively. The turbine is a full admission reaction type. At the design condition, the turbine delivers 3,607 horsepower at a total pressure ratio of 1.84.

To my family

AFIT/GAE/ENY1/08-M01

Acknowledgments

I would like to express my sincere appreciation to my faculty advisor, Maj Richard R. Branam, for his guidance and support throughout the course of this thesis effort. I greatly appreciate his insight and experience. To the DEAN team, Captain John McCall, Captain William Strain and Lieutenant David Martin, it was a blast. I would like to thank Dr. Edward Childs of Concepts NREC Inc. I would like to thank the AFIT/AFRL library staff, Dawn French and Renate Hannaford for their persistence in finding critical reference documents.

To all my grade school teachers and college professors, thank you for your commitment to teaching. I would like to thank my wife for her constant motivation and patience.

Michael A. Arguello

.

Table of Contents

Page

Abstract iv
Acknowledgments vi
List of Figures x
List of Tables xiv
Nomenclature xvi
1. Introduction 1
1.1 Background 1
1.2 Problem Statement 3
1.3 Research Objectives 4
1.4 Investigative Questions 4
2. Literature Review 5
2.1 Chapter Overview 5
2.2 DEAN TPH Design Concept 5
2.3 Materials 6
2.4 Turbopump Bearings 8
2.5 RL10 Upper Stage 13
2.6 MB-XX Upper Stage 16
2.7 VINCI Upper Stage 18
2.8 Demonstrator Upper Stage 19

3. Turbomachinery Theory 22

3.1 Chapter Overview 22

3.2 Impeller Inlet and Exit Modeling 22

3.3 Vaneless Diffuser Modeling 25

3.4 Volute Modeling 26

4. Methodology 27

4.1 Chapter Overview 27

4.2 Power Balance 28

4.3 Preliminary Pump Impeller Design 34

4.4 Detailed Pump Impeller Design 37

4.5 Volute Design 45

4.6 Pump Impeller Design Analysis Mode 48

4.7 Turbine Impeller Design 49

4.8 Axial Bearing Load 53

4.9 DEAN Shaft 54

5. Analysis and Results 56

5.1 Chapter Overview 56

5.2 Stage 1 Impeller layout 56

5.3 Stage 1 Off-Design Operating Range 60

5.4 Stage 2 Impeller Layout 63

5.5 Stage 2 Off-Design Operating Range 64

5.6 Turbine Layout 67

5.7 Turbine Off-Design Operating Range 70

5.8 Bearing and Shaft 74

6. Conclusions and Recommendations 76

6.1 Conclusions 76

6.2 Recommendations 77

Appendix A. Pumpal® Wizard Steps 79

Appendix B RITAL® Wizard Steps 91

Bibliography 100

Vita 103

List of Figures

Page

Figure 1 IHPRPT Boost/Orbit Transfer Payoff and Spacecraft Propulsion Payoff 3

Figure 2 DEAN TPH Design Process 6

Figure 3 Roller Ball Bearing 10

Figure 4 Series-Hybrid Fluid Film Rolling Element Bearing 11

Figure 5 Foil Journal Bearing 12

Figure 6 RL10A-3-3A Schematic of Propellant Flow 14

Figure 7 Cross Section of Fuel Pump and Turbine 15

Figure 8 MB-XX Engine Cycle Schematic 17

Figure 9 Advanced Expander Engine Cycle Schematic 20

Figure 10 Component View of ALH Turbopump 21

Figure 11 Impeller Inlet Velocity Triangle Tangential Format 23

Figure 12 Impeller Exit Velocity Triangles Tangential Format 24

Figure 13 Concepts NREC Turbomachinery Design Process 27

Figure 14 DEAN System Schematic 33

Figure 15 Hybrid Pump Diffusion Ratio Model 39

Figure 16 Axial Thrust Forces 54

Figure 17 DEAN Liquid Hydrogen Pump Configuration 56

Figure 18 DEAN Stage 1 Impeller 57

Figure 19 Stage 1 Head Rise Operating Range 61

Figure 20 Stage 1 Volumetric Flow Rate (USgpm) vs. Stage Efficiency TT 61

Figure 21 Stage 1 Volumetric Flow Rate (USgpm) vs. Stage Power (hp) 62

Figure 22 Stage 1 Ns vs. Stage Efficiency TT 62
Figure 23 DEAN Stage 2 Impeller 63
Figure 24 Stage 2 Head Rise Surge Line 65
Figure 25 Volumetric Flow Rate (USgpm) vs. Stage Efficiency TT 65
Figure 26 Stage 2 Volumetric Flow Rate (USgpm) vs. Stage Power (hp) 66
Figure 27 Stage 2 Ns vs. Stage Efficiency TT 66
Figure 28 DEAN Turbine Cross-Sectional Layout 68
Figure 29 DEAN Radial Turbine 68
Figure 30 Stage Velocity Ratio U/C vs. Stage Efficiency TT 71
Figure 31 Stage Velocity Ratio U/C vs. Stage Efficiency TS 71
Figure 32 vs. Expansion Ratio TT vs. Corrected Mass Flow Rate 72
Figure 33 Turbine Power Output vs. Stage Efficiency TT 72
Figure 34 Volumetric Flow Rate (gpm) vs. Stage Power (hp) 73
Figure 35 Turbine Reaction vs. Mass Flow Rate lbm/s 73
Figure 36 DEAN Conceptual Bearing Layout 74
Figure 37 DEAN Liquid Hydrogen Turbopump Rotor Assembly Solid Model 75
Figure 38 Pumpal® Wizard Step One 79
Figure 39 Pumpal® Wizard Step Two 79
Figure 40 Pumpal® Wizard Step Three 80
Figure 41 Pumpal® Wizard Step Four 80
Figure 42 Pumpal® Wizard Step Five 81
Figure 43 Pumpal® Wizard Step Six 81
Figure 44 Pumpal® Wizard Step Seven 82

Figure 45 Pumpal® Wizard Step Eight 82
Figure 46 Pumpal® Wizard Step Nine 83
Figure 47 Pumpal® Wizard Step 10 83
Figure 48 Pumpal® Wizard Step 11 84
Figure 49 Pumpal® Wizard Step 12 84
Figure 50 Pumpal® Wizard Step 13 85
Figure 51 Pumpal® Wizard Step 14 85
Figure 52 Pumpal® Wizard Step 15 86
Figure 53 Pumpal® Wizard Step 16 86
Figure 54 Pumpal® Wizard Step 17 87
Figure 55 Pumpal® Wizard Step 18 87
Figure 56 Pumpal® Wizard Step 19 88
Figure 57 Pumpal® Wizard Step 20 88
Figure 58 Pumpal® Wizard Step 21 89
Figure 59 Pumpal® Wizard Step 22 89
Figure 60 Pumpal® Wizard Step 23 90
Figure 61 Pumpal® Wizard Step 24 90
Figure 62 RITAL® Wizard Step One 91
Figure 63 RITAL® Wizard Step Two 91
Figure 64 RITAL® Wizard Step Three 92
Figure 65 RITAL® Wizard Step Four 92
Figure 66 RITAL® Wizard Step Five 93
Figure 67 RITAL® Wizard Step Six 93

Figure 68 RITAL® Wizard Step Seven 94
Figure 69 RITAL® Wizard Step Eight 94
Figure 70 RITAL® Wizard Step Nine 95
Figure 71 RITAL® Wizard Step 10 95
Figure 72 DEAN Stage 1 Impeller 96
Figure 73 DEAN Stage 2 Impeller 97
Figure 74 DEAN Turbine 98

List of Tables

Page

Table 1 IHPRPT Goals for Boost and Orbit Transfer and Spacecraft Propulsion..... 2

Table 2 Atlas IIA and Centaur IIA upper stage 3

Table 3 Turbopump Materials 8

Table 4 Liquid Hydrogen Foil Bearing Test Results 12

Table 5 Bearing System Comparison 13

Table 6 RL10A-3-3A Engine On Design Performance 15

Table 7 RL10A-3-3A Fuel Turbopump Performance Parameters..... 15

Table 8 MB-35 and MB-60 Comparisons 17

Table 9 MB-XX Demonstrator Fuel Turbopump Performance Parameters..... 17

Table 10 VINCI Fuel Turbopump Performance Parameters 19

Table 11 Demonstration Engine Performance 21

Table 12 ALH Turbopump Performance Parameters 21

Table 13 Initial Power Balance Results 30

Table 14 NPSS Inputs..... 32

Table 15 NPSS Power Balance Results 32

Table 16 Power Balance Comparison of NPSS and Spreadsheet (S.S)..... 33

Table 17 Preliminary Pump Impeller Sizing 35

Table 18 Pumpal® Volute Parameters..... 45

Table 19 Pumpal® Wizard Inputs Preliminary Impeller Inlet/Exit Design..... 47

Table 20 Impeller Design Criteria 47

Table 21 RITAL® Preliminary Sizing Default Settings..... 50

Table 22 Turbine Impeller Design Criteria 52
Table 23 Stage 1 Impeller On-Design Performance Pumpal® Results 58
Table 24 Pump Stage Efficiency Sensitivity Analysis 59
Table 25 Pump Head Rise Sensitivity Analysis 59
Table 26 Volute Exit Pressure Sensitivity Analysis 59
Table 27 Power Required Sensitivity Analysis 59
Table 28 Impeller Tip Radius Sensitivity Analysis 60
Table 29 Stage 2 On-Design Performance Pumpal® Results 63
Table 30 Stage 2 Horsepower Requirement at Various Mass Flow Fractions 67
Table 31 Turbine On-Design Performance RITAL® Results 68
Table 32 Turbine Impeller Total Stage Efficiency Sensitivity Analysis 69
Table 33 Turbine Impeller Power Sensitivity Analysis 69
Table 34 DEAN Theoretical Shaft and Bearing Size 75
Table 35 Axial Load Results 75
Table 36 DEAN TPH Upstream Conditions 81
Table 37 RITAL® Upstream Conditions 92

Nomenclature

Greek Symbols	**Description**	**Units**
π	3.14	radians
α'	Absolute angle with tangential direction	degrees
ω	Angular speed	radians/second
β	Blade angle	degrees
ρ	Density	lbm/ft^3 (kg/m^3)
δ	Deviation angle	degrees
Δ	Difference between exit and inlet	
η	Efficiency	
ϕ	Flow coefficient	
ψ	Head coefficient	
ν	Jet speed ratio	
φ	Loading coefficient	
λ	Nozzle Efficiency; swirl parameter	
ε	Nozzle expansion ratio	
γ	Ratio of specific heats	
β'	Relative angle with tangential direction	
ξ	Rotor meridional velocity ratio	
χ	Secondary flow mass fraction	
σ	Slip factor; stress	
θ	Tangential coordinate	
ε_r	Tip clearance	inches (m)
τ	Torque; torsional stress	ft.lbs (N.m)

Station Numbering

0	Stagnation state
1	Pump Impeller inlet or eye
2	Pump Impeller tip or outlet
3	Pinch location for vaneless diffuser
4	Diffuser throat
5	Diffuser exit
7	Volute throat
8	Stage exit, shaft

Subscripts

ps	Allowable pressure rise
b	Blade height
c	Chamber
cool	Cooling jacket
e	Exit
feed	Feed system
f	Flow; front face
$_\infty$	Freestream
h	Hub
inj	Injector
i	Inlet
a	Inlet region
is	Isentropic-to-Static
m	Meridional; mean
opt	Optimum
recirc	Recirculation
req	Required
p	Required pressure rise; primary zone
sp	Specific
t	Tip; throat
TS	Total-to-static
TT; tt	Total-to-total
trat	Turbine pressure ratio
v	Vapor

Acronyms/Variables	**Description**	**Units**
C	Absolute velocity	ft/s
ALH	Advanced Liquid Hydrogen	
Al	Aluminum	
AR	Aspect Ratio	
AxLngth	Axial Length	inches
Beta2b	Blade exit angle	degrees
B2	Blade Height	inches
B; BLK1	Blockage	
DN	Bearing bore size x Rotational speed	mm x rpm
constants	C1,C2,C3,C4,C5	
c*	Characteristic Exhaust Velocity	m/s
CLRF	Clearance	inches
CLRR	Clearance	inches
L_c	Clearance loss	
K_c	Clearance loss constant	
CCV	Combustion Control Valve	

CFD	Computational Fluid Dynamics	
k	Constant	
DELTA	Deviation angle	degrees
D	Diameter	inches
DivAng	Diffuser divergence angle	degrees
DR	Diffusion ratio	
C_D	Discharge Coefficient	
h	Enthalpy	ft^2/s^2
s	Entropy	
ZR	Exit blade number	
F.S	Factor of Safety	
T_c	Flame Temperature	^oR
ALPHA	Flow angle	degrees
A	Flow area	ft^2
FBP	Fuel Boost Pump	
FTP	Fuel Turbopump	
R	Gas Constant	
GUI	Graphical User Interface	
g_o	Gravitational Constant	m/s^2
H	Head rise	ft
BETA1HB	Hub blade angle	degrees
TPH	Hydrogen turbopump	
L_i	Incidence loss	
PHI	Inclination angle	degrees
BETAB1	Inlet blade angle	degrees
Z1	Inlet blade number	
r	Inlet radius	inches
C	Inlet tangential absolute velocity	ft/s
C_o	Isentropic Spouting Velocity	ft/s
L	Inducer inlet hub-to-tip diameter	
LH2	Liquid hydrogen	
LN2	Liquid nitrogen	
LC	Loss coefficient	
Ma	Mach number	
MFV	Main Fuel Valve	
MOV	Main Oxygen Valve	
$\dot{m}$	Mass flow rate	lbm/s
BETA1MB	Mean blade angle	degrees
MTBR	Mean Time Between Removal	
E	Modulus of elasticity	psi
I	Moment of inertia	$inches^4$
NIST	National Institute of Standards and Technology	
NPSHR	Net Positive Suction Head Required	ft

NREC	Northern Research Engineering Corporation	
n	Number of stages	
na	Not applicable	
NPSS	Numerical Propulsion Simulation System	
O/F	Oxygen to Fuel Ratio	
OBP	Oxygen Boost Pump	
OTP	Oxygen Turbopump	
O/B	Overboard	
b	Passage depth	inches
L_p	Passage loss	
K_p	Passage loss constant	Recommended value = 0.3
J	Polar momentum of inertia	$inches^4$
P	Power	ft.lbs/s
PWA	Pratt and Whitney	
p	Pressure	psia
Pr	Pressure Ratio	
PR	Pressure ratio (TT)	
RTP	Radial Turbine Program	
r	Radius	inches
W	Relative flow speed	ft/s
rpm	Revolution per minute	
N_r	Rotational speed	rad/s
f	Shaft deflection	inches
c	Shaft radius	inches
SIG2	Slip Factor	
C_{slip}	Slip velocity	ft/s
c_p	Specific heat	BTU/lbm^oR
N_s	Specific Speed	rpm*(USgpm)^0.5/ft^0.75
N	Speed	rpm
T	Temperature	^oR
F	Thrust	lb_f
T/W	Thrust to weight ratio	
BETA1TB	Tip blade angle	degrees
Ti	Titanium	
TPA	Turbopump assembly	
unk	Unknown value	
U/C	Velocity ratio	
Q	Volumetric flow rate	USgpm
w	Weight of impeller	lbs
U	Wheel speed	ft/s
$\dot{W}$	Work per unit mass flow rate	BTU/lbm/s

THE CONCEPT DESIGN OF A SPLIT FLOW LIQUID HYDROGEN TURBOPUMP

1. Introduction

1.1 Background

In 1994, the Integrated High Payoff Rocket Propulsion Technology Program (IHPRPT) was initiated. This program was to be the harbinger of development and demonstration for rocket propulsion technology. National Association of Space Administration (NASA), Department of Defense (DoD), and commercial industry all agreed to lend their expertise to achieve the IHPRPT goals. The program goal is to double U.S rocket propulsion capability by 2010. The overarching figures of merit used to justify programmatic progress are cost and performance. U.S government agencies and industry have worked together to develop time-phased technology goals. Table 1 outlines these phases. Figure 1 depicts the significance of achieving the IHPRPT.

The IHPRPT program identifies three mission application areas. These mission application areas are Boost and Orbit Transfer, Spacecraft, and Tactical. There are five technology areas within each mission application. The five technology areas are Propellants, Controls, Propellant Management Devices, Combustion and Energy Conversion Devices, and Demonstrators. The propellant management device (PMD) technology area is the focus of the following research.

The IHPRPT performance goals for I_{sp}, T/W, and MTBR will guide the overall design. The significance of increasing I_{sp} is best revealed in a financial analysis. Table 2 shows a financial analysis for the Atlas IIA with a Centaur IIA upper stage fitted with an

RL10-A-4 model engine. The results show an average cost savings of approximately $199,000 for the Atlas IIA per second increase in I_{sp}. This dollar amount was calculated using 1993 dollars and the total cost per kilogram of payload of $11,935[12]. The results reveal that a 26-second I_{sp} increase would result in approximately a $3.2 million dollar savings and ensure an increase of 267.3 kg of payload. This number was adjusted to the 2007 dollar value using the GDP index of 1.2677[13]. The cost savings is an estimated $4.1 million. The next generation rocket engine will deliver more payload mass into orbit for each dollar spent.

Table 1 IHPRPT Goals for Boost and Orbit Transfer and Spacecraft Propulsion[1]

Boost and Orbit Transfer Propulsion	**Phase I**	**Phase II**	**Phase III**
Reduce Stage Failure Rate	25%	50%	75%
Improve Mass Fraction (Solids)	15%	25%	35%
Improve I_{sp} (Solids)	2%	4%	8%
Improve I_{sp} (sec) (Liquids)	14	21	26
Reduce Hardware Cost	15%	25%	35%
Reduce Support Costs	15%	25%	35%
Improve Thrust to Weight (Liquids)	30%	60	100%
Mean Time Between Removal (Mission Life: Reusable)	20	40	100
Spacecraft Propulsion			
Improve Istot/Mwet (Electrostatic/Electromagnetic)	20%/200%	35%/500%	75%/1250%
Improve I_{sp} (Bipropellant/SolarThermal)	5%/10%	10%/15%	20%/20%
Improve Density: I_{sp} (Monopropellant)	30%	50%	70%
Improve Mass Fraction (Solar Thermal)	15%	25%	35%

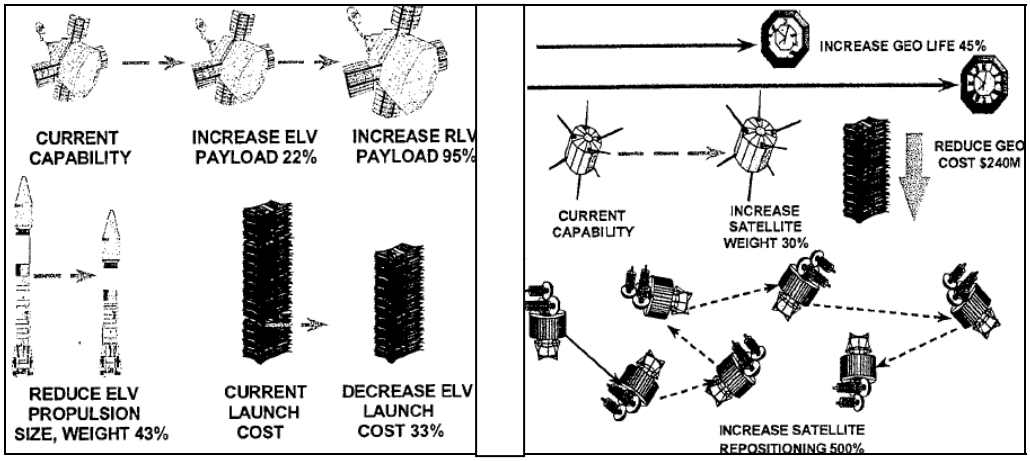

Figure 1 IHPRPT Boost/Orbit Transfer Payoff and Spacecraft Propulsion Payoff [1]

Table 2 Atlas IIA and Centaur IIA upper stage

I_{sp} (sec)	Payload (kg)	Payload Increase from baseline (kg)	% Payload Increase	Cost per kg of Payload ($/kg)	Total Cost Savings $M(1993)
449	7122.0	-	-	11,935	-
460	7307.2	185.2	2.6%	11,633	2.2
465	7389.3	267.3	3.8%	11,878	3.2

1.2 Problem Statement

The next generation upper stage engine will use a dual expander cycle. The engine will require a liquid hydrogen turbopump that will have improve performance, safety and reliability over the baseline. To satisfy these requirements the turbopump will incorporate a split flow design. A split flow design will reduce the fuel flow into the second stage by splitting the mass flow at the exit of stage one. This should reduce the stage two horsepower consumed and reduced the overall horsepower required of the turbine, leading to increase reliability. Current multistage pumps are full flow designs that split the working fluid outside the turbopump assembly and have equal power

consumption levels for each stage, thus requiring greater turbine power output. The conceptual turbopump design must provide the predicted mass flow, exit pressure, head rise, and efficiency for steady state operation. A size requirement derived from the baseline footprint must be satisfied.

1.3 Research Objectives

The objectives of this research are

- Provide a conceptual fuel pump design to satisfy the operating conditions for the Dual Expander Aerospike Nozzle (DEAN) upper stage engine.
- Provide proof of stable operation over a throttling range.
- Select potential component material that may satisfy reliability requirements.
- Provide a design process to develop the next generation upper stage rocket fuel pump.

1.4 Investigative Questions

What is the conceptual TPA configuration that will satisfy the power balance outputs for a dual expander annular aerospike rocket engine? What are the component materials necessary to ensure a reliable design? Will the conceptual design satisfy the phase III IHPRPT goals? Does the turbopump have throttle capability?

2. Literature Review

2.1 Chapter Overview

In the following chapter the goals for the DEAN TPH are outlined. An outline is completed for several past and present turbopump projects. The goal is to leverage each pump design to provide a competent recommendation for the pump type, layout, component materials and bearing system.

2.2 DEAN TPH Design Concept

The DEAN TPH must provide the necessary head rise and mass flow to maintain steady operation at the design condition. The TPH entire assembly must be comparable to current/past designs in layout, size, and weight. The materials used must be hydrogen compatible and commercially available. The DEAN TPH concept will use a minimum number of pump and turbine impellers on a single shaft. All impellers will be unshrouded. For a given rotational speed the diameters of each impeller must be minimized. The pump and turbine design will be centrifugal and radial type. The bearing system must be available and provide increased reliability and life. Figure 2 shows the design process used to complete the liquid hydrogen turbopump design.

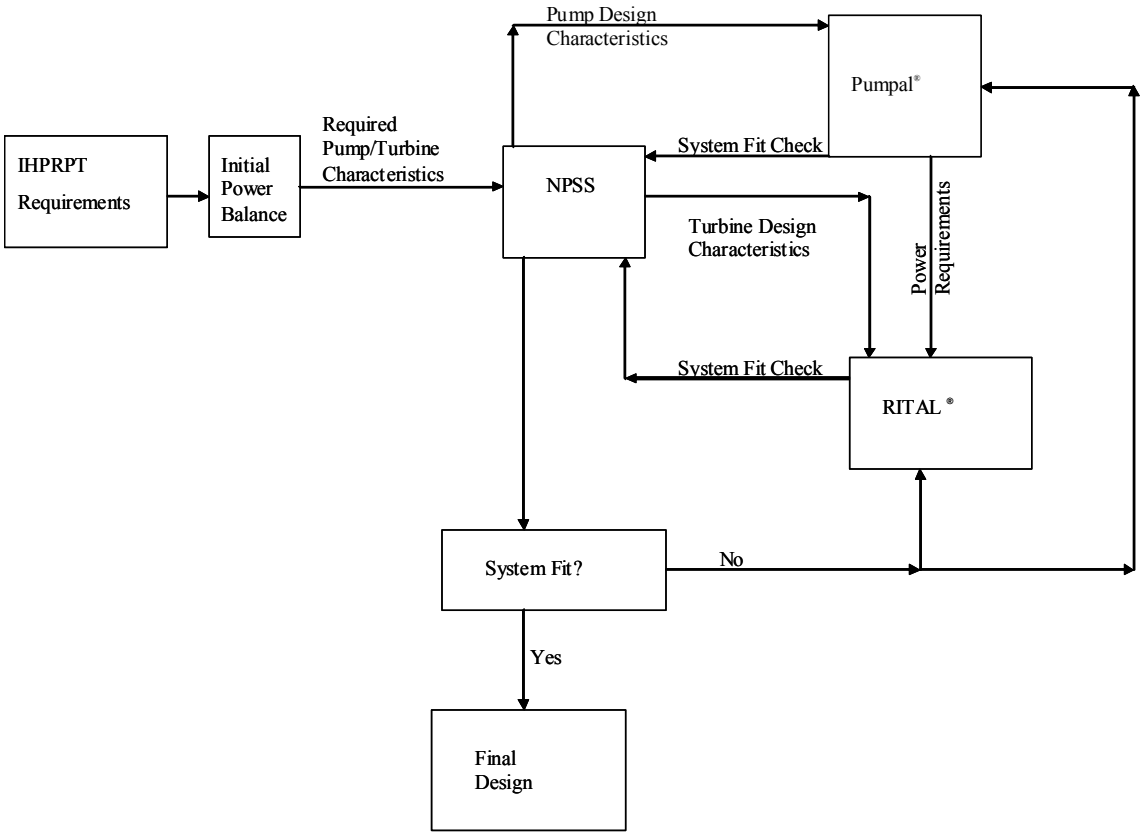

Figure 2 DEAN TPH Design Process

2.3 Materials

The liquid hydrogen environment is only compatible with certain materials. For this reason, a limited number of materials are used in rocket turbopumps. Hydrogen embrittlement is one of the serious concerns when attempting to select the appropriate material. Hydrogen embrittlement occurs when hydrogen contacts the surface of a material and atomic hydrogen dissolves into the material. The absorption of atomic hydrogen within the molecular structure causes degradation in mechanical properties. The current operational materials typically employed include; aluminum, stainless steel, nickel alloys, and titanium alloys. By breaking out the purpose of the components within

the turbopump, the choice of material type becomes evident. The purposes include, stiffness driven components, warm temperature applications and cryogenic applications. The stiffness driven components transfer loads from one to another, these include flanges and support structures. These components may or may not be exposed to the working fluid but are subject to moderate thermal and chemical environments. Current systems use nickel-based superalloys for both high stiffness and compatibility. Quantitatively high stiffness would require moduli greater than 32 ksi (220 GPa).[14] The warm temperature applications are related to the turbine components. These components include, ducting, housing, rotating and stationary elements. The rotating machinery has the most severe requirements in this area. Rotating components directly exposed to hydrogen gas require both creep and fatigue resistance. Nickel-based superalloys are typically used for these components.[14] The cryogenic components must operate at 38^{o}R (21K) this includes: inducer, impellers, stationary guide vanes, and housings. The need to account for varying shrinkage between components, hydrogen compatibility, and fatigue resistance leads current designer to use forged and machined titanium alloys.[14] For a single stage pump the typical material strength requirement is approximately 125 ksi (862 MPa).[14] Table 3 is a list of materials used in current turbopump designs.

Table 3 Turbopump Materials

Upper Stage Engine	Inducer/ Impeller	Pump Housing	Pump Volute	Turbine Housing	Turbine Volute	Turbine Impeller	Shaft
RL10	4135 Al-Alloy	4130 Al-Alloy	4130 Al-Alloy	unk	unk	4127 Al-Alloy	5667 Nickel-Alloy
MB-60	Ti-Alloy	unk	unk	unk	unk	Inconel 718	unk
VINCI	Ti-(Powder)	Inconel 718	Inconel 718	Inconel 718	Inconel 718	Ti 6-4	Ti 6-4
ALH	PWA Ti-1240	Inconel 718	Inconel 718	Waspaloy	Waspaloy	PWA Ti-1240	PWA Ti-1240

2.4 Turbopump Bearings

A designer may choose from four common types of bearing systems; ball, hybrid-ball, hydrostatic, and foil bearings. The bearing selected is based on four primary factors, speed, load, life and environment. The type of load the bearing will sustain during operation, axial or radial, defines the directional loading capability. The load capacity is a direct function of bearing size. The qualitative criterion used to select a suitable bearing system is, the pump design speed shall not exceed the speed limits of the bearing system. A quantitative measure of this criterion is given by the product of the bearing bore, D, in millimeters and the rotational speed, N, in revolutions per minute (DN). An upper speed limit is related to bearing size and to the required operating life for a given radial and axial load of a rotating assembly. However, DN does not give a complete description of speed severity because it does not account for rolling element size of the bearing internal geometry. A bearing system should be designed to a minimum DN value

and number of bearings. The bearing system must provide mechanical balancing and hydraulic balancing of impeller forces.

For low speed application (DN < 0.5E6) a sufficiently large bearing may be used.[2] For high speed applications the DN method may be inadequate. A dynamic analysis must be used to determine speed effects and the interactions of high-speed bearing stresses, life, stiffness, dynamic forces, and velocities. The radial stiffness is a controlling factor in critical speed control. Radial stiffness is defined as the ability of the bearing to maintain the shaft in its ideal location during operation. This is important because the slightest departure from ideal conditions may result in failure. Moreover, the radial stiffness is a controlling factor in shaft critical speed control and the location of the bearing on the turbopump shaft. The stiffness capability of a bearing is measured in lb_f/in. In throttle type engines roller bearing are sometimes used with a stiffness range of 1.5-2.0E6 lb_f/in.[2]

The mission needs define the bearing life requirement. The generally accepted life rating for ball and roller bearings is the B-10 life standard.[15] The numerical designator denotes the reliability percentage of the bearing. For example, a B-10 life results in 90 percent reliability. In general turbopump bearings are designed for a B-10 life of at least 100 hours.[15] This rating would result in a 10 hour life with 99 percent reliability and 1 hour life with 99.9 percent reliability.

2.4.1 Ball Bearings

Ball bearings are able to support a combined radial and axial load, a thrust load in both axial directions, and moment loading.[2] In 2005, Snecma reported successful test

results for an LH2 ceramic ball bearing at DN values up to 3E6.[16] In comparison to fluid bearings, rolling contact bearings are used because of the following characteristics listed below.[2] Figure 3 shows a roller ball bearing schematic.

- Large capacity-to-volume
- Ability to operate independently of external pressurizing systems
- Ability to operate satisfactorily after ingesting foreign material
- Tolerance for short periods of coolant/lubrication starvation
- High radial spring rate
- Low heat generation and coolant/lubrication consumption

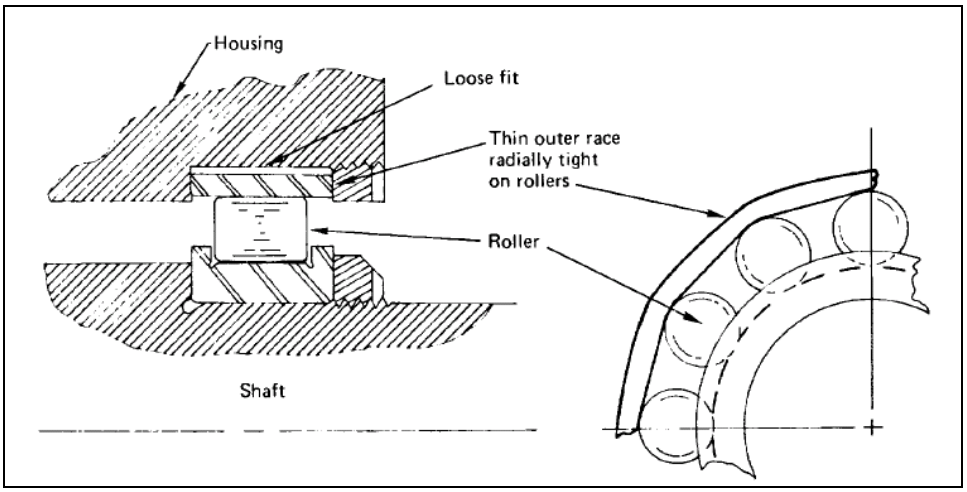

Figure 3 Roller Ball Bearing[2]

2.4.2 Hydrostatic Bearing

A hydrostatic bearing uses a fraction of the working fluid injected at a nominal pressure to create a fluid cushion layer preventing rubbing. The hydrostatic bearing is not limited by a DN value in comparison to ball bearings. However, the shortfall of

hydrostatic bearings occurs during transients. During startup the pump head is insufficient to feed the hydrostatic bearing. Furthermore, the limited viscosity of LH2 prevents the creation of a hydrodynamic effect and contact between the bearing stator and shaft is common.

2.4.3 Hybrid Hydrostatic Ball Bearing

A hybrid-hydrostatic ball bearing takes advantage of the strengths of both the hydrostatic and ball bearing systems. The hybrid bearing system is a ball bearing unit in series with a hydrostatic fluid ports.[3] While operating at the on-design condition the fluid film mode offsets the loading forces and centers the shaft. This design allows for high DN values. In transient operation, the ball bearing system offsets the loading forces and centers the shaft. The RL60 program has tested hybrid ball bearings to DN values greater than 3E6.[17] Figure 4 shows the schematic diagram of a typical series-hybrid fluid film rolling element bearing.

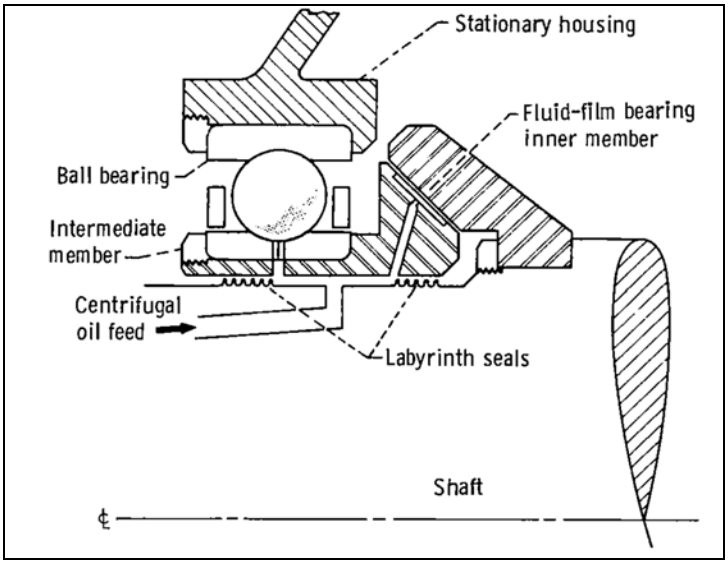

Figure 4 Series-Hybrid Fluid Film Rolling Element Bearing[3]

2.4.4 Fluid-Foil Bearing

The fluid foil bearing concept consists of several foils overlapped and wrapped around the shaft. The foils maintain contact with the shaft when at rest. The foils are designed with a specific radius of curvature and thickness. The motion of the shaft develops a fluid film and the foils lift off from the shaft. At a minimum speed contact between the shaft and foils is minimized. A protective coating is applied to the foils to safeguard the shaft from wear during stop and start transient operation. Figure 5 shows the components used in the foil bearing system. In 1991, NASA Lewis Research Center tested a foil bearing. [4] Table 4 shows the test results. Table 5 shows a summary of the bearing systems used for each turbopump.

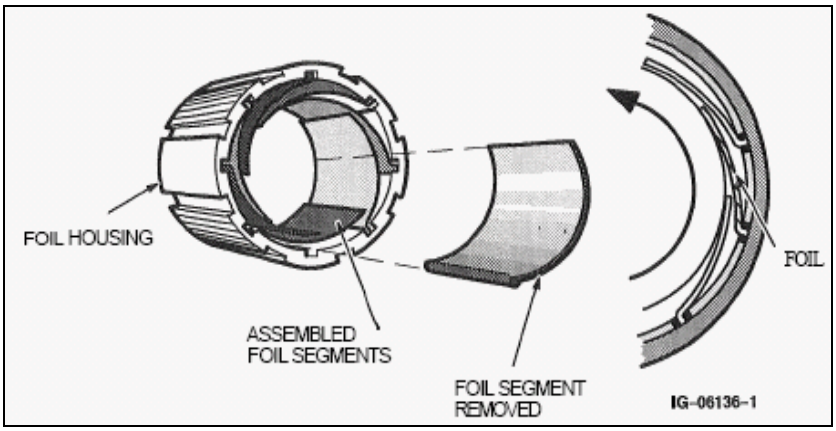

Figure 5 Foil Journal Bearing[4]

Table 4 Liquid Hydrogen Foil Bearing Test Results [4]

Achieved 240-psi load capacity in LH2
Ran stably at all speeds (20,000 to 97,000 rpm)
Over 150 start/stop cycles with no noticeable bearing wear
Demonstrated negligible cross-coupling stiffness
Achieved 300-psi load capacity in LN2
Accumulated run time: 4 hr in LH2 and 5 hr in LN2

Table 5 Bearing System Comparison

Type	Bearing Type	Number of Bearings	DN Value	Configuration	Material Type
RL10	Ball	2	unk	Inboard	Steel AMS 5630
MB-60	Hybrid Angular Contact	2	$3x10^6$	Inboard	Ceramic Balls
VINCI	Angular Contact	2	$2.8x10^6$	Inboard	Si_3N_4 Balls
ALH	Split Ring Hydrostatic	2	6.4E6	Inboard	Titanium Shell

2.5 RL10 Upper Stage

The United States mission of delivering space assets in a timely and cost effective manner has fallen solely on the Centaur. The Atlas and now retired Titan launch platforms use the Centaur. On November 17, 1963, the Centaur demonstrated the first ever in-flight burn of liquid hydrogen/liquid oxygen. The Centaur was officially the first United States high-energy upper stage launch vehicle. For the next 40 years, the Centaur would be the upper stage of choice. The RL-10 family of engines is the common thread for the U.S. launch platforms. In 1958, Pratt and Whitney signed a contract with the United States Air Force to develop the RL10 engine. This engine operates using an expander cycle. This type of engine cycle utilizes the liquid hydrogen to cool the main combustion chamber. The thermal energy added to the fuel is used to rotate the turbine, thus rotating oxidizer and fuel pump impellers. Figure 6 shows a diagram of the engine layout. A gearbox connects the fuel and oxidizer pumps. Table 6 shows the engine

performance values during steady state operation. To center the shaft the turbopump uses steel ball bearings. The majority of the other components are made of aluminum alloy. Figure 7 shows the cross sectional layout of the liquid hydrogen turbopump. The layout depicts a two-stage centrifugal pump. The impellers are mounted back-to-back to minimize thrust unbalance. The velocity head is recovered by a straight conical diffuser connected to a volute. A three-bladed axial flow inducer is located upstream of the first-stage impeller. The nominal clearance between the blade and housing contours for stage one and two are 0.055 and 0.061 inches.[18] Table 7 shows the predicted performance of the liquid hydrogen turbopump during steady state operation.

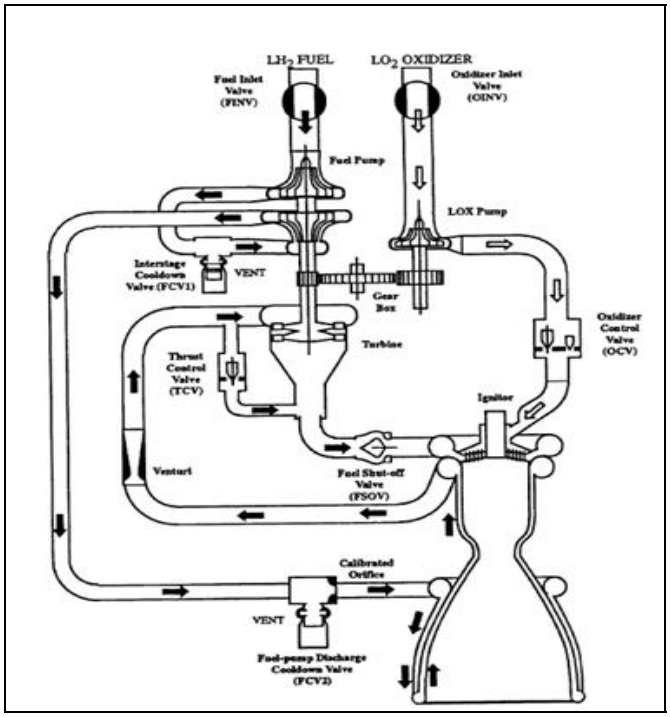

Figure 6 RL10A-3-3A Schematic of Propellant Flow[5]

Table 6 RL10A-3-3A Engine On Design Performance[5]

Propellants	Units	LOX/LH2
I_{sp}	sec	444
F	lb_f	16,500
p_c (at injector face)	psia	475
T/W[19]		54

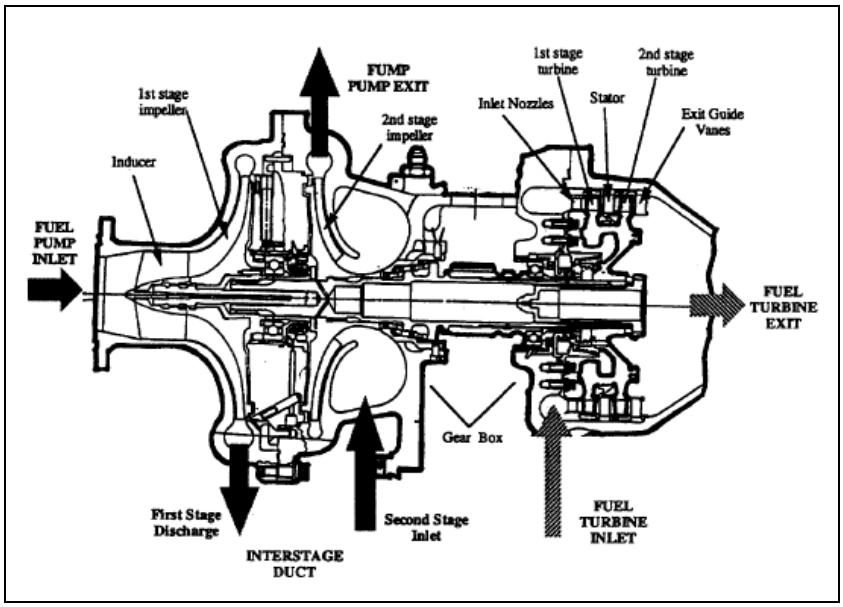

Figure 7 Cross Section of Fuel Pump and Turbine[5]

Table 7 RL10A-3-3A Fuel Turbopump Performance Parameters[5]

Pump	Units	Stage 1	Stage 2
η		0.59	0.57
ψ		0.57	0.61
ϕ		0.041	0.043
Q	USgpm	637.8	641
P_{req}	hp	323	350
H	ft	16,858	17,900
N	rpm	31,537	31,537

Turbine	Units	Combined Stages
η_{tt}		0.74
U/C_o		0.46
P_{trat}		1.39
P_{req}	hp	789
N	rpm	31,537

2.6 MB-XX Upper Stage

The current Japanese launch vehicle is the H-IIA. The family of MB-XX engines powers the upper stage of the HIIA. Two versions of the engine are the MB-35 and MB-60, each provide 35 klb_f and 60 klb_f of thrust. They are intended replace the RL10 engine.[6] The MB-XX engines use an expander bleed cycle. Figure 8 shows the engine cycle schematic. A fraction of the hydrogen flow is routed around the main combustion chamber, heated, and then expanded through turbines to power the high pressure pumps.[6] The engine incorporates boost pump for both turbopumps. The MB-35 design uses a common set of interfaces as the RL10, thus no significant changes are required to the stage.[6] The MB-60 is designed to provide substantial payload launch capability as an expendable upper stage. The potential applications include the Boeing Delta IV, Lockheed Martin Atlas V and the Japanese H-IIA launch vehicles.[6] Table 8 MB-35 and MB-60 Comparisons shows a comparison of both engines.

The MB-XX engine demonstrator was tested with results published in 2006. The MB-XX demonstrator engine is a development version of the MB-60 cryogenic upper stage propulsion system.[9] The turbopump was tested at a thrust level of 40 klb_f. The MB-XX demonstrator FTP is a two-stage pump, powered by a velocity compounded two-stage turbine. Table 9 shows the FTP operating conditions. To center the shaft an angular contact ceramic ball bearing is used.[9] Japan's National Aerospace Laboratory (NAL) reported a DN value of up to 3E6.[9]

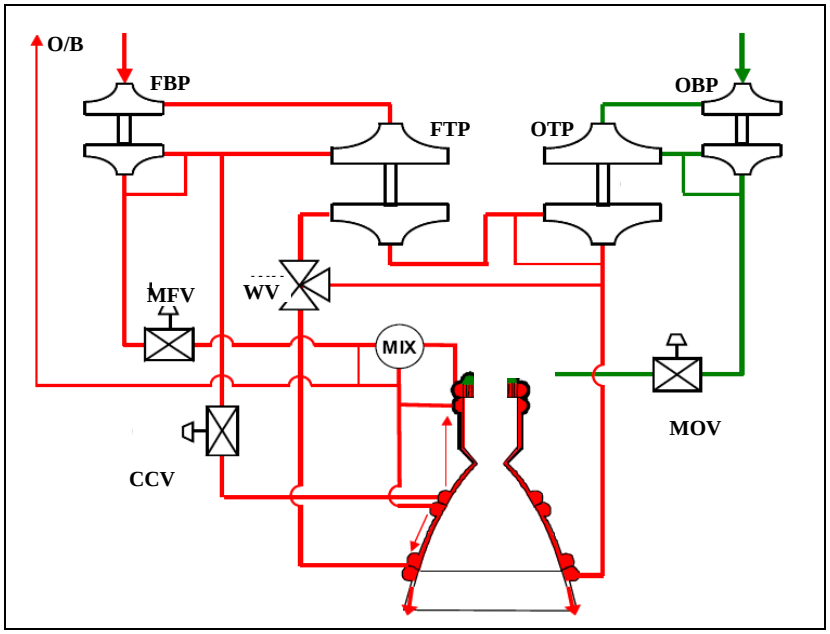

Figure 8 MB-XX Engine Cycle Schematic[6]

Table 8 MB-35 and MB-60 Comparisons[6]

	Units	MB-35	MB-60	MB-XX Demo
Propellants		LOX/LH2	LOX/LH2	LOX/LH2
I_{sp}	sec	468	467	466.6
F	lb_f	35,000	60,000	40,000
p_c	psia	1,500	1,950	1,950
Weight	lb_f	760	1300	-
T/W		46	46	-

Table 9 MB-XX Demonstrator Fuel Turbopump Performance Parameters[9]

Parameter	Units	Stage 1	Stage 2
$\dot{m}$	lbm/s	13.8	13.8
N	rpm	56,300	56,300
H	psia	2,010	
P_{req}	hp	2,609	

2.7 VINCI Upper Stage

The European launch platform is the Ariane 5. The VINCI engine will serve as the power plant for the ESC-B upper stage. The VINCI is an expander cycle engine that uses liquid oxygen and hydrogen as propellants. The VINCI engine delivers 40,400 lb_f of thrust at 464 seconds of I_{sp}.[20] The engine provides multiple firing capability. Gaseous hydrogen returning from the cooling jacket of the nozzle powers both turbines.

The hydrogen turbopump has the following features: powder metallurgy impellers, and ceramic bearings. The TPH is a two stage centrifugal pump with shrouded impellers. An inducer is located upstream of the first stage. The pump impellers are made of titanium with Isoprec® powder.[21] The turbine is a single stage full admission axial turbine.[21] The turbine impeller is unshrouded and made of titanium. The inducer, pump impellers and turbine are on a single shaft. Four cast pieces each made of Inconel 718 make up the TPH housing.[21] The bearing system is ceramic ball type. The bearings are rated to operate up to a DN value of 2.8E6.[10] In a single test a ceramic bearing was tested at 120,000 rpm for 500 seconds at steady state conditions.[10] An Axial Balancing System (ABS) offsets the axial forces. The ABS flows pressurized fluid to the backplane of the second stage impeller.[21] The turbopump operates between the second and third critical speeds.[21]

Table 10 VINCI Fuel Turbopump Performance Parameters[10]

Pump	Units	Stage 1	Stage 2
$\dot{m}$	lbm/s	12.79	12.79
N	rpm	90000	90000
Δp	psia	3336	
P_{req}	hp	3353	
Turbine			
$\dot{m}$ [20]	lbm/s	10.8	-
D_2 [20]	in	4.72	-
p_1 [20]	psi	2756	-

2.8 Demonstrator Upper Stage

Under contract with the United States Air Force Research Laboratory, the Pratt and Whitney Company built a technology demonstrator rocket engine. The engine was design as an expander cycle with a 50 klb_f thrust level. The effort was in support of the IHPRPT boost/orbit transfer propulsion area phase 1 goals for an LH2/LOX upper stage. Figure 9 shows the expander engine cycle schematic. The pumps rotate using gaseous hydrogen passed through each turbine. Table 11 shows the engine steady state performance values.

Figure 10 shows the components of the ALH assembly. The ALH turbopump design minimized weight and cost by integrating flow paths and components into complex housings. The requirements drove the design toward maximizing rotor speeds to obtain high impeller tip speeds to achieve a minimum impeller diameter. A main concern was rotor dynamic instability at high speed. Using the conventional bearing DN limits, this would have been a significant concern. Therefore, the ALH turbopump

design incorporated a fluid film support system. The rotor support system provided optimized rotor dynamic operation, accurate rotor position and control minimizing rotor stresses and bearing loads.[22] The reduced part count of the turbopump, resulted in reduced costs and improved reliability.[22] The ALH rotor is made of PWA 1240 titanium.[22] The rotor consists of an integral inducer, first and second stage uncovered impellers, and an integrally bladed radial inflow unshrouded turbine.[23] Cast Inconel 718 makes up the pump housing. The pump housing contains internal diffuser passages from the first stage impeller discharge to the second stage impeller inlet.[23] Also, it contains an integral volute to collect the pump discharge flow. The turbine housing is cast of weldable Waspaloy and it incorporates an as-cast volute inlet manifold.[23] To complete the ALH assembly the pump and turbine housing bolt together. The ALH was used as a design help guide. Table 12 shows the TPH performance parameters at steady state condition.

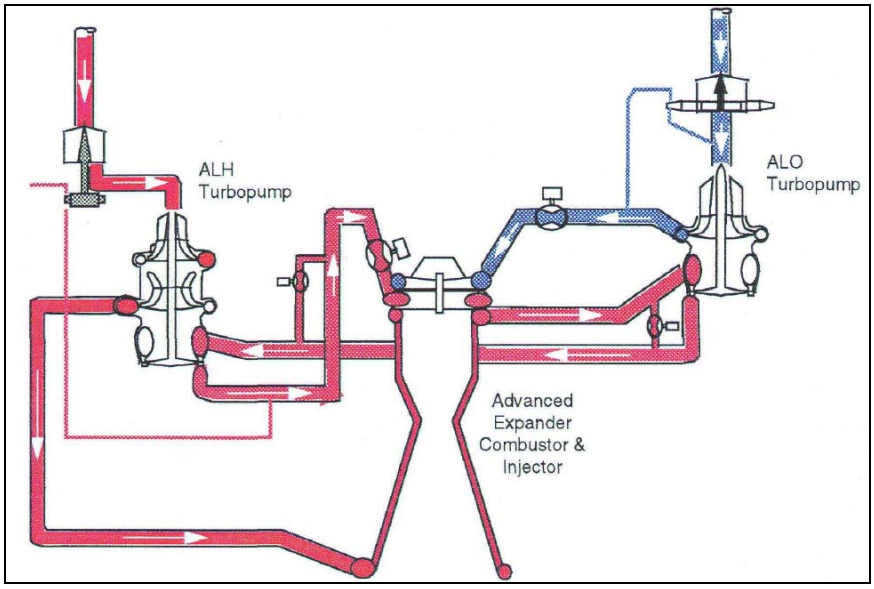

Figure 9 Advanced Expander Engine Cycle Schematic[7]

Table 11 Demonstration Engine Performance[11]

Propellants	Units	LOX/LH2
I_{sp}	sec	450.6
F	lb_f	50,334
p_c	psia	1,375
Weight Estimate	lbs	715
T/W		70.4

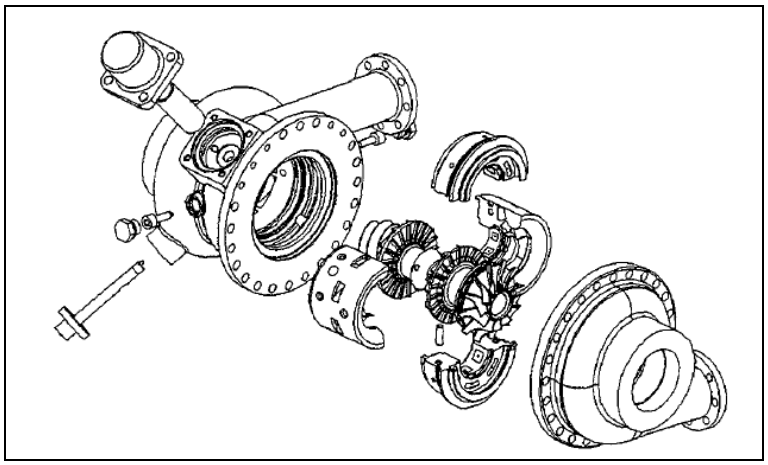

Figure 10 Component View of ALH Turbopump[7]

Table 12 ALH Turbopump Performance Parameters[7]

Pump	Units	100%
η		0.67
ψ		0.462
ϕ		0.147
Ns		17,000
Q	gpm (US)	1,600
P_{req}	hp	5,900
N	rpm	166,700
H_{total}	ft	136,700
U_{2t}	ft/s	2,182

Turbine	Units	
η_{tt}		0.78
U/C (actual)		0.633
P_{trat}		2.16
P_{req}	hp	5,900
N	rpm	166,700
U_{2t}	ft/s	2,327

3. Turbomachinery Theory

3.1 Chapter Overview

The following section will outline the basic fluid dynamic theory used in modeling a liquid pump stage.

3.2 Impeller Inlet and Exit Modeling

A preliminary method of solving the flow state at the inlet or exit of the impeller is the one-dimensional meanline analysis. In a meanline analysis, the assumption is the average flow characteristics, mass or energy, gives the correct representation for the entire flow field. The principal characteristics of the flow state are solved at various locations within the pump. The conservation of mass is the first principle that must be satisfied. The conservation of mass equation is shown in Equation (1.1). Equation (1.1) sets the meridional velocity at any location. Next Newton's Second law of motion must be satisfied for an angular coordinate system. The change in angular momentum is shown in Equation (1.2). The angular momentum change can be related to the change in work using Equation (1.3). The substitution of Equation (1.2) into (1.3) yields the Euler's turbomachinery equation. Equation (1.4) is the fundamental equation at the heart of the modeling process.

$$\dot{m} = \rho A_f C_m \tag{1.1}$$

$$\tau = \dot{m}\left(r_a C_{\theta a} - r_b C_{\theta b}\right) \tag{1.2}$$

$$W = \omega\tau \tag{1.3}$$

$$\dot{W} = \frac{W}{\dot{m}} = \Delta h_0 = U_a C_{\theta a} - U_b C_{\theta b} \tag{1.4}$$

The Euler turbomachinery equation reveals the work input (enthalpy rise) is set by the change in angular momentum. A velocity triangle at the impeller inlet helps visualize the magnitude of the velocity. The velocity triangle is important in determining the work input, or pressure rise. It helps provide insight into pressure variations with changes in mass flow. Figure 11 shows the tangential format sign convention at the impeller inlet. The equations governing the inlet are (1.5) - (1.10).

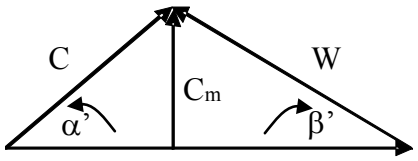

Figure 11 Impeller Inlet Velocity Triangle Tangential Format

$$i = \beta_{blade} - \beta \tag{1.5}$$

$$U = 2\pi r N \tag{1.6}$$

$$C_m = \frac{\dot{m}}{\rho A_f} \tag{1.7}$$

$$p_0 = p + \frac{1}{2}\rho C^2 \tag{1.8}$$

$$C = \left(C_m^2 + C_\theta^2\right)^{\frac{1}{2}} \tag{1.9}$$

$$W = \left[\left(U - C_\theta\right)^2 + C_m^2\right]^{\frac{1}{2}} \tag{1.10}$$

Figure 12 shows the exit velocity triangle in tangential format. The governing equations are (1.11)-(1.14). An important characteristic of the Euler equation shown in (1.11) is it does not account for disk friction, leakage or backflow. The ability to model these phenomena will result in a more practical design. Each component is discussed in the following section.

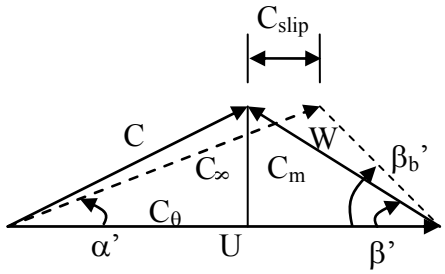

Figure 12 Impeller Exit Velocity Triangles Tangential Format

$$\dot{W} = U_2 C_{\theta 2} - U_1 C_{\theta 1} \tag{1.11}$$

$$C_{\theta 2} = U_2 - C_{m2} \cot \beta_{2b} - C_{slip} \tag{1.12}$$

$$U_2 = 2\pi r_2 N \tag{1.13}$$

$$C_{m2} = \frac{\dot{m}}{\rho_2 A_{f2}} \tag{1.14}$$

$$p_{02} = p_2 + \frac{1}{2}\rho C^2 \tag{1.15}$$

$$\eta_{rotor} = \frac{\dot{W}_{isentropic}}{W_{actual}} = \frac{\Delta p_0 / \rho}{\dot{W}} \tag{1.16}$$

The Δp_0 in (1.16) is the difference of the total exit and inlet pressures at station two and zero. The slip velocity shown in (1.12) is a result of the exit flow angle not precisely following the blade angle. Equation (1.17) shows the American definition of the slip factor as opposed to the European form in equation (1.18). The American definition of slip factor is used. To ensure realistic flow deviation the slip factor, σ, must be modeled accurately. A description of the how the slip factor is modeled is given in subsequent sections.

$$\sigma = 1 - \frac{C_{slip}}{U_2} \tag{1.17}$$

$$\sigma' = \frac{C_{\theta 2}}{C_{\theta 2\infty}} \tag{1.18}$$

3.3 Vaneless Diffuser Modeling

Next, the states of the vaneless diffuser discharge are modeled. Equations (1.19)-(1.21) give a first approximation of the station states. As the flow proceeds through the vaneless diffuser, the impeller exit angular momentum is reduced. Using the

conservation of mass the meridional velocity component is calculated. The flow angle, α, is determined from the results of the conservation of mass and angular momentum.

$$rC_\theta \cong \text{constant} \tag{1.19}$$

$$\rho C_m A_f \cong \text{constant} \tag{1.20}$$

$$\tan\alpha = \frac{C_\theta}{C_m} \cong \frac{k_1 / r}{k_2 / \rho 2\pi r b C_D} = \rho b k_3 \tag{1.21}$$

$$C_D = \frac{A_{eff}}{A_{geo}} = 1 - B \tag{1.22}$$

$$B = 1 - \left(\frac{A_{flow}}{A_{geo}} \right) \tag{1.23}$$

3.4 Volute Modeling

The conservation of mass and angular momentum must be satisfied for the volute states. Equation (1.24) shows a typical operating characteristic at constant speed. The tangential velocity leaving the impeller and diffuser is constant. Equation (1.25) shows the effective velocity passing through the volute throat depends on the mass flow and flow area.

$$C_{\theta 5} \cong \text{constant along a speed line} \tag{1.24}$$

$$\mathrm{C}_7 = \frac{\dot{m}}{\rho_7 A_{f7}} \tag{1.25}$$

4. Methodology

4.1 Chapter Overview

Figure 13 shows a complete design process for turbopump development presented by Concepts NREC. This research employed this methodology to produce a new design. The cycle analysis and meanline design steps were completed. The cycle analysis (power balance) was completed using two different tools, a first order, engineering relationship and a higher fidelity system simulation approach (Numerical Propulsion Simulation System). The meanline design of the pumps and turbine were completed using Pumpal® and RITAL®, software developed by Concepts NREC Inc. A solid model of the pump impellers and turbine were generated using Axcent®.

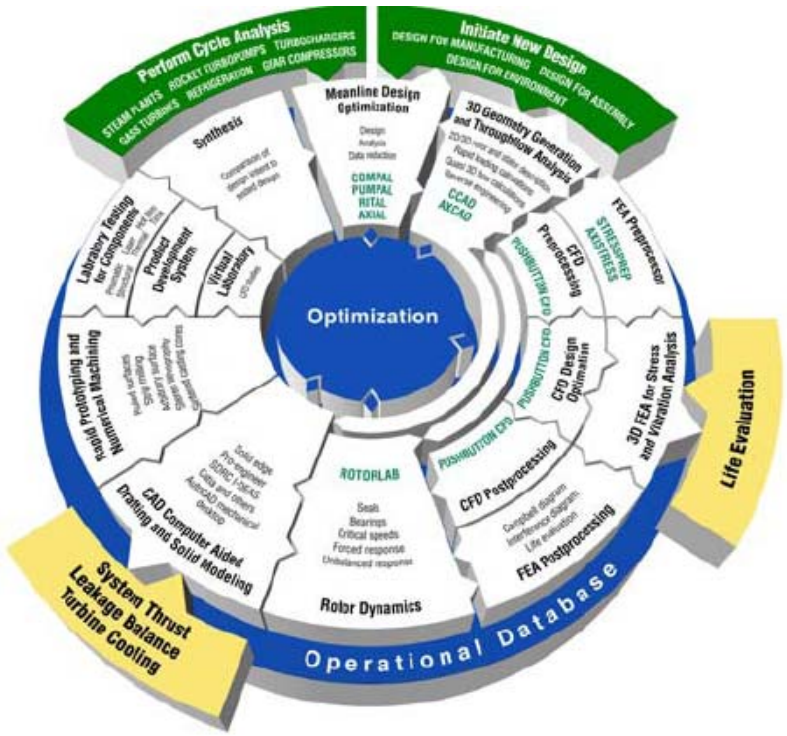

Figure 13 Concepts NREC Turbomachinery Design Process (Used with permission from Concepts NREC)

4.2 Power Balance

The power balance was completed first using an engineering approach employing empirical correlations and idealized theory. This result was then used to initiate a higher fidelity system simulation approach (Numerical Propulsion Simulation System). The power balance phase defined the thermodynamic outputs for the turbopump.

4.2.1 Initial Power Balance

Following the method outlined by Humble, et al. the preliminary power balance, pump and turbine size calculations were completed. The overall design requirement is the power required by the pump can be provided by the turbine. The governing equation relating all three major variables: flow rate, pressures, and power is shown in Equation(1.32). Equation (1.32) is the power required by the turbine to drive the pump.

First, the initial I_{sp} and thrust level goals for the total engine system must be satisfied. The specific impulse was calculated using Equations (1.26) - (1.29). This performance parameter is a strong function of combustion temperature and propellant choice with a weaker dependence on chamber pressure.

$$I_{sp} = \lambda \left\{ \frac{c^* \gamma}{g_0} \sqrt{\left(\frac{2}{\gamma - 1}\right)\left(\frac{2}{\lambda + 1}\right)^{\frac{\gamma+1}{\gamma-1}} \left[1 - \left(\frac{p_e}{p_c}\right)^{\frac{\gamma-1}{\gamma}}\right]} + \frac{c^* \varepsilon}{g_0 p_c}\left(p_e - p_a\right) \right\} \qquad (1.26)$$

$$c^* = \frac{\eta_{c^*} \sqrt{\gamma R T_c}}{\gamma \left(\frac{2}{\gamma + 1}\right)^{\frac{\gamma+1}{2\gamma-2}}} \qquad (1.27)$$

$$\frac{p_e}{p_c} = \left[1 + \frac{\gamma - 1}{2} M_e^2\right]^{\frac{\gamma}{1-\gamma}} \tag{1.28}$$

$$\varepsilon = \frac{1}{M_e}\left[\left(\frac{2}{\gamma + 1}\right)\left(1 + \frac{\gamma - 1}{2} M_e^2\right)\right]^{\frac{\gamma+1}{2\gamma-2}} \tag{1.29}$$

The mass flow rate required is set by the thrust level. The mass flow rate through the pumps was calculated using Equation (1.30) - (1.31). The thermodynamic properties; γ, c_p, and ρ, were gathered using the National Institute of Standards and Technology (NIST) thermophysical database.

$$\dot{m} = \frac{p_c A_t}{c^*} \tag{1.30}$$

$$A_t = \frac{\dot{m}\sqrt{\gamma R T_c}}{\eta_{c^*} p_c \gamma \left(\frac{2}{\gamma + 1}\right)^{\frac{\gamma+1}{2\gamma-2}}} \tag{1.31}$$

The turbine pressure ratio was adjusted to satisfy the I_{sp} goal. A typical turbine pressure ratio is approximately 1.5 for expander cycles.[24] Table 13 shows the initial power balance results.

$$P_{req} = \frac{g_0 \dot{m} H}{\eta_p} = \eta_t \dot{m} c_p T_i \left[1 - \left(\frac{1}{p_{trat}}\right)^{\frac{\gamma-1}{\gamma}}\right] \tag{1.32}$$

$$Q = \frac{\dot{m}}{\rho} \tag{1.33}$$

$$H = \frac{\Delta p}{g_0 \rho} \tag{1.34}$$

To complete the preliminary calculations and to support T/W goals, the mass of the turbopump was estimated using Equations (1.35) - (1.36). The empirical coefficient, A, ranges from (1.3-2.6) and the empirical exponent, B, ranges from (0.6-0.667).[24] For conceptual designs, A =1.5 and B=0.6.[24] SI units were used in the computation and converted to lbm in the final output. Therefore, the pump shaft torque, τ, is in (N*m), the power required, P_{req} (W), and the pump rotational speed, N_r (rad/s). The turbopump total mass is estimated to be 262 lb_f.

$$\tau = \frac{P_{req}}{N_r} \tag{1.35}$$

$$N_r = \frac{N\pi}{30} \tag{1.36}$$

$$m_{tp} = A\tau^B \tag{1.37}$$

Table 13 Initial Power Balance Results

	Units	Stage 1	Stage 2	Turbine
$\dot{m}$	lbm/s	15.1	7.6	7.6
ρ	lbm/ft^3	4.34	3.99	1.076
Q	gpm	1562	850	3151
Head Rise	ft	66792	73811	-
P_{req}	hp	-2157	-1192	3349
P_{in}	psi	45.0	2035	3663
P_{out}	psi	2035	4080	2035
T_{in}	R	38.6	80.7	298
T_{out}	R	80.7	103	215
P_{ratio}		-	-	1.80
η_{tt}		0.85	0.85	0.9

4.2.2 Numerical Propulsion Simulation System

The NASA Numerical Propulsion Simulation System was used further the fidelity of the power balance results.

The NPSS program was created by NASA Glenn Research Center, in conjunction with the U.S. aeropropulsion industry and the Department of Defense. The NPSS program is capable of supporting detailed aerothermodynamic computer simulations of complete aircraft and rocket engines. NPSS is a component-based object oriented engine cycle simulator. It can perform cycle design, steady state and transient off-design performance prediction and test data matching.[25] NPSS uses a NIST compliant thermodynamic gas-properties package. NPSS is supplemented with a rockets package that includes different modeling components, thermodynamic packages, and flow station functions. For example, SuperTrapp and Gaspak, are the thermodynamic packages included in the NPSS Rockets supplement. The CEA thermodynamics package is frequently used for modeling combustion and products of combustion and captures varying thermodynamic properties.[25]

Table 14 shows the NPSS input parameters and Table 15 shows the NPSS results. Table 16 shows a comparison of the initial power balance and the NPSS results. The comparison revealed that the results were within reasonable range of one another. The NPSS results became the inputs for Pumpal® and RITAL® impeller sizing due to the enhanced fidelity of the thermodynamic models.

Table 14 NPSS Inputs

Engine	Units	Value	
O/F		7.0	
ε		125	
P_c	psi	1,740.5	
A_t	in^2	15.9	
Pump		Stage 1	Stage 2
Pr		45.0	2.0
N	rpm	110,000	110,000
$\dot{m}$	lbm/s	15.1	7.55
P_i	psi	45.0	2,025
Turbine			
P_{trat}		1.85	
η_{tt}		0.9	
N	rpm	110,000	
$\dot{m}$	lbm/s	7.55	
P_i	psi	4,080	

Table 15 NPSS Power Balance Results

Engine	Units	Value	
I_{sp}	sec	472	
F	lbs	57,232	
P_c	psi	1,739	
Pump		Stage 1	Stage 2
Q	gpm	1,579	766
T_i	R	40.0	65.7
T_e	R	65.7	82.9
P_e	psi	2,025	4,050
H	ft	65,441	64,016
P_{req}	hp	-2,527	-1,046
η_{tt}		0.80	0.83
Turbine			
P_{trat}		1.84	
Ti	R	609.7	
P_e	psi	1,967	
P_{req}	hp	3,573	
η_{tt}		0.90	

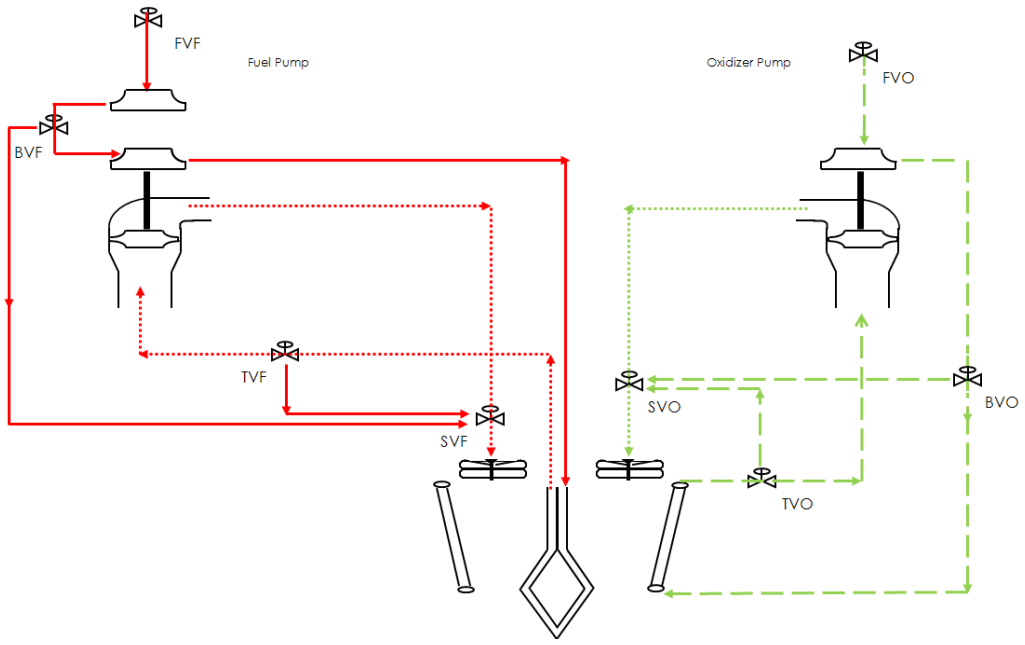

Figure 14 DEAN System Schematic

Table 16 Power Balance Comparison of NPSS and Spreadsheet (S.S)

Engine	Units	NPSS	S.S	|Δ|	NPSS	S.S	|Δ|
I_{sp}	sec	472	465	7			
F	lbs	57232	50000	7232			
P_c	psi	1739	1740	1			
Pump		Stage 1			Stage 2		
Q	gpm	1579	1562	17	766	850	84
T_i	R	40.0	38.6	1.4	65.7	80.7	15
T_e	R	65.7	80.7	15	82.9	103	20.1
P_i	psi	45.0	45.0	0			
P_e	psi	2025	2035	10	4050	4080	30
P_{req}	hp	-2527	-2157	370	-1046	-1192	146
η_{tt}		0.80	0.85	0.05	0.83	0.85	0.02
Turbine							
P_{trat}		1.84	1.80	0.04			
T_i	R	609.7	298	311.7			
P_i	psi	3626	3663	37			
P_e	psi	1967	2035	68			
P_{req}	hp	3573	3349	224			
η_{tt}		0.90	0.90	0			

4.3 Preliminary Pump Impeller Design

A two part process was used to design and size the pump. The first part is to chose the preliminary layout and calculate the impeller size.[24] Table 17 shows the results of the preliminary impeller sizing.

The initial step in the first process was to determine the number of stages. Equation (1.38) provides this function. The required pump pressure rise Δp_p in (Pa) was calculated using Equation (1.39). The tank pressure, p_{tank}, was set to 45.0 psi (0.3 MPa). The typical range of tank pressure varies from 29 psi (0.2 MPa) to 72.5 psi (0.5 MPa) and average about 43.5 psi (0.3 MPa).[24] The Δp_{ps} is the allowable pressure rise over a single stage. This value was set to 2,321 psia (16 MPa).[24] The next highest integer value for the ratio is the number of stages required. The dynamic pressure is a function of the liquid propellant density and the flow velocity. The flow velocity was set to 32.8 ft/s.[24] The pressure drop in the feed system was chosen at the upper end of the typical range seen for this application of 4.4-7.3 psia (30,000–50,000Pa) [24]. The upper end allows for longer feed lines in comparison to lower end. For a regenerative cooling system the pressure drop in the cooling jacket, Δp_{cool}, can vary between values of 10% to 20% of the chamber pressure.[24] The injector pressure drop, Δp_{inj}, was selected to ensure throttling capability design.[24]

Table 17 Preliminary Pump Impeller Sizing

Parameter	Units	Stage 1	Stage 2
Q	gpm	1,562	850
r	lbm/ft3	4.340	3.99
H	ft	66,792	73,811
NPSH	ft	887	--
Nr	rad/s	1,833	1,833
N	rpm	110,000	110,000
Ut	ft/s	1,339	1,407
D1t	in	1.94	1.58
D2t	in	2.79	2.93

$$n \geq \frac{\Delta p_p}{\Delta p_{ps}} \tag{1.38}$$

$$\Delta p = p_c + \Delta p_{dynamic} + \Delta p_{feed} + \Delta p_{cool} + \Delta p_{inj} - p_{tank} \tag{1.39}$$

$$\begin{aligned} \Delta p_{dynamic} &= \frac{1}{2}\rho V^2 \\ \Delta p_{cool} &= 0.15 p_c \\ \Delta p_{inj} &= 0.3 p_c \end{aligned} \tag{1.40}$$

Next, the shaft rotational speed was calculated using Equation (1.43). The lesser value of the two calculations for, N_r (rad/s) was used to calculate the shaft speed, N.[24] The suction specific speed, u_{ss}, and specific speed, N_s, were assigned values of 130 and 2.0 for liquid hydrogen.[24]

$$N_r = \frac{u_{ss}\left(NPSH\right)^{0.75}}{\sqrt{Q}} \tag{1.41}$$

$$N_r = \frac{N_s\left(\frac{H}{n}\right)^{0.75}}{\sqrt{Q}} \tag{1.42}$$

$$N = \frac{30 N_r}{\pi} \tag{1.43}$$

Equation (1.44) was used to calculate the pump impeller tip speed, here SI units are used for the gravitational constant and head rise. A value of 0.60 was used for the pump head coefficient.[24] Equation (1.45) is used to determine the pump impeller inlet and exit diameters, D_{1t} and D_{2t}. The inlet flow coefficient value was set to 0.10.[24] The inducer inlet hub-to-tip diameter ratio was set to 0.3.[24] The Net Positive Suction Head (NPSH) for stage one was calculated using Equation (1.47). Equation provides the the vapor pressure.[26] The temperature units must be in Kelvin, and the vapor pressure is calculated in Pascal. In Equation (1.48) the coefficient were set to the following values C1=12.69 C2=-94.896, C3=1.1125, C4=3.291E-0.4, and C5=2.0. all are based on an empirical curve fit.[26] The NPSH value is a crucial parameter. The pump head rise must not exceed this value or cavitation will occur. The cavitation phenomenon is the formation of bubbles in a low-pressure region. The bubbles collapse in a high-pressure region. This occurs when the pressure in the system falls below the liquid vapor pressure. The formation and collapse of the bubbles may cause noise, pressure drop, efficiency decrease, and compression stress levels that may cause the material to fail.

$$u_t = \sqrt{\frac{g_0 H}{n\psi}} \tag{1.44}$$

$$D_{1t} = \sqrt[3]{\frac{\left(4/\pi\right) Q}{\phi N_r \left(1 - L^2\right)}} \tag{1.45}$$

$$D_{2t} = \frac{2u_t}{N_r} \tag{1.46}$$

$$NPSH = \frac{p_i - p_v}{g_0 \rho} \tag{1.47}$$

$$P_{vapor} = \exp(C1 + \frac{C2}{T} + C3 * \ln(T) + C4 * T^{C5}) \tag{1.48}$$

4.4 Detailed Pump Impeller Design

The second step was the completion of a detailed design of the pump impellers. The following section will outline the steps taken to use Pumpal® and complete a detailed design of the pump impeller.

The Pumpal® software uses an extensive database to calculate the impeller inlet and exit radius, blade angles, and exit depth. The following assumptions are made with respect to the meanline design and analysis. First, there is a mean streamline running through the machine such that the fluid flow states and velocities on this streamline at any point are representative of the mean of the whole cross-section. Second, the radial and circumferential variations of all the flow parameters are neglected. Lastly, the objective of a meanline analysis is not to reveal the full details of the flow state and velocity, but to determine the overall performance of the machine (the analysis mode) or the combination of overall geometric parameters which provide the maximum efficiency (the design mode). To initiate a new design the Pumpal® software is equipped with a graphical user interface (GUI), the design wizard. An outline of the steps taken within the wizard and the mathematical relationships used in Pumpal® is given the following paragraphs.

The first step is to choose the technology base. There are three technology bases, CETI Two-zone model, CETI Single-Zone model, NREC single-zone model. The CETI Two-zone model is based on the Concepts ETI, Inc. technology. Within the CETI two-zone model, a primary zone corresponding to the jet flow, is assumed to be isentropic, and there is a secondary zone corresponding to the low momentum wake flow region. The primary zone diffusion ratio and the secondary zone size must be modeled or specified by the user. The NREC model uses different correlations to model the individual losses such as friction, blade loading, and end wall. In addition, a blockage factor must be modeled to resolve the impeller exit conditions. The CETI-Two-zone model was selected as the technology base for this effort.

4.4.1 CETI-Two-Zone Model

At the impeller exit the flow is divided into two zones: primary zone and secondary zone. The following two assumptions apply

1. The flow in the primary zone is assumed to have reached the impeller exit plane through an isentropic process. All the loss inside the impeller passage is assumed to be concentrated inside the secondary zone.[8]
2. The primary and secondary zone reach static pressure balance at the impeller exit.[8]

To solve the primary zone the relative exit velocity, W_{2p}, must be calculated. To complete this calculation the diffusion ratio, DR2 is specified by the user or a diffusion model is selected.

$$W_{2p} = W_{1t} * DR2 \tag{1.49}$$

There are eight methods within Pumpal® to estimate the value of the diffusion ratio. The Hybrid diffusion model was selected. Figure 15 shows the correlation used in the Hybrid model. To ensure a solution of the two-zone model the diffusion must be calculated accurately.

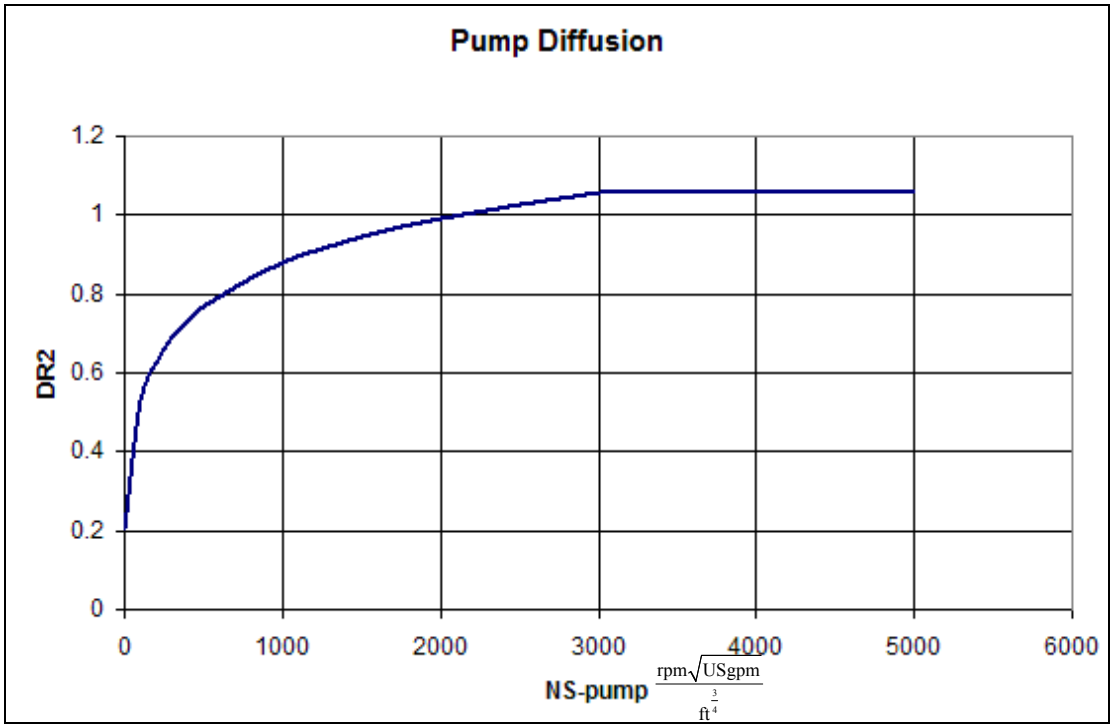

Figure 15 Hybrid Pump Diffusion Ratio Model[8]

The next calculation is the static enthalpy, h_{2p}.

$$h_{2p} = \left(\frac{h_1 + W_1^2}{2\left(2 - U_1^2\right)} \right) - \frac{W_{2p}^2}{2} + \frac{U_2^2}{2} \tag{1.50}$$

This calculation is carried out using Equation (1.51) the rothalpy conservation from inlet to exit, as implied by assumption one. Rothalpy, I, is a fundamental property that is constant for an adiabatic irreversible flow process relative to a rotating component.

$$I = h_{2p} + \frac{W_{2p}^2}{2} - \frac{U_2^2}{2} = h_1 + \frac{W_1^2}{2} - \frac{U_1^2}{2} \tag{1.51}$$

By employing the assumption of an isentropic flow the exit flow entropy is defined

$$s_{2p} = s_1 \tag{1.52}$$

With the static enthalpy and entropy at the exit defined, all other thermodynamic properties can be calculated. Finally, the primary flow angle, β_{2p}, is calculated using Equation (1.53) and the primary zone velocity triangle is completely defined.

$$\beta_{2p} = \beta_{2b} + DELTA2p \tag{1.53}$$

To solve the secondary zone, the mass fraction of the primary zone, χ, is calculated using Equation (1.54). With a known value of the mass fraction the secondary area fraction, ε, and the secondary exit relative velocity are calculated as shown in Equations (1.55)-(1.56).

$$1 - \chi = \frac{\rho_{2p}(1-\varepsilon) A_2 W_{2p} \cos(\beta_{2p})}{\dot{m}} \tag{1.54}$$

$$\varepsilon = 1 - \frac{(1-\chi)\dot{m}}{\rho_{2p} A_2 W_{2p} \cos(\beta_{2p})} \tag{1.55}$$

$$W_{2s} = \frac{\chi \dot{m}}{\varepsilon \rho_{2s} A_2 \cos(\beta_{2s})} \tag{1.56}$$

The conservation of rothalpy can be applied to calculate the static enthalpy of the secondary zone, h_{2s}.

$$h_{2s} = \left(h_1 + \frac{W_1^2}{2} - \frac{U_1^2}{2} \right) - \frac{W_{2s}^2}{2} + \frac{U_2^2}{2} \tag{1.57}$$

To complete the calculations the assumption that the primary and secondary zone reach static pressure balance, $p_{2s} = p_{2p}$, is applied. With the exit static enthalpy and pressure defined all other thermodynamic properties are calculated. Equation (1.58) shows the secondary flow angle is calculated from the exit blade angle,β_{2b}, and the secondary deviation angle, DELTA2s. The secondary zone velocity triangle is completely defined by the secondary relative exit velocity and flow angles.

$$\beta_{2s} = \beta_{2b} + DELTA2s \tag{1.58}$$

To complete the CETI-Two Zone model it is assumed that the primary and secondary zone achieve uniform state instantly at the impeller exit through a mixing process.[8] Equations (1.59) - (1.61) show the conservation of mass and momentum equations.

$$\rho_{2m} C_{m_{2m}} A = \rho_{2p} C_{m_{2p}} (1-\varepsilon) A + \rho_{2s} C_{m_{2s}} \varepsilon A \tag{1.59}$$

$$\left(p_{2p} - p_{2m} \right) A = \rho_{2m} C_{m_{2m}}^2 A - \left\{ \rho_{2p} C_{m_{2p}}^2 (1-\varepsilon) A + \rho_{2s} C_{2s}^2 \varepsilon A \right\} \tag{1.60}$$

$$C_{t_{2m}} = \chi C_{t_{2s}} + (1-\chi) C_{t_{2p}} \tag{1.61}$$

The energy equation assumes a parasitic power loss that results from front and rear leakage, P_{fleak} and P_{rleak}, disk friction P_{df} and recirculation P_{recirc}. The overall after-mixing energy is calculated using Equation (1.65). The disk friction was modeled using the Stepanoff method, shown in Equations (1.62)-(1.64). To obtain the after mixing conditions at station 2m, the fluid equation of state and Equations (1.59)-(1.65) are solved using an iterative process.

$$P_{df} = \frac{1}{2} K \rho U_2^3 R_2^2 \tag{1.62}$$

$$K = \frac{0.0402}{\mathrm{Re}^{\frac{1}{5}}} \tag{1.63}$$

$$\mathrm{Re} = \frac{U_2 R_2}{\nu} \tag{1.64}$$

$$h_{02m} = h_{02a} + \frac{\left(P_{fleak} + P_{rleak} + P_{df} + P_{recirc}\right)}{\dot{m}} \tag{1.65}$$

4.4.2 Deviation/Slip Modeling

The results of the impeller exit calculations from the CETI-Two-Zone model allow for the calculation of the deviation angle, DELTA2p, and the slip factor, σ. There are two slight variations of the definition for slip factor, the American convention shown in Equation (1.66) and the European, shown in Equation (1.67). The American convention is used in this design effort.

$$\sigma = 1 - \frac{C_{slip}}{U_2} = 1 - \frac{C_{\theta 2\infty} - C_{\theta 2}}{U_2} \tag{1.66}$$

$$\sigma_\theta = \frac{C_{\theta 2}}{C_{\theta 2\infty}} \tag{1.67}$$

There are eight slip model choices. The Weisner-Buseman Model was selected. According to Japiske et al, the Weisner-Buseman correlation is appropriate, especially when very good flow passages such as highly loaded rocket turbopump impellers are designed. The Wiesner-Buseman equation for slip is shown in Equation (1.68).

However, this model suffers a major defect, in that it depends only on geometric parameters, yet the slip factor may vary substantially along an operating speed line. The Wiesner-Buseman model may give a DELTA2p greater than zero. In this case the model is not used and slip is calculated using Equation (1.66).[8] The primary zone deviation values range from 0^o to -4^o for a good backswept rotor, although it can be as much as -20^o for a radial or any flat plate blade.[8]

$$\sigma = 1 - \frac{\sqrt{\cos \beta_{2b}}}{Z_2^{0.7}} \tag{1.68}$$

The next step is to solve the impeller inlet. There are two optimization methods, minimize the relative tip speed or the NPSHR. The W_{1tmin}, minimum relative tip speed method, corresponds to minimum loss and is selected for this research. The W_{1tmin} is calculated using Equation (1.69). The minimum relative tip speed can be found from the derivative of Equation (1.69). For an axial inlet flow design, the minimum relative tip speed is achieved when Equation (1.70) is satisfied. The inlet blade angle from hub to tip is then calculated. This angle is set based on the optimum incidence angle and the flow angle, the calculation is shown in Equation (1.71) for the hub, mean, and tip blade angle.

$$W_{1t} = \left(U_{1t}^2 + C_{m1}^2\right)^{\frac{1}{2}} = \sqrt{\left(\frac{2\pi R_{1t} N}{60}\right)^2 + \left(\frac{Q}{\pi\left(R_{1t}^2 - R_{1h}^2\right)}\right)^2} \tag{1.69}$$

$$R_{1t} = \left(\frac{30\sqrt{2}Q}{\pi^2 N\left(1 - \left(\frac{R_{1h}}{R_{1t}}\right)^2\right)}\right)^{\frac{1}{2}} \tag{1.70}$$

$$\begin{aligned}\beta_{1tb} &= \beta_{1t} + I_{1t\_opt} \\ \beta_{1mb} &= \beta_{1m} + I_{1m\_opt} \\ \beta_{1hb} &= \beta_{1h} + I_{1h\_opt}\end{aligned} \tag{1.71}$$

The impeller exit geometry is solved using the option to optimize the impeller outlet diameter (R2) and impeller exit width (B2). The impeller outlet radius is calculated based on the specified head rise and is adjusted until the specified pressure rise is matched. The impeller exit width is calculated by setting the exit swirl angle as a function of the specific speed. The exit swirl coefficient is defined as the ratio of the exit absolute tip speed to the absolute mean speed. This setting allows the user to select a tip model secondary mass flow fraction. The mass fraction was set to 0.05. This value is within the range (0.02-0.10) for typical high performance pumps.[27]

A vaneless diffuser was chosen to ensure a wide range of operation.[27] The lack of diffuser vanes means the absence of a vane-driven vibratory coupling with the impeller blades. This could lead to possible fatigue failure of the leading edges, or impeller blades. The vaneless diffuser entry is not pinched. Table 19 shows the complete list of inputs for the first stage.

4.5 Volute Design

To simulate the split flow of the liquid hydrogen, a volute is chosen for both pump stages. Both stages use a right overhung volute. At the volute exit of stage one and two, the objective is to provide 2,025 psia and 4,050 psia of pressure. Table 18 shows the preliminary volute parameters.

Table 18 Pumpal® Volute Parameters

Parameter	Value	Note
D8/D7	1.1	Designer Choice
LC57	0.45	Designer Choice
Nominal Area Fraction at 0^o	0.03	Designer Choice

There are three stations within the volute providing the necessary information to model the volute. Station 5 is the inlet to the volute. The following inlet conditions are transferred from the upstream element; p_o, T_o, C and α. Station 7 is the volute throat location. The properties at station 7 are calculated using the Equations (1.72), (1.73), and (1.74). Station 8 is the volute exit. The pressure and mass flow rate at station must be equal to power balance values. To be able to complete the calculation of the station 7 parameters, the loss coefficient parameter LC57 must be calculated.

$$p_{07} = p_{05} - LC57 \times \left(p_{05} - p_5 \right) \tag{1.72}$$

$$T_{07} = f\left(p_{07,} h_{05} \right) \tag{1.73}$$

$$s = f\left(p_{07,} T_{07} \right) \tag{1.74}$$

The modeling technique used to calculate LC57 for a simple overhung volute was created by Young and reported by Japiske.[27] The model is based on a geometric area ratio as define in Equation(1.75), where A_5 and A_7 are the volute inlet and exit areas. Incompressible flow is assumed. The inlet and exit velocities are calculated using Equations (1.76) and (1.78). The inlet swirl parameter, λ, is equal to the ratio of the absolute tangential velocity and the absolute meridional velocity as shown in Equation (1.77). An approximate relationship for the loss coefficient LC57 is shown in Equation (1.79). The pressure recovery coefficient CP57 can also be set in Pumpal®. The default value of zero for CP57 was used for the preliminary design. The volute can be designed to accelerate the flow or diffuse the flow. If the product, λAR, designated as LAMAR in Pumpal® is greater than 1.0 the flow is diffused, if less than or equal to 1.0 the flow is accelerated.[27]

$$AR = \frac{A_7}{A_5} = \frac{\pi D_7^2 / 4}{2\pi r_5 b_5} \tag{1.75}$$

$$C_5 = \left(Q / A_5 \right) \left(1 + \lambda^2 \right)^{\frac{1}{2}} \tag{1.76}$$

$$\lambda = \frac{C_{\theta 5}}{C_{m5}} \tag{1.77}$$

$$C_7 = Q / A_7 \tag{1.78}$$

$$LC57 = \frac{p_{05} - p_{07}}{p_{05} - p_5} \tag{1.79}$$

The second stage is a clone of the first stage. The total head rise is selected as the critical solution parameter. The horsepower required is the critical solution parameter for

the first stage. This algorithm will ensure the critical parameter is satisfied for each solution. The bypass is simulated using the interstage transfer selected from the drop down menu Multistage. A multiplier of 1.0 for temperature, pressure, and speed was set. To simulate a 50% bypass, a multiplier of 0.5 was set for the flow. A zero multiplier was set for the swirl. Table 19 shows the preliminary input values. The values were chosen using the noted reference and criteria. This concludes the user inputs necessary to define both stages. Table 20 shows the criteria for a successful pump design.

Table 19 Pumpal® Wizard Inputs Preliminary Impeller Inlet/Exit Design

Pumpal® Symbol	Units	Value	Guidance
Z1		3	ALH Design
Z2	-	15	ALH Design
Bex/B2	-	1.0	No Pinch
Rex/R2	-	1.1	Designer Choice
R1H/R1T	-	0.3	Typical ratio[24]
p_0	psi	1967	NPSS
β_1	deg	0	Simulate Axial
i	deg	0	pg. 506[27]
PHI1	deg	65.0	Designer Choice
CLR	in	0.0397	Designer Choice
PHI2	deg	90	Simulate Radial
Beta2b	deg	65.0	pg. 515[27]

Table 20 Impeller Design Criteria

Symbol	Units	Criteria	Note
η_{tt}	-	≥ 0.80	NPSS
M2M_ABS	-	≤ 1.0	Zero Shock Loss
R_{2tip}	inches	≤ 7.07	RL10 Size[5]
H_p	ft	≥ 66792	NPSS value
H_p	ft	≥ 73811	NPSS value
P_{08} Stage 1	psi	≥ 2035	Power Balance
P_{08} Stage 2	psi	≥ 4080	Power Balance

4.6 Pump Impeller Design Analysis Mode

After a satisfactory design is found in Design Mode, the user switches to Analysis mode. This mode allows the user to generate performance maps. This step aids in predicting the throttle range of the concept design. Within Analysis mode the geometry of the impeller is set. The impeller inlet calculations are not based on an optimization method, as in the Design Mode. The velocity triangle and static conditions at the impeller inlet are calculated using an iterative process. This process is based on the known upstream conditions, total pressure and temperature. The equations used in the iterative process are shown in Equations (1.80)-(1.85). The CETI-Two-zone modeling technique is used to solve for the impeller exit conditions and geometry. Within the Analysis mode the pump maps are generated using the multiple point analysis option. The user must specify the speed and flow range within the option window.

$$p_0^1 = \frac{\left(p_\infty + LC1 * p_1\right)}{\left(1 + LC1\right)} \tag{1.80}$$

$$h_0^1 = h\left(T_\infty, p_\infty\right) \tag{1.81}$$

$$s_1 = s\left(h_{01}, p_{01}\right) \tag{1.82}$$

$$C_{m_1} = \frac{\dot{m}}{\rho_1 A_1 \left(1 - B1\right)} \tag{1.83}$$

$$C_1 = \frac{C_{m_1}}{\cos(ALPHA1)} \tag{1.84}$$

$$h_1 = h_{01} - \frac{1}{2} C_1^2 \tag{1.85}$$

$$\rho_1 = \rho\left(h_1, s_1\right) \tag{1.86}$$

4.7 Turbine Impeller Design

The preliminary design of the radial turbine impeller was completed using the RITAL® software. RITAL® utilizes flow models based on extensive past design and test experience. There are three different types of solvers to calculate the geometry of the turbine: RITAL®, RITDAP, and RTP. The RITAL® and RITDAP solvers are heritage algorithms and were retained for projects originally developed using the RITDAP program or older versions.[28] The RTP solver was used to complete the conceptual design of the turbine. An outline of RTP is given below and the steps taken to complete a conceptual design of a meanline turbine is given in the preceding sections.

4.7.1 Radial Turbine Program

The RTP solver is recommended for all new projects and was used to design the conceptual hydrogen turbine. The solver is able to solve for subsonic, transonic and supersonic flow. RTP uses real fluid properties extracted from an internal database. The RTP is a pressure-based solver. This means in order to balance the mass flow for each component process adjusts the pressure for each station. Also, the flow conditions from the upstream component passed to the next component are not mixed and aerodynamic blockage is preserved. The rotor and nozzle models are validated by Concepts NREC.[28]

4.7.2 Preliminary Impeller Sizing

The user interface with RITAL® is similar to Pumpal®, a design wizard. Appendix B describes in detail each step. One of two methods is chosen to size the turbine. The first design method is based on the flow and loading coefficients. The second design method is based on the optimum specific speed and blade-to-jet ratio.

These reference values do not reflect the final design parameters exactly. Equations (1.87) and (1.88) define the RITAL® default parameters.

Table 21 RITAL® Preliminary Sizing Default Settings

Variable	Default Value
ϕ	0.25
φ	0.9
ξ	1.0
$C_{\theta 6}$	0
δ_6	5
R_{4h}/R_3	0.3
R_1/R_2	1.25
R_{5h}	0
A_5/A_4	1.5
DivAng	4.5

$$\phi = \frac{C_{m6}}{U_4} \tag{1.87}$$

$$\varphi = \frac{\Delta h_0}{U_4} \tag{1.88}$$

The actual enthalpy change, Δh_0, shown in Equation (1.89) is related with the isentropic enthalpy change, Δh_{is}, through the total-to-static efficiency, η_{TS}, as shown below in Equation (1.89).

$$\Delta h_0 = \eta_{TS} * \Delta h_{is} \tag{1.89}$$

The second design method is based on specific speed, N_s, and jet speed ratio, ν. These parameters are defined in Equations (1.90) and (1.91). The specific speed is a function of, Q_6, and the isentropic total-to-static enthalpy drop, Δh_{is}, from the rotor inlet to exit.

$$N_s = \frac{2\pi * N * \sqrt{Q_6}}{60 * \left(\Delta h_{is}\right)^{\frac{3}{4}}} \tag{1.90}$$

$$\nu = \frac{U_4}{C_j} = \frac{U_4}{\sqrt{2\Delta h_{is}}} \tag{1.91}$$

The rotor meridional velocity ratio, ξ, is the ratio of the inlet to exit velocity, defined in Equation (1.92). The design is based on the flow and loading coefficient.

$$\xi = \frac{C_{m_4}}{C_{m_6}} \tag{1.92}$$

4.7.3 Rotor Loss Model

A specific type of passage loss model can be used in the calculation of the rotor losses. The rotor losses include; incidence, clearance, trailing edge, and passage. The incidence loss is modeled as a decrement in tangential kinetic energy due to the turning of the flow. The incidence is a function of the relative rotor inlet velocity, W_4, as shown below in Equation (1.93).

$$L_i = \frac{1}{2} W_4^2 \sin^2 i \tag{1.93}$$

Equation (1.94) shows the clearance loss is model. The clearance loss, L_c, is a function of the ratio of the tip clearance, ε_r, to the exducer blade height, b_5. The recommended value of K_c is unity.[28]

$$L_c = K_c \left(\frac{\varepsilon_r}{b_5} \right) \tag{1.94}$$

This research employed the NASA passage loss model. Equation (1.95) shows the passage loss is a function of the mean passage kinetic energy. The coefficient K_p, is an empirical parameter, its recommended value is 0.3.[28] The design criteria for the turbine impeller are given in Table 22.

$$L_p \frac{1}{2} K_p \left(W_4^2 \cos^2 i + W_5^2 \right) \tag{1.95}$$

$$i = \beta_4 - \beta_{4,opt} \tag{1.96}$$

Table 22 Turbine Impeller Design Criteria

Parameter	Units	Criteria	Guidance
D_{2m}	inches	$\leq$ 5.4	RL10 Size
η_{tt}		$\geq$ 0.90	NPSS
Ma		$\leq$ 1.0	Zero Shock Loss
P_0	psi	$\geq$ 2035	NPSS
P_{req}	hp	$\geq$ 3602	NPSS/Pumpal®

4.8 Axial Bearing Load

The net axial thrust is the summation of the component forces shown in Equations (1.97)-(1.103). A diagram of the vector forces is shown in Figure 16. The DN value is limited to 3E6. The RL60 has achieved this value. [17]

$$F_1 = \dot{m} C_{m1} \sin\phi_1 - \dot{m} C_{m2} \sin\phi_2 \tag{1.97}$$

$$F_2 = \frac{p_{1h} + p_{1t}}{2} \pi \left(R_{1t}^2 - R_{1h}^2 \right) \tag{1.98}$$

$$F_3 = p_{1t} \pi \left(R_1^{'2} - R_{1t}^2 \right) \tag{1.99}$$

$$F_4 = \frac{\pi}{2} A_f \left(R_{2t}^4 - R_1^{'4} \right) + \pi B_f \left(R_{2t}^2 - R_1^{'2} \right)$$

where

$$A_f = \frac{\rho}{2} \left(1 - F_f^2 \right) \left(2\pi\omega \right)^2 \tag{1.100}$$

and

$$B_f = p_2^{'} - \frac{\rho}{2} \left(1 - F_f^2 \right) U_1^{'2}$$

$$F_5 = p_2 \pi \left(R_{2t}^2 - R_{2h}^2 \right) \tag{1.101}$$

$$F_6 = \frac{\pi}{2} A_f \left(R_{2h}^2 - R_{8h}^4 \right) + \pi B_f \left(R_{2h}^2 - R_{8h}^2 \right)$$

where

$$A_f = \frac{\rho}{2} \left(1 - F_f^2 \right) \left(2\pi\omega \right)^2 \tag{1.102}$$

and

$$B_f = p_8^{'} - \frac{\rho}{2} \left(1 - F_f^2 \right) U_8^{'2}$$

$$F_8 = p_{1h} \pi R_{1h}^2 \tag{1.103}$$

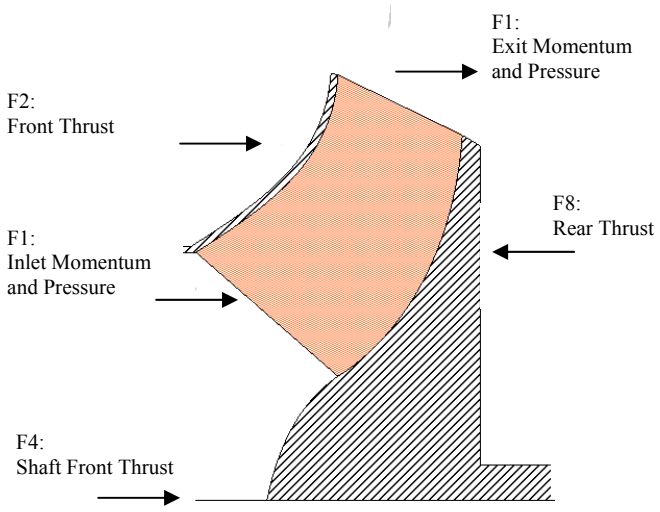

Figure 16 Axial Thrust Forces

4.9 DEAN Shaft

The preliminary shaft material is chosen to be TI-6Al-4V extra low interstitial, (ELI) grade. The Ti-6Al-4V has moderate sensitivity to hydrogen embrittlement.[29] The ELI grade has high damage-tolerance at cryogenic temperatures.[29] Equations (1.104)-(1.107). are used to determine the shaft radius. A pure torsional load is assumed. The power required, P_{req}, was converted to units of (in.lb/s). The rotational speed, N, was converted to units of revolution per second. A factor of safety, F.S, equal to 1.2 is used in the design.[30] The yield stress for TI-6Al-4V ELI that is beta annealed is 115 ksi.[29] The tensile yield stress for recrystallization annealed ELI was found to be 125 ksi.[29] Equation (1.107) provides the radius of the shaft.

$$T = \frac{P_{req}}{2\pi N} \tag{1.104}$$

$$J = \frac{1}{2}\pi c^4 \tag{1.105}$$

$$F.S = \frac{\sigma_{yield}}{\tau_{allowable}} \tag{1.106}$$

$$\frac{J}{c} = \frac{T}{\tau_{allowable}} \tag{1.107}$$

Equation (1.108) is used to calculate the shaft length. The deflection is assumed to be 0.005 inches.[31] The modulus of elasticity is 16.5E6 psi. The loading coefficient, C is set to unity. While these preliminary estimates for shaft dimensions provide for the pump and turbine loading, the design process often increases shaft diameters to accommodate rotordynamic phenomenon. Typically, these shafts operate supercritical speeds, above the first vibrational mode. The larger shaft ensures adequate stiffness to handle these operating conditions.

$$f = \frac{wl^3}{CEI} \tag{1.108}$$

$$I = \frac{\pi d^4}{64} \tag{1.109}$$

5. Analysis and Results

5.1 Chapter Overview

This chapter provides the predicted performance maps of the pumps and turbine. The results of a preliminary shaft and bearing size are given.

5.2 Stage 1 Impeller layout

Figure 17 shows the layout of the DEAN liquid hydrogen turbopump. The red shaded area identifies the fluid path created by the impeller blade. The blue shaded area identifies the vaneless diffuser and volute. The stage two impeller does not incorporate a diffuser. The grey shaded area without hash marks identifies the shaft. The fluid path between stages is not modeled as a physical component, such as a cross over, but the interstage transfer allows for the transfer of the thermodynamic properties from stage one into stage two.

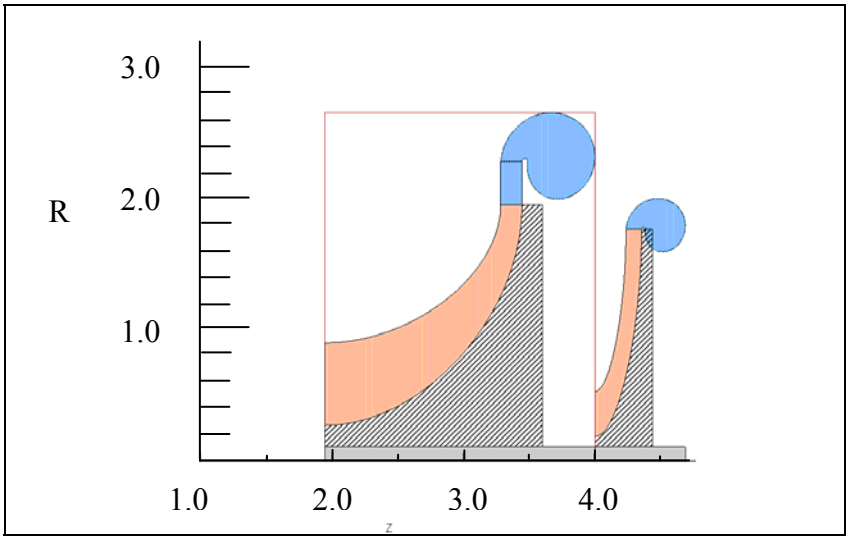

Figure 17 DEAN Liquid Hydrogen Pump Configuration

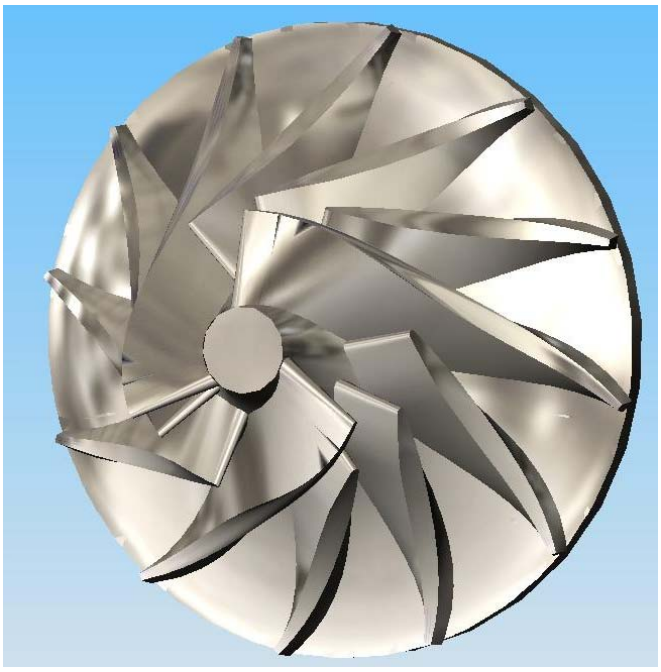

Figure 18 DEAN Stage 1 Impeller

Figure 18 shows the stage 1 impeller design with 3 main blades and 12 exit blades. Stage 1 is a centrifugal axial inflow impeller. The impeller is unshrouded. An unshoruded impeller reduces weight, manufacturing time and cost. However, this design is not as efficient as a shrouded impeller. To increase the range of operation a 60^{o} blade backsweep is incorporated. Table 23 presents the results of the initial and final pump design. The initial design required modification. The head rise and exit pressure proved to be the critical parameters. The engine cycle must receive the appropriate pressure rise and total pressure to ensure on-design performance. The volute parameter VR7/D5 was incremented until the satisfaction of the criteria. The exit pressure from the volute meets the power balance specification. The increase of the impeller diameter is consistent with an increase in required power. The impeller size for each is comparable to current designs. The design did not meet the cavitation criteria as expected. The preliminary

calculations suggest an inducer will be required. This is consistent with current state-of-the-art pump designs. The impact of not meeting the efficiency goal may result in a mission loss. The turbine is designed to accommodate this variation.

Table 23 Stage 1 Impeller On-Design Performance Pumpal® Results

Symbol	Units	Criteria	Run1	Final
η_{tt}	-	≥ 0.80	0.77	0.77
H	ft	≥ 65,441	64,823	70,355
P_{req}	hp	≥ 2,527	2,158	2,523
P_{08}	psi	≥2,025	1,988	2,320
$\dot{m}$	lbm/s	≤15.1	15.1	15.1
NPSHR	ft	≤ 841	7,076	7,076
D_{2t}	inches	≤ 6.0	3.39	3.88
VR7/D5		na	1.0	3.0

5.2.1 Pump Sensitivity Analysis

A sensitivity analysis was completed to reveal the pump stage variable influences on the critical performance parameters. Equation (1.110) shows the method use to determine sensitivity, the ratio of the performance parameter, P, for a given incremental change in variable, Q. The impeller characteristics are numbered according to their degree of influence. The value shown in the far right column of Table 24 - Table 28 Impeller Tip Radius Sensitivity Analysis is the sensitivity value. The most influential is ranked number 1.

$$\text{Sensitivity} = \Delta P \times \frac{Q}{\Delta Q} \tag{1.110}$$

Table 24 Pump Stage Efficiency Sensitivity Analysis

Rank	D8/D7	N	R_{ex}/R_{in}	D7/D5	ZR	$\Delta\eta_{tt}$
		rpm				
Baseline	1.1	110000	1.1	1.0	15	-
1	1.11					-0.11
2		11100				-0.11
3			1.11			-0.10
4				1.1		0.07
5					16	-0.02

Table 25 Pump Head Rise Sensitivity Analysis

Rank	D8/D7	R_{ex}/R_{in}	D7/D5	N	R_{1h}/R_{1t}	ΔH_{tt}
				rpm		
Baseline	1.1	1.1	1.0	110000	0.3	-
1	1.11					-10198
2		1.11				-7197
3			1.1			6365
4				111000		-6259
5					0.0303	-2874

Table 26 Volute Exit Pressure Sensitivity Analysis

Rank	D8/D7	R_{ex}/R_{in}	D7/D5	N	R_{1h}/R_{1t}	Δp_{08}
				rpm		
Baseline	1.1	1.1	1.0	110000	0.3	-
1	1.11					-274
2		1.11				-217
3			1.1			192
4				111000		-190
5					0.0303	-87

Table 27 Power Required Sensitivity Analysis

Rank	N	D7/D5	R_{ex}/R_{in}	ΔP_{req}
	rpm			
Baseline	110000	1.0	1.0	-
1	111000			-0.44
2		1.1		0.11
3			1.1	0.10

Table 28 Impeller Tip Radius Sensitivity Analysis

Rank	N	ZR	ΔR_{2t}
	rpm		
Baseline	110000	15	-
1	111000		-1.9
2		12	-0.1

5.3 Stage 1 Off-Design Operating Range

A plot of mass flow versus total head rise best describes the off-design performance. Figure 19-Figure 22 show stage 1 can operate at a wide range of speed and mass flow. This fact is important for throttle operation. Figure 19 shows a red dashed line to indicate the surge line. The turbopump should not operate to the left of this line because the stage performance would be severely degraded. At 110,000 rpm the stage can operate in a mass flow range of 12.1 lbm/s to 15.1 lbm/s. Figure 19 shows within this range the head rise is sufficient for on design performance. Figure 20 and Figure 21 show at the design speed of 110,000 rpm, the efficiency maximizes and the power required minimizes at a flow rate of 12.1 lbm/s. Figure 22 predicts the appropriate combination for optimum performance at an off-design point. The combination of 44,000 rpm and specific speed, Ns of 835 produces the highest efficiency. This fact is not promising for the current design. Ideally, the on design point should yield the optimum combination and ensure the highest efficiency since the greatest amount of operational time will spent at this combination value. This suggests the impeller shall need further design optimization.

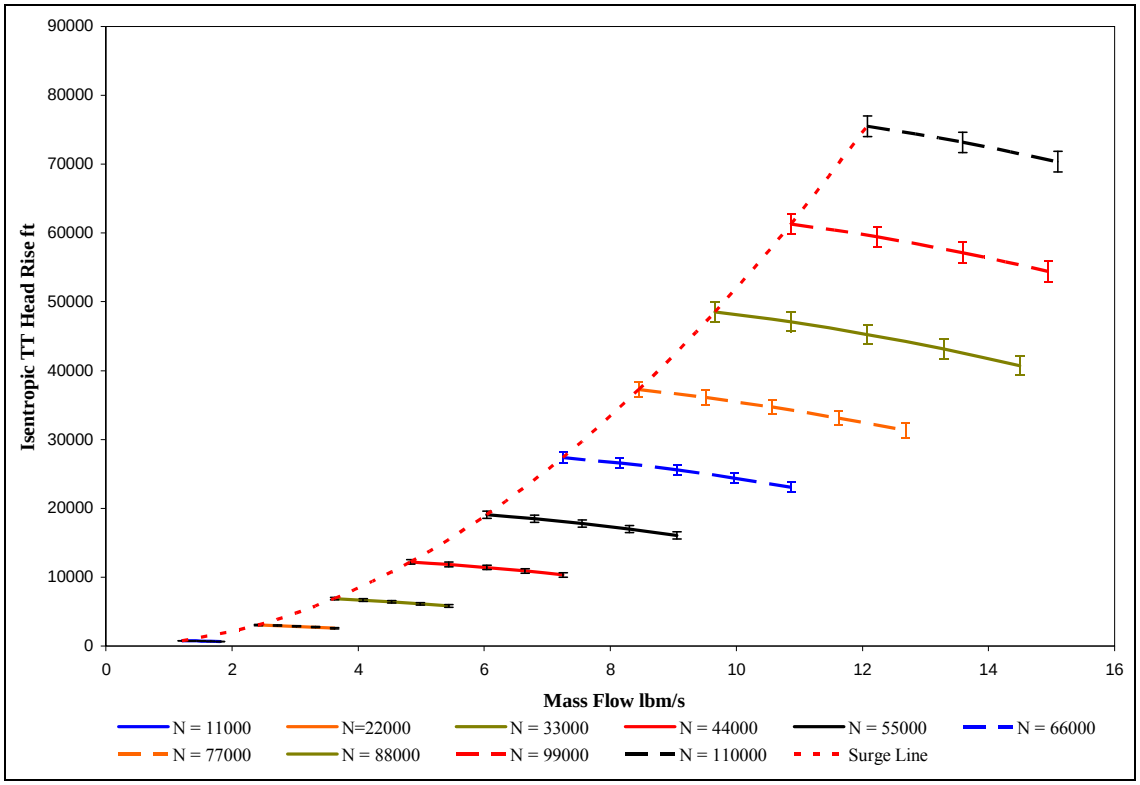

Figure 19 Stage 1 Head Rise Operating Range

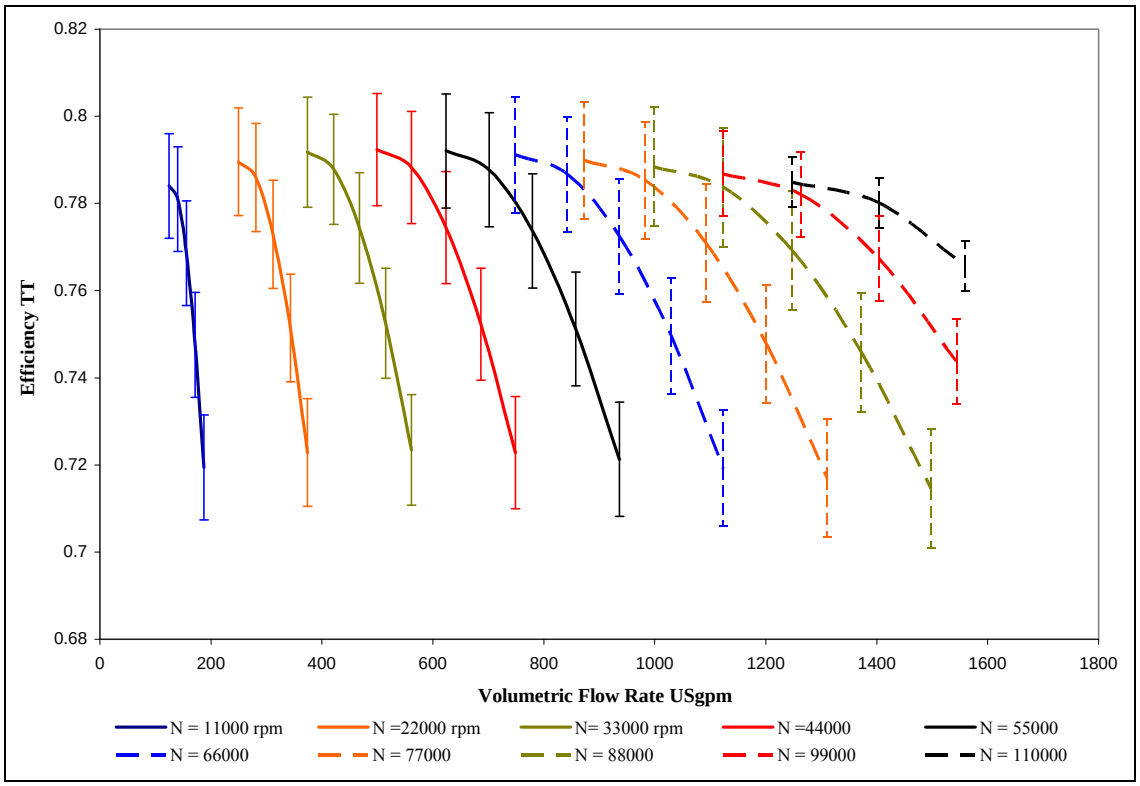

Figure 20 Stage 1 Volumetric Flow Rate (USgpm) vs. Stage Efficiency TT

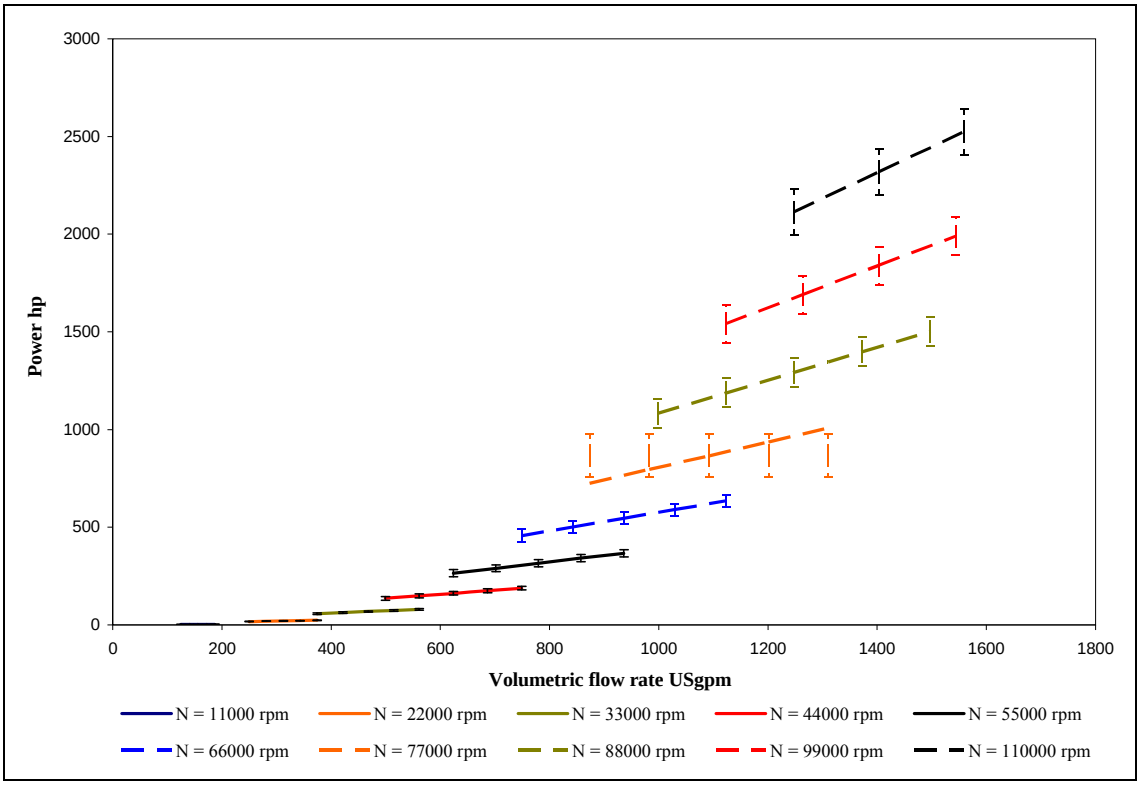

Figure 21 Stage 1 Volumetric Flow Rate (USgpm) vs. Stage Power (hp)

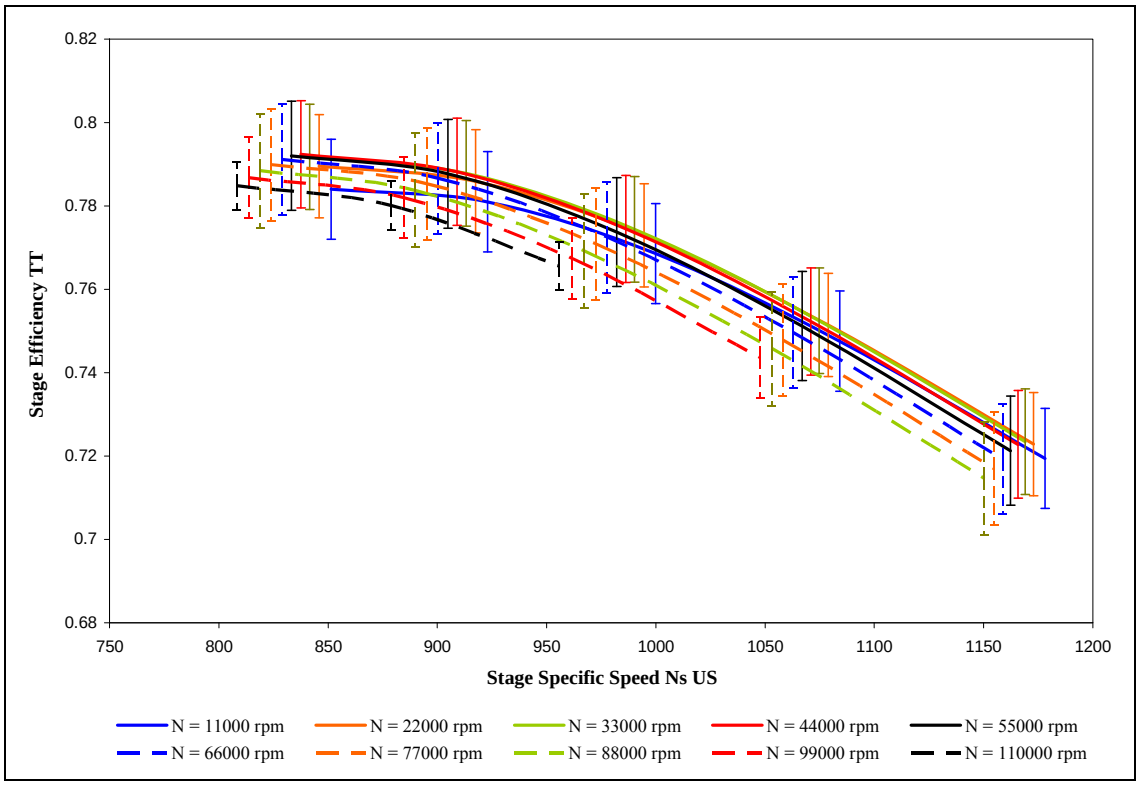

Figure 22 Stage 1 Ns vs. Stage Efficiency TT

5.4 Stage 2 Impeller Layout

Stage 2 of the fuel pump is designed as a centrifugal unshrouded impeller. An unshoruded impeller reduces manufacturing time and cost, however is not as efficient as a shrouded impeller. Stage 2 is design with a 35^{o} blade back sweep. Table 29 shows the predicted performance results. The results show that the on-design criteria set by NPSS were met.

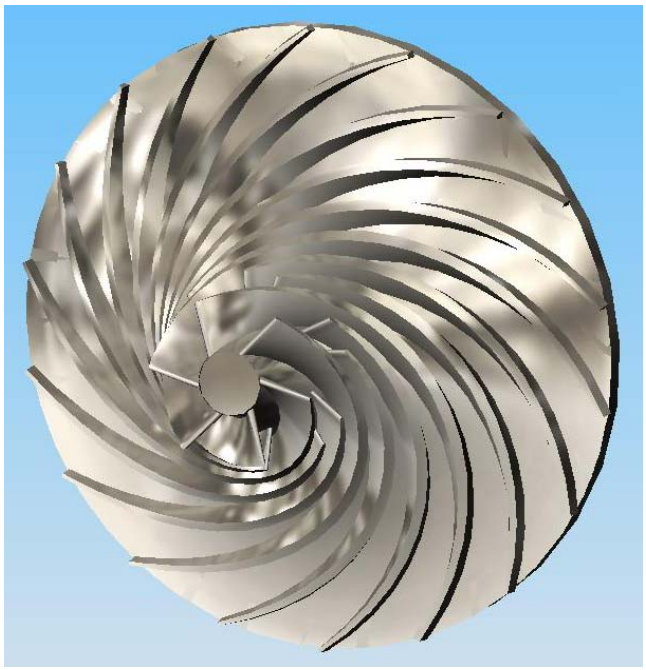

Figure 23 DEAN Stage 2 Impeller

Table 29 Stage 2 On-Design Performance Pumpal® Results

Symbol	Units	Criteria	Run1	Final
η_{tt}	-	≥ 0.80	0.78	0.80
H	ft	≥ 64021	61856	65840
P_{req}	hp	≥ 1046	1046	1079
P_{08}	psi	≥4050	3928	4050
$\dot{m}$	lbm/s	≤ 7.6	7.55	7.55
D_{2t}	inches	≤ 6.0	3.55	3.52

5.5 Stage 2 Off-Design Operating Range

In each graph the circle indicates the on-design condition. The off-design performance of stage 2 is best described with a plot of mass flow versus total head rise. Figure 24 shows the surge line as a red dashed line. The impeller should not operate to the left of the surge line. Within this region the stage performance would be severely degraded. At the on-design speed of 110,000 rpm the stage can operate at a mass flow of 6.0-7.55 lbm/s. Figure 24 shows the head rise is sufficient for this range of mass flow. Figure 24 - Figure 27 predict stage 2 can operate at a wide range of speed and mass flow. This fact is important for throttle operation. Figure 27 is a chart of the stage efficiency as a function of specific speed. The results show that the stage efficiency maximizes at an off-design point of 22,000 rpm and Ns =814.

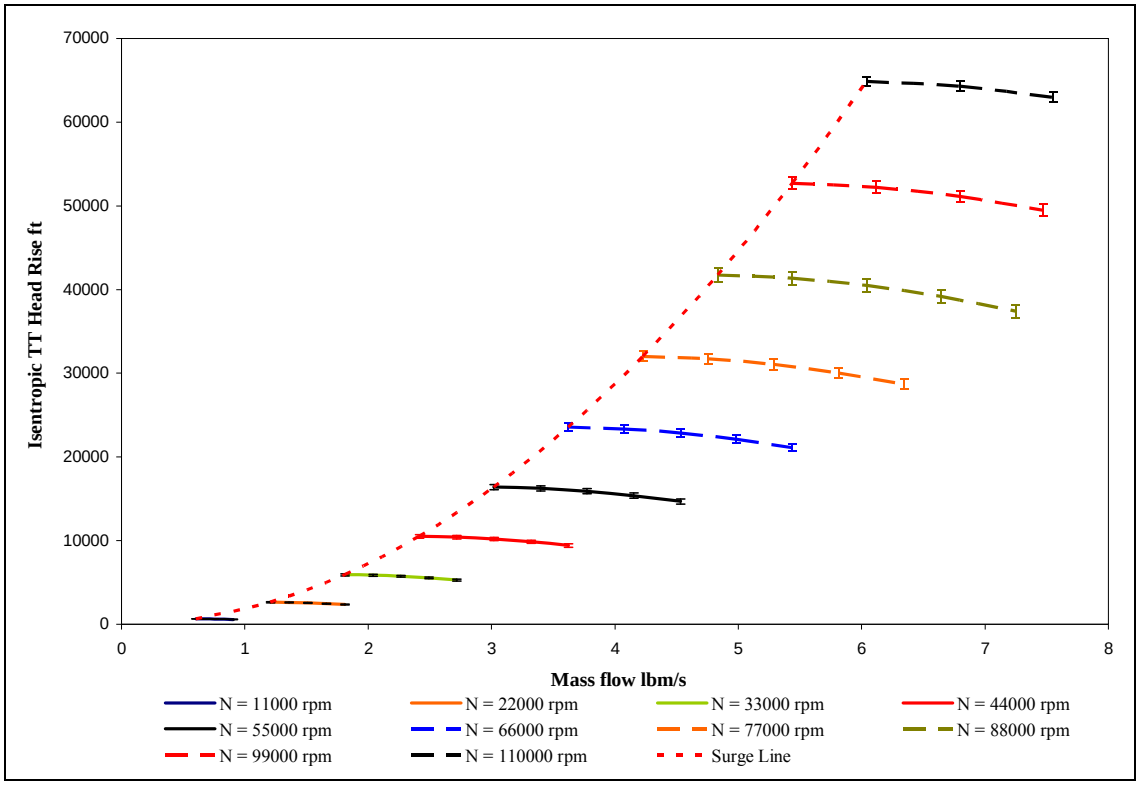

Figure 24 Stage 2 Head Rise Surge Line

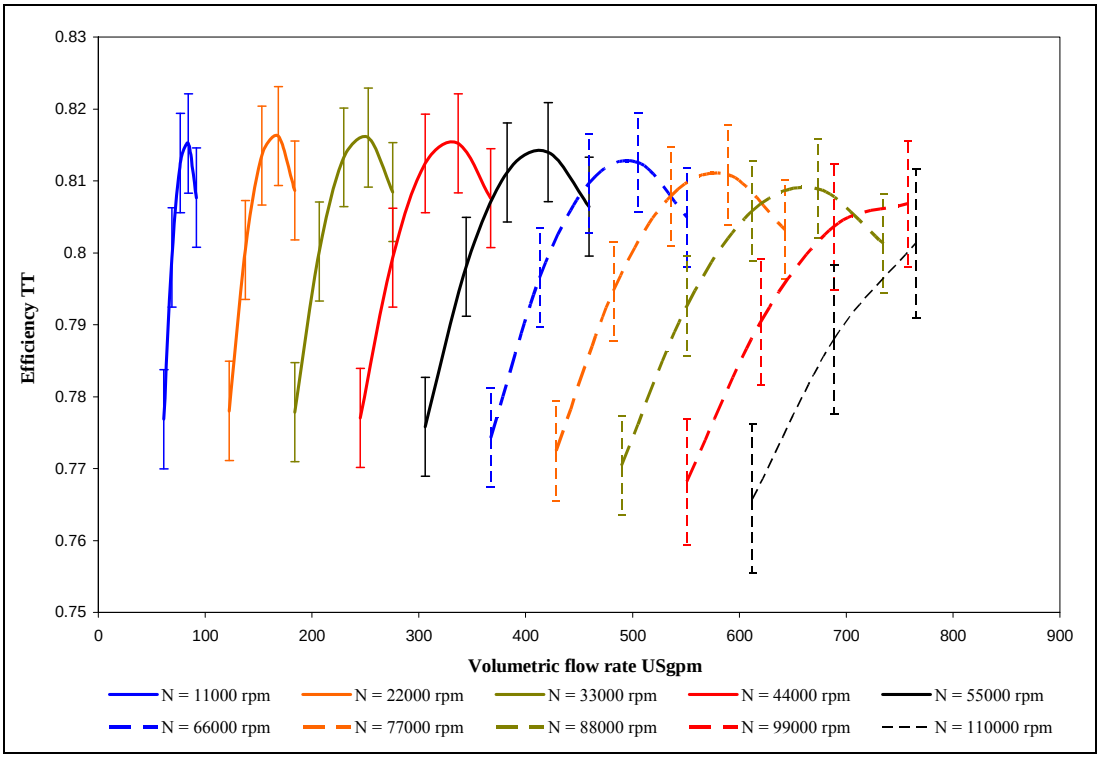

Figure 25 Volumetric Flow Rate (USgpm) vs. Stage Efficiency TT

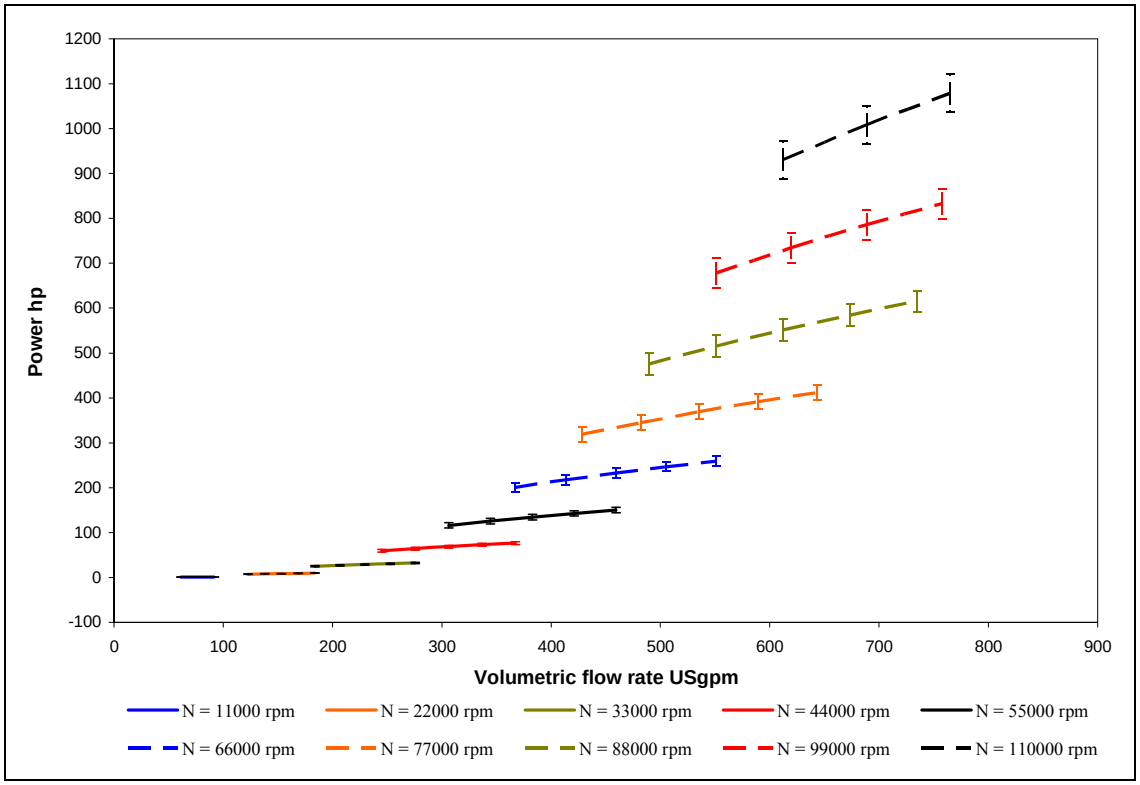

Figure 26 Stage 2 Volumetric Flow Rate (USgpm) vs. Stage Power (hp)

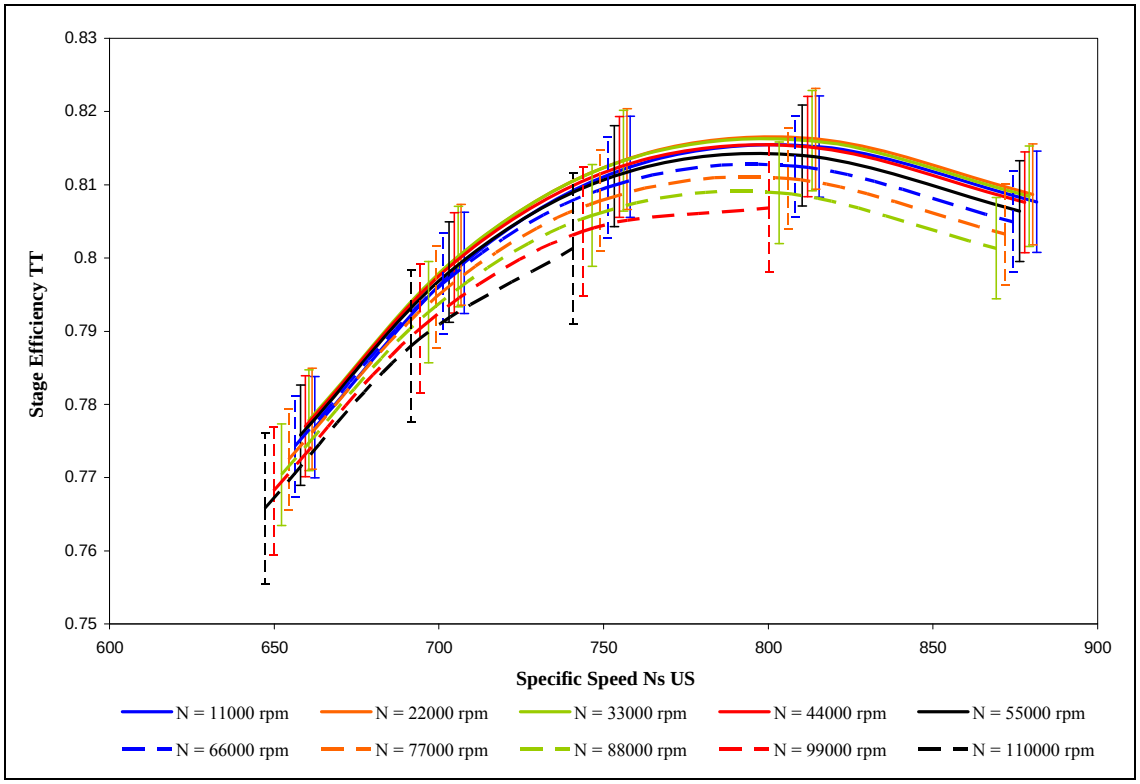

Figure 27 Stage 2 Ns vs. Stage Efficiency TT

5.5.1 Split Bypass

The interstage transfer feature was used to verify a benefit existed in splitting the flow between stages. Table 30 shows the horsepower required and efficiency for each mass flow fraction. The 50% flow fraction yielded the desired efficiency at the least power required.

Table 30 Stage 2 Horsepower Requirement at Various Mass Flow Fractions

T_1	p_{08}	N	H	Flow Fraction	P_{req}	η_{tt}
R	psi	rpm	ft	%	hp	
65.71	2025	110000	64026	0.25	556	0.758
65.71	2025	110000	64026	0.5	1053	0.80
65.71	2025	110000	64026	0.75	1533	0.824
65.71	2025	110000	64026	1.0	2044	0.824

5.6 Turbine Layout

Figure 28 shows a full admission, radial turbine with an unshrouded impeller. Figure 29 shows the turbine disk with short blade heights and lengths. This design characteristic is incorporated in the ALH turbine design. This design should allow for high loading during operation. Table 31 shows the turbine design meets all performance requirements for on-design performance set forth by the power balance.

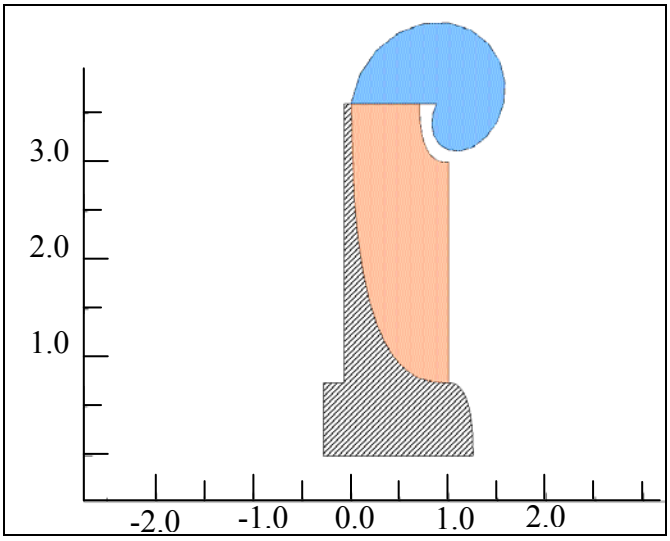

Figure 28 DEAN Turbine Cross-Sectional Layout

Table 31 Turbine On-Design Performance RITAL® Results

Symbol	Units	Criteria	Final
η_{tt}	-	≥ 0.90	97.7
P_{req}	hp	≥ 3606	3607
P_0	psi	≥2038	2035
$\dot{m}$	lbm/s	≤ 7.6	7.55
D_{2t}	inches	≤ 6	6.2

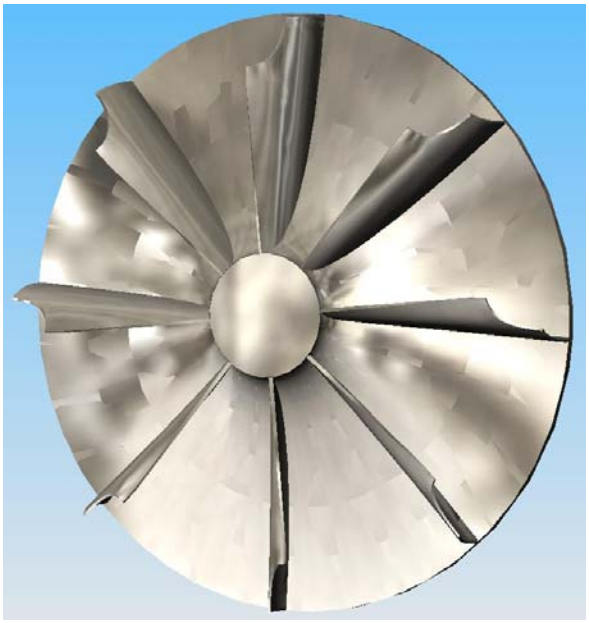

Figure 29 DEAN Radial Turbine

5.6.1 Sensitivity Analysis

To guide the design a sensitivity analysis was completed. Equation (1.111) shows the calculation used to determine the magnitude in change of the performance parameter, P, for a given change of the impeller variable, Q. Shown in Table 32 and Table 33 are the top five most influential parameters for stage efficiency and power output. The preliminary baseline is shown as the reference. The value shown in the far right column of each table is the sensitivity value. The most influential is ranked number 1.

$$\text{Sensitivity}=\Delta P \times \frac{Q}{\Delta Q} \tag{1.111}$$

Table 32 Turbine Impeller Total Stage Efficiency Sensitivity Analysis

Run	N	T_{inlet}	R_{1t}	R_{1h}	R_{2t}	$\Delta\eta_{tt}$
	rpm	R	in	in	in	
Baseline	110,000	388	3.535	3.535	3.0	0.925
1	111,100					-0.2
2		391.8				0.1
3			3.5			0.1
4				3.5		0.1
5					2.97	0.1

Table 33 Turbine Impeller Power Sensitivity Analysis

Run	T_{inlet}	Mass Flow	B_1	β_2	CLR_{axial}	ΔP
	R	lbm/s	in	deg	in	
Baseline	388	7.5	0.7	30.0	0.0039	-
1	391.8					2,563
2		7.65				2,419
3			0.707			94
4				30.3		90
5					0.00394	70

5.7 Turbine Off-Design Operating Range

The circle designates the on design point. Figure 30 and Figure 31 show the predicted turbine stage efficiency during off-design operation. The range of operation shown is 20% up to 110% of the design speed. Figure 32 shows the expansion pressure ratio versus corrected mass flow. The map the predicted on-design point will not operate at choked flow, thus the turbine does not reach Mach 1.0. The lack of a knee followed by a horizontal trend at high-pressure ratios supports this conclusion. This meaning of this result is shock loss should not occur and add a detrimental effect on performance. Figure 33 shows the predicted results show that at the on-design condition the turbine should operate at its most efficient for a given power output. This is a favorable trait because the engine should operate at the on-design value for the majority of the mission. Figure 34 shows the predicted volumetric flow rate and power output for a given speed. The on-design power level meets the predicted power output calculated using NPSS. Figure 35 shows the turbine reaction values at a given speed and mass flow. The degree of reaction is a significant figure of merit in that it defines the expansion process through the rotor stator. The predicted reaction value indicates the enthalpy and pressure drop across the impeller. At the on-design condition the reaction is approximately 0.43. This indicates the flow accelerates while passing through the impeller.

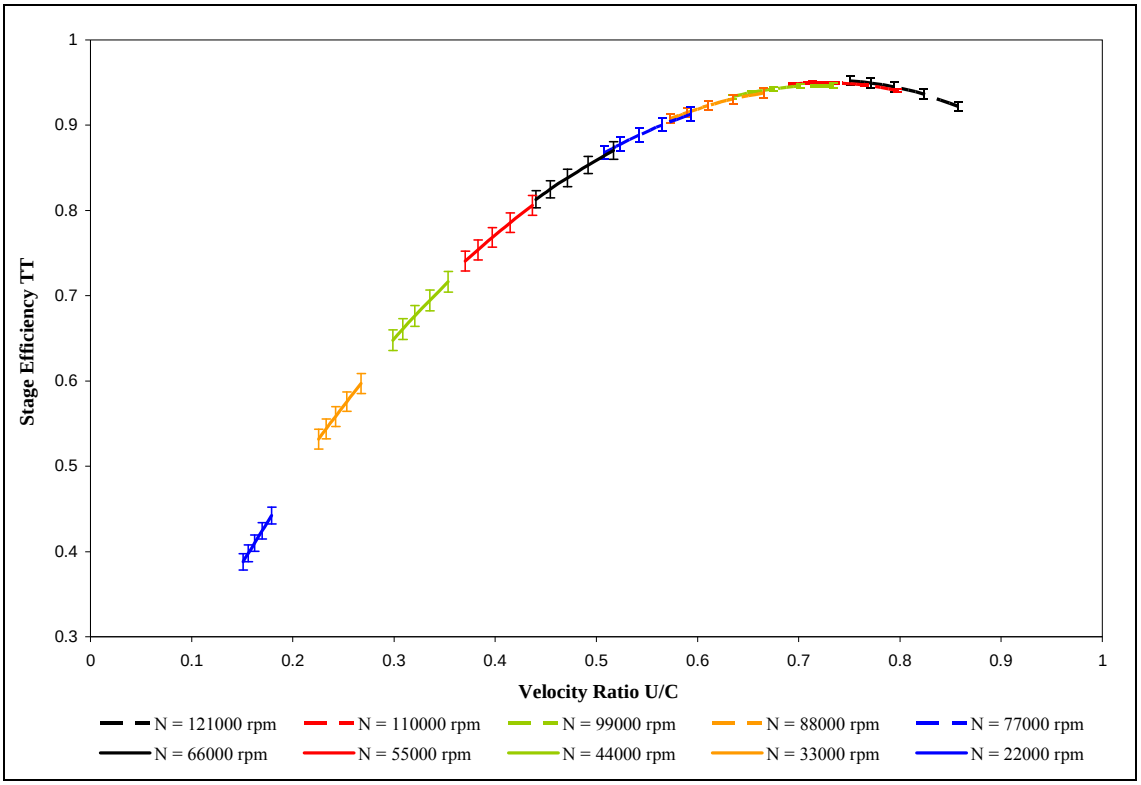

Figure 30 Stage Velocity Ratio U/C vs. Stage Efficiency TT

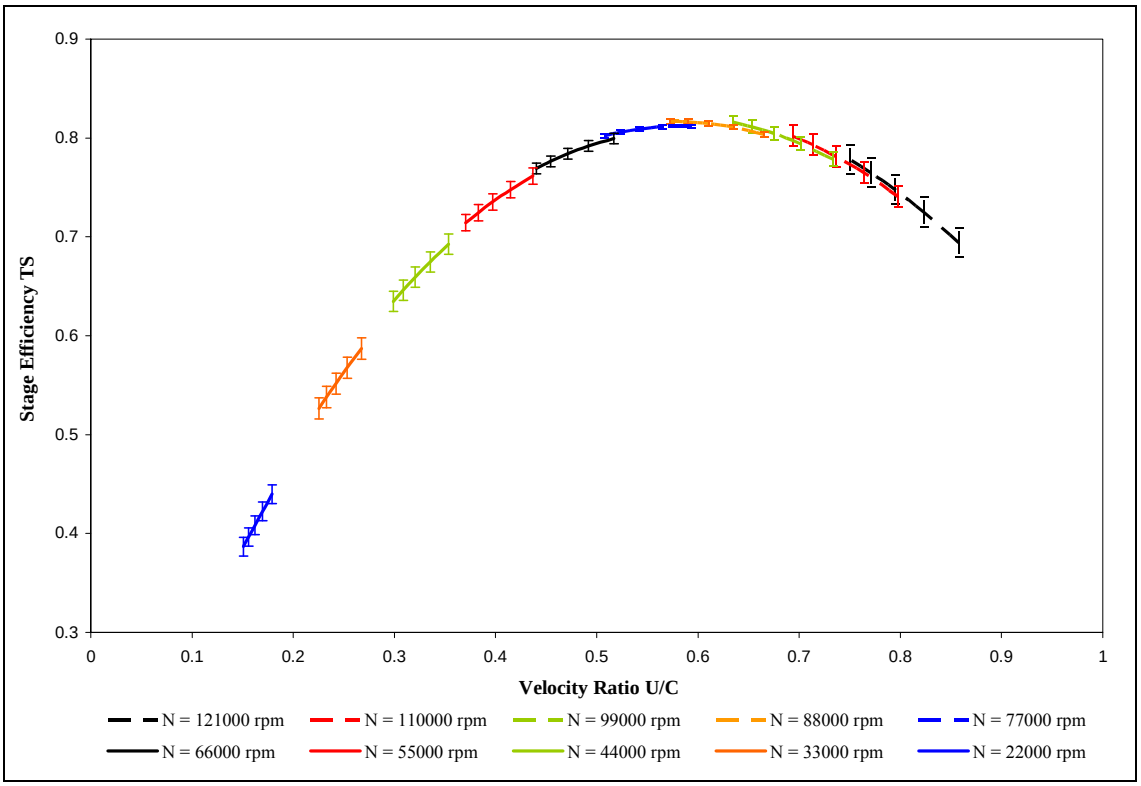

Figure 31 Stage Velocity Ratio U/C vs. Stage Efficiency TS

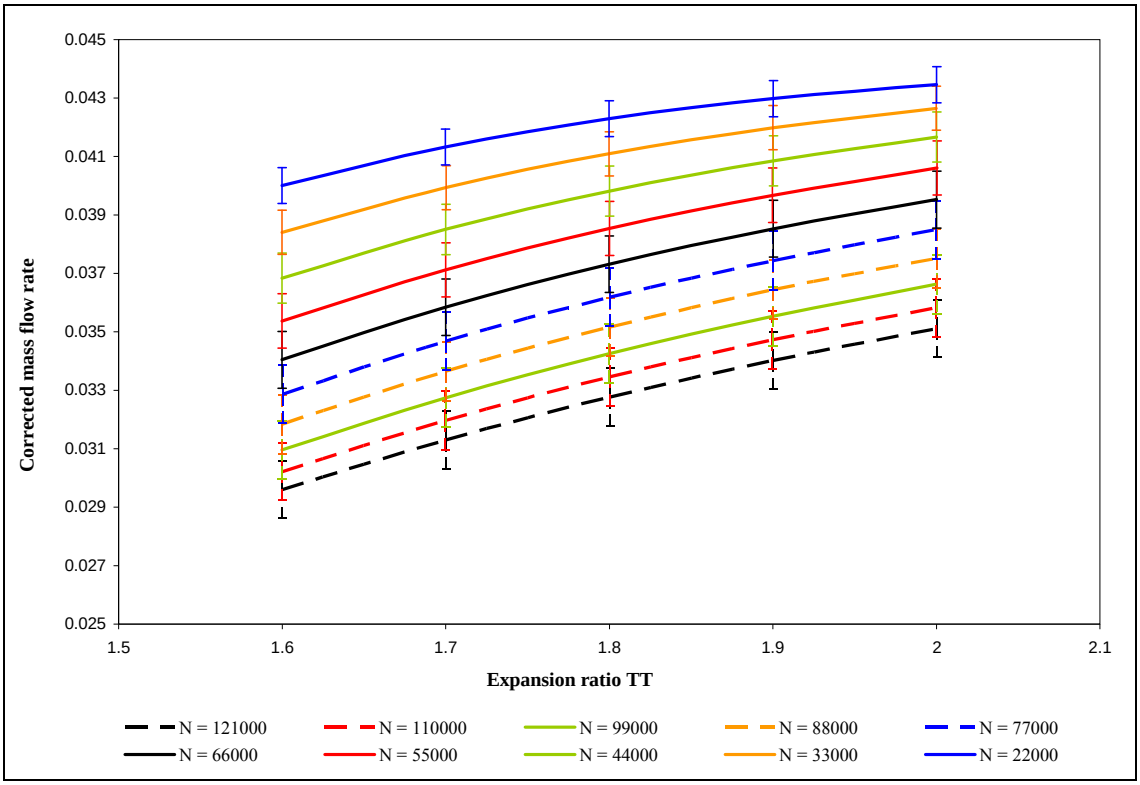

Figure 32 vs. Expansion Ratio TT vs. Corrected Mass Flow Rate

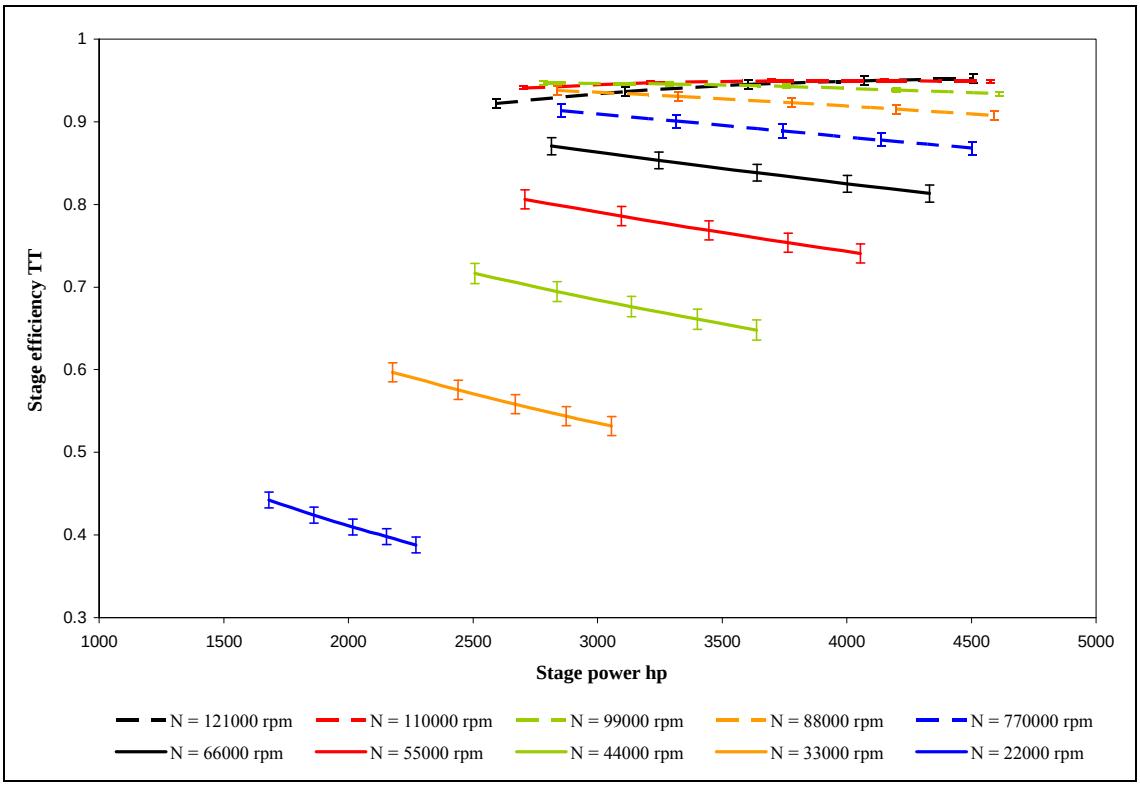

Figure 33 Turbine Power Output vs. Stage Efficiency TT

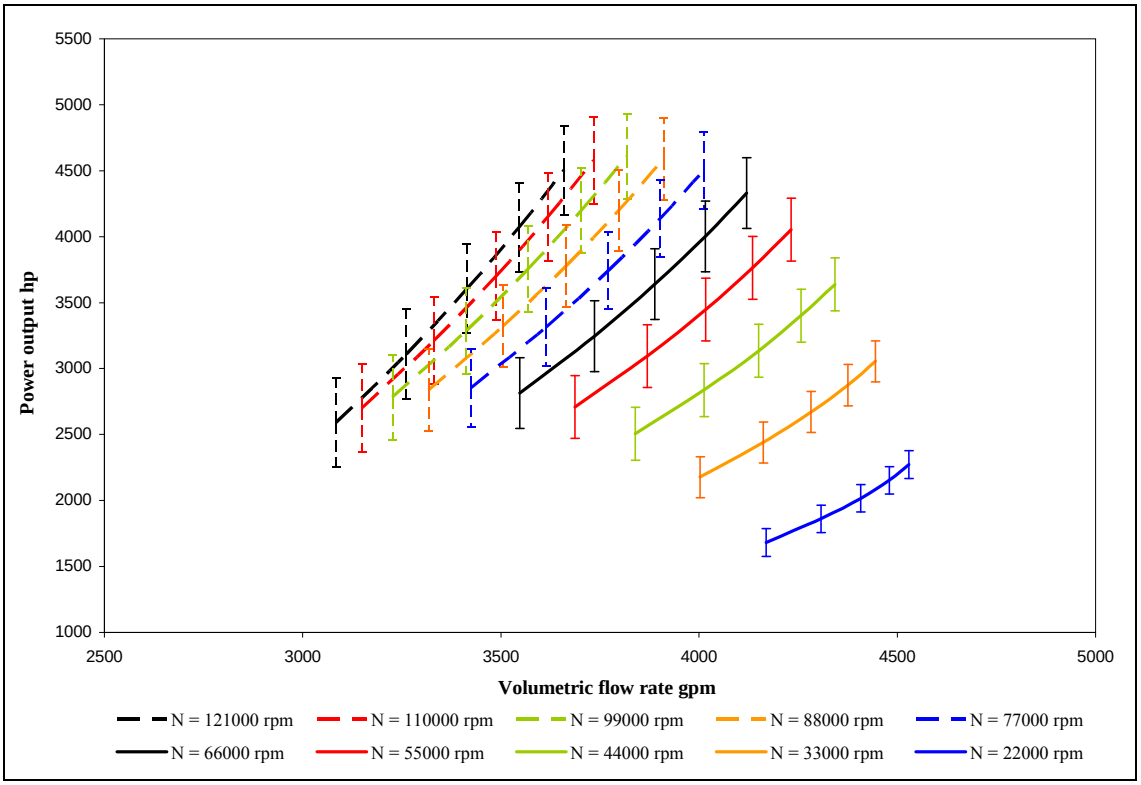

Figure 34 Volumetric Flow Rate (gpm) vs. Stage Power (hp)

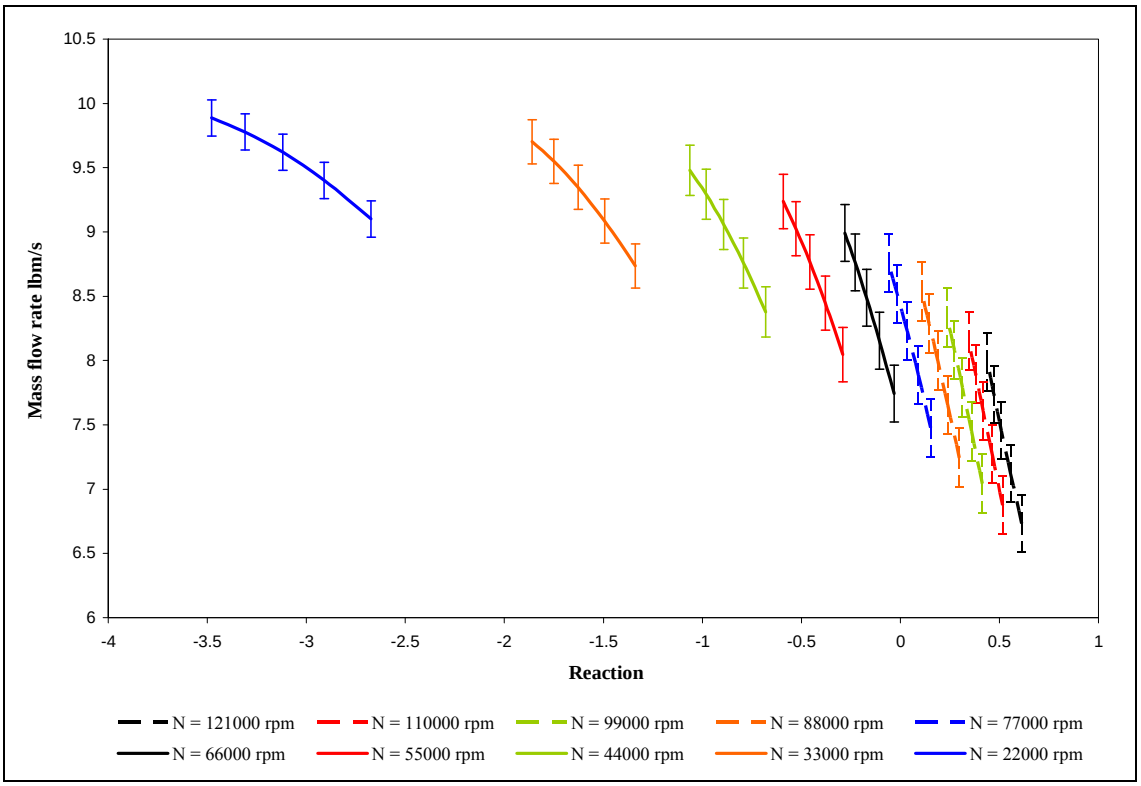

Figure 35 Turbine Reaction vs. Mass Flow Rate lbm/s

5.8 Bearing and Shaft

The trade study resulted in the selection of a ceramic Hybrid/Ball bearing system. This bearing type will take advantage of the axial loading capabilities of a ball bearing while providing the increased life of a hydrostatic bearing during steady state operation. A preliminary decision has been made to place the bearings in board, with a minimum number of two bearings. Figure 36 shows a conceptual bearing configuration. This layout is consistent with the trade-study presented in the previous section. Table 34 DEAN Theoretical Shaft and Bearing Size presents the results of the preliminary calculations for the shaft size and bearing DN value. Table 35 shows the axial thrust force for each pump stage using Pumpal®. The resultant axial load is calculated to be 127.8 lb_f towards the turbine. The turbine axial force was calculated assuming a pure axial force. The multiplication of the exit pressure and frontal area provided the preliminary turbine axial thrust force.

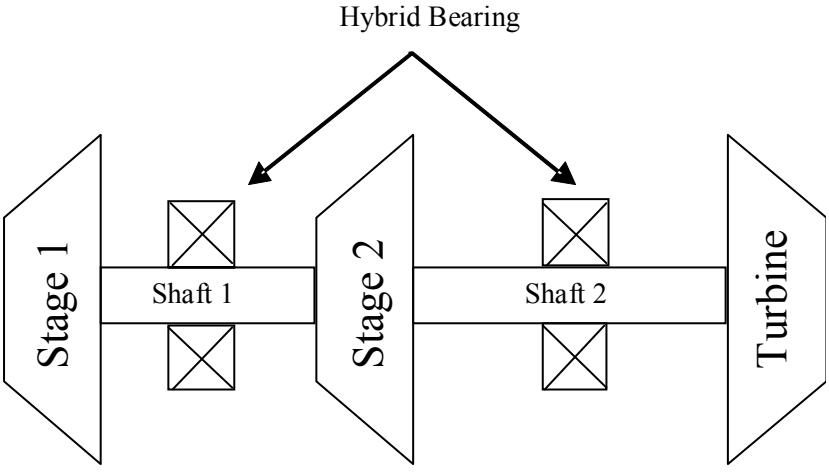

Figure 36 DEAN Conceptual Bearing Layout

Table 34 DEAN Theoretical Shaft and Bearing Size

Shaft #	D (in)	L (in)	P_{req} (in*lb/s)	T (lb*in)	σ_{yield} (psi)	$\tau_{allowable}$ (psi)	DN
1	0.21	0.32	16678200	1448	125000	104167	5.8E+05
2	0.23	0.39	23806200	2067	125000	104167	6.5E+05

Table 35 Axial Load Results

Axial Thrusts	Units	Stage 1	Stage 2	Turbine
Front	lb_f	5413.4	22186.4	
Rear	lb_f	-5486.5	-23906.6	
Inlet Momentum	lb_f	55.3	40.7	
Inlet Pressure	lb_f	74.0	1529.7	
Exit Momentum	lb_f	0	0	
Exit Pressure	lb_f	0	0	
Shaft Front	lb_f	7.6	213.8	
Total	lb_f	+63.8	+64.0	-61438

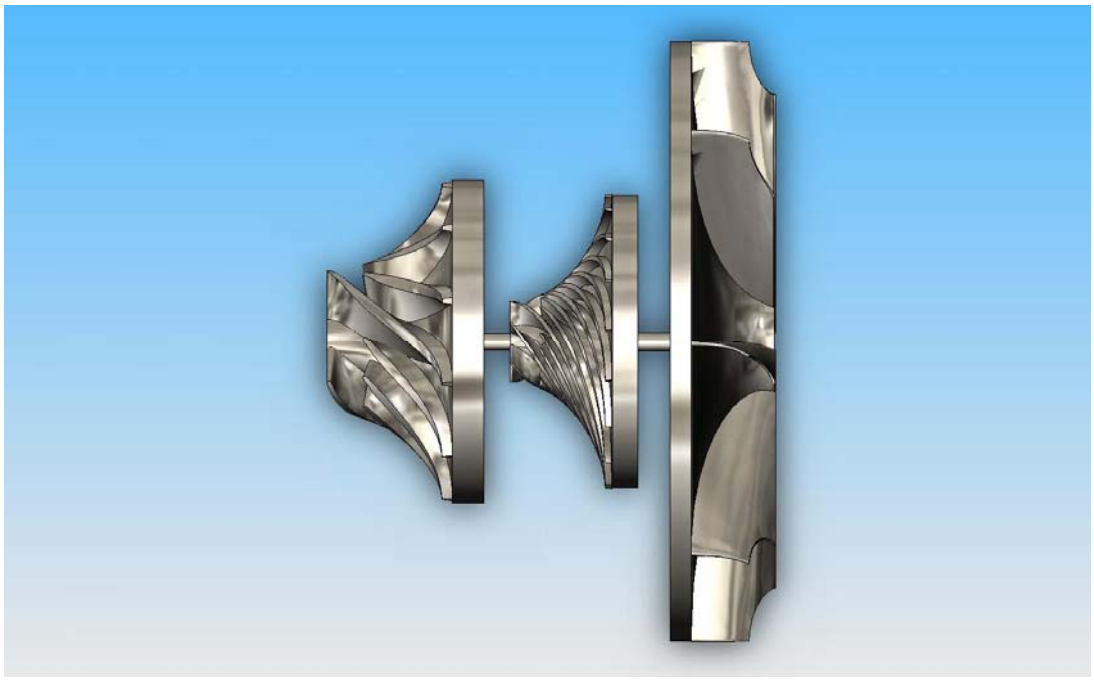

Figure 37 DEAN Liquid Hydrogen Turbopump Rotor Assembly Solid Model

6. Conclusions and Recommendations

6.1 Conclusions

The primary goal of the research was to provide a conceptual design of a turbopump satisfying the operating conditions of the DEAN upper stage engine. The primary performance parameter requirements are, exit pressure, pump head rise, stage efficiency and power required. The conceptual pump and turbine design presented fulfills the primary requirements.

Second, the split flow design does reduce the power required for the second stage. The results are shown in Table 30. The full flow horsepower requirement is 52% more than split flow design. A lower turbine power requirement is desirable because this would effectively reduce the operating stress level and increase the rotor life. Furthermore, a lower horsepower requirement effectively reduces the turbine impeller size. A smaller impeller is desirable to satisfy the geometric footprint requirement

Third, the off design operation was clarified in the pump and turbine maps. Both pump stages are predicted to operate satisfactorily at speeds levels of 20-100% the design speed. The performance prediction show the turbine can operate at 20-110 % the design speed. The concpetual design show the potential to provide a wide throttle range.

Fourth, the Pumpal® and RITAL® software steps outlined in the Methodolgy section are shown in Appendix A and B. The design was completed using empirical data when applicable. As the designer it is advisable to know the established ranges for each impeller variable. For example, the useful range of the blade exit angle is small 50^{o}-60^{o} and non-convergence occurs frequently when outside of this range. The solution time

was reduced because the preliminary design was outlined in sufficient detail. A sensitivity analysis aided the thought process for incremental change of input variables. This step should be accomplished first to ensure a good engineering approach to incremental design changes.

6.2 Recommendations

1. The conceptual design of the pump impellers and turbine should be progressed through a complete design process as outlined in Figure 13 Concepts NREC Turbomachinery Design Process.
2. Complete an inducer design to ensure the NPSHR for stage 1 is satisfied.
3. A stress analysis on each component should be completed to ensure the material integrity throughout the range of operation and cycle life.
4. A water flow test of the conceptual impeller design can be accomplished and test results compared using the Pumpal® design tool Data Reduction.

This Page Intentionally Left Blank

Appendix A. Pumpal® Wizard Steps

.

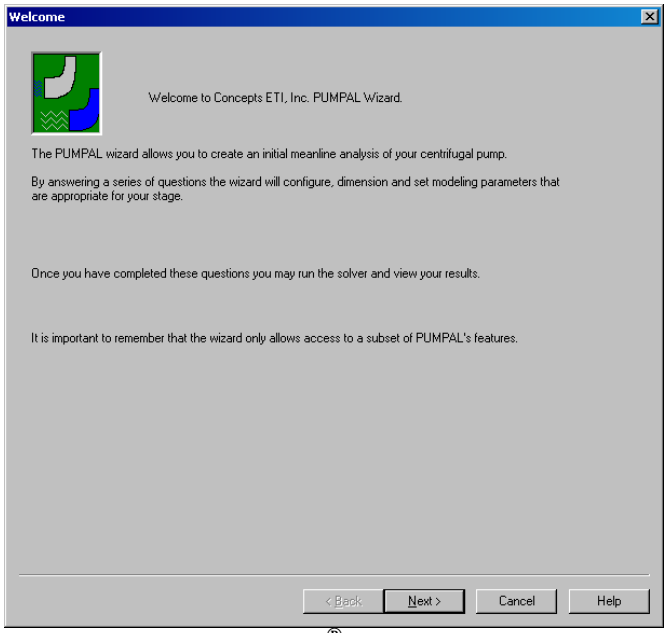

Figure 38 Pumpal® Wizard Step One

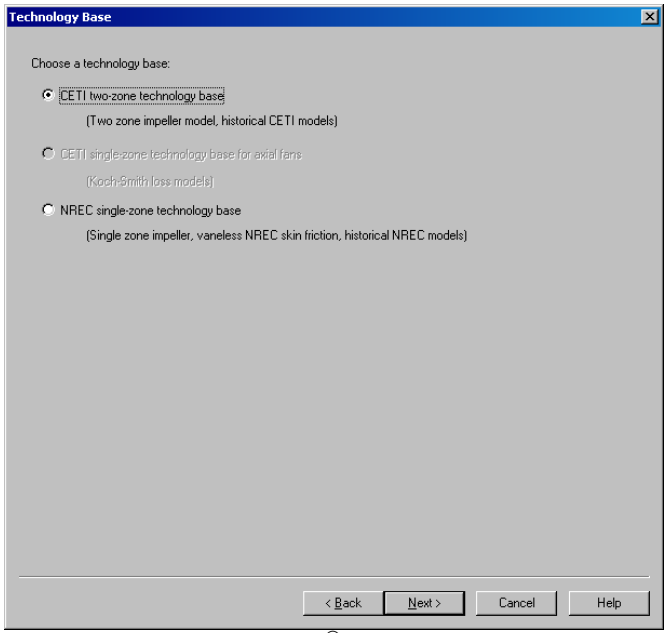

Figure 39 Pumpal® Wizard Step Two

Figure 38 shows the first step the user will take to initiate a new pump design in Pumpal

Figure 39 shows the second step where the user is required to select the technology base. The DEAN TPH used the CETI Two-Zone.

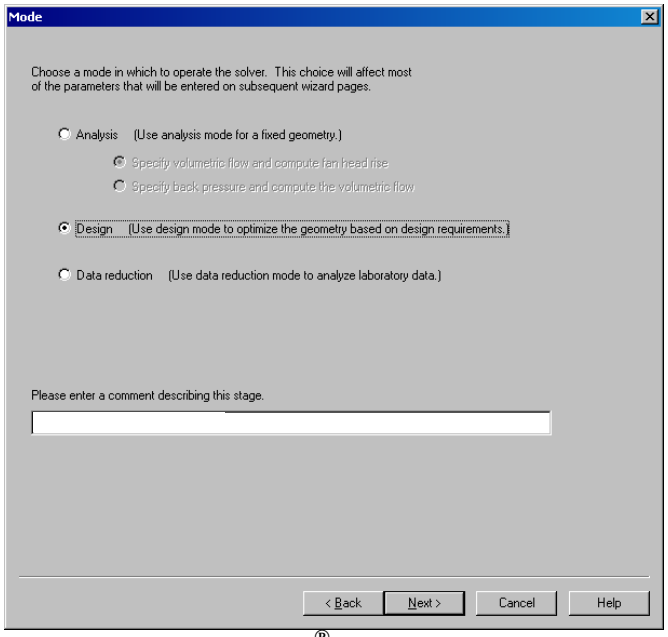

Figure 40 Pumpal® Wizard Step Three

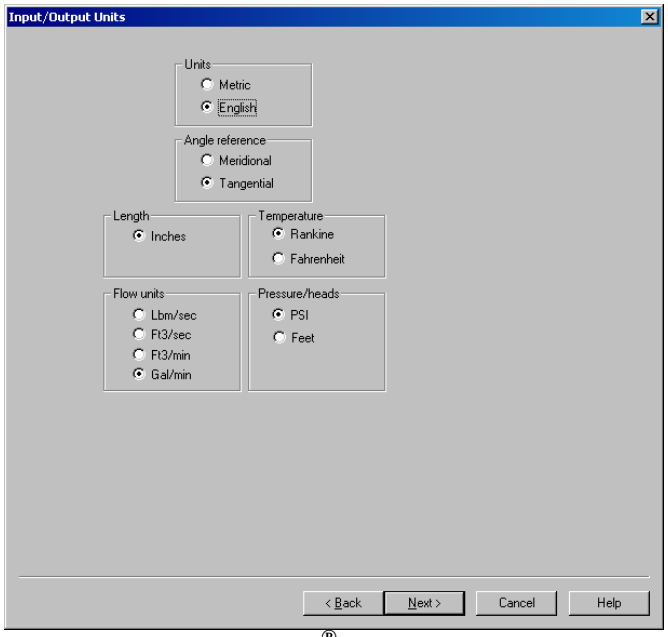

Figure 41 Pumpal® Wizard Step Four

Figure 40 shows the third step where the user must select the design mode. Pumpal® can operate in three different solver modes, Design, Analysis and Data Reduction. The Design mode calculates the impeller dimensions and blade settings from the user specified operating conditions. In Analysis mode, the impeller geometry is frozen and the performance can be run across the various speed lines. If test data is available for an existing impeller, this may be incorporated in the Data Reduction mode.

Figure 41 shows step four. Here the user makes various selections for the input/output unit type. The DEAN TPH design used English units and tangential angle references. The length and temperature are set to, inches and Rankine. The flow rate and pressure/heads were set to, gallon per minute (gpm) and pounds per square inch (psi).

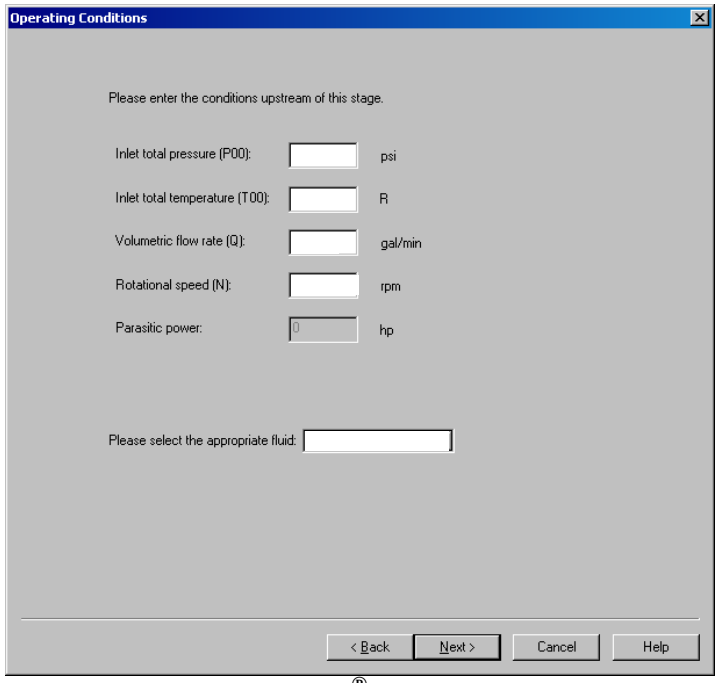

Figure 42 Pumpal® Wizard Step Five

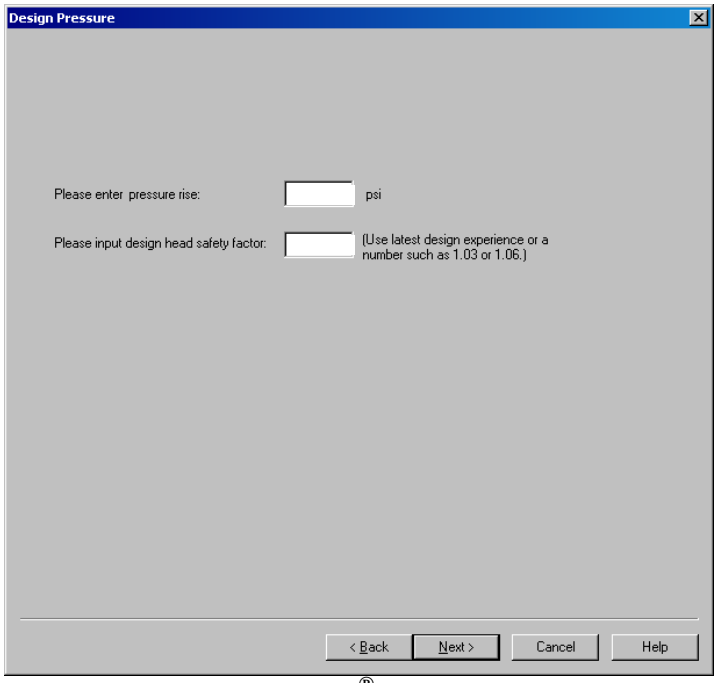

Figure 43 Pumpal® Wizard Step Six

Figure 42 shows step five here the inlet conditions are set. Table 36 shows the DEAN upstream conditions.

Table 36 DEAN TPH Upstream Conditions

Parameter	Units	Value
T_{01}	R	40.0
P_{01}	psi	45.0
Q	gpm	1579
N	rpm	110,000

Figure 43 shows step six. The user is required to input total head rise and safety factor. The heard rise values is taken from the power balance and the safety factor is set according to design criteria. For the DEAN TPH the safety factor is set to unity.

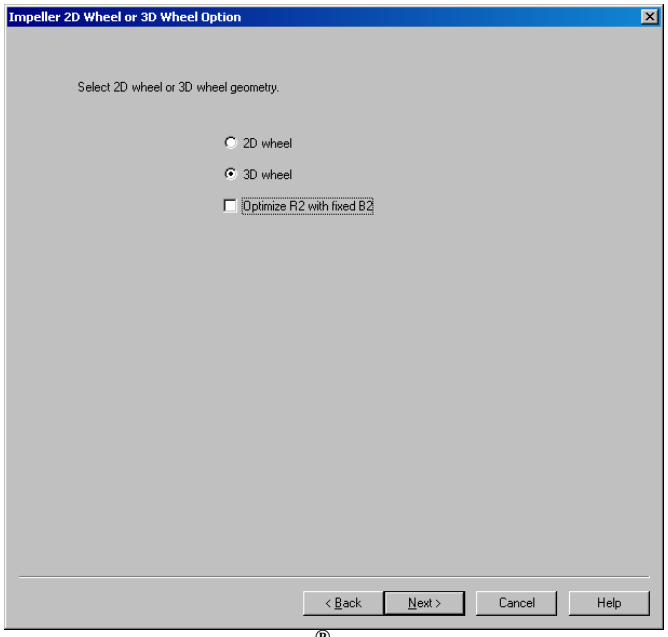

Figure 44 Pumpal® Wizard Step Seven

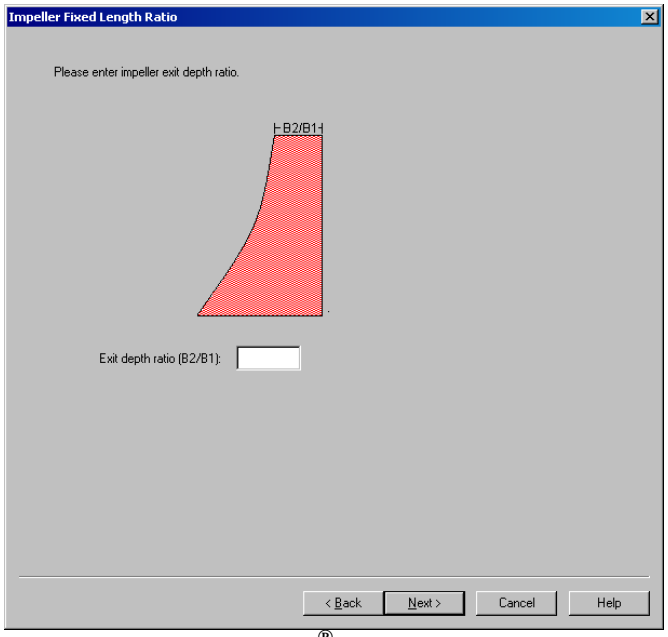

Figure 45 Pumpal® Wizard Step Eight

Figure 44 shows step seven where the impeller wheel option is set. The 2D wheel option will set the PHI1 to zero and the 3D wheel will allow the user to set the PHI1 value. A PHI1 value of zero indicates an axial inlet flow. For a 2D wheel the inlet tip radius, R1T, and the inlet hub radius, R1H, are set equal to one another. This sets the impeller inclination angle PHI1 to zero. For a 3D wheel, R1T is greater than R1H, thus PHI1 angle is greater than zero. The 3D wheel option was selected. The blade inclination angle (PHI1) and the inclination angle at impeller exit (PHI2) are set to 0 and 90 degrees to simulate an axial and radial element leading edge.

Figure 45 shows the eighth step where the user is asked to provided an impeller exit depth ratio.

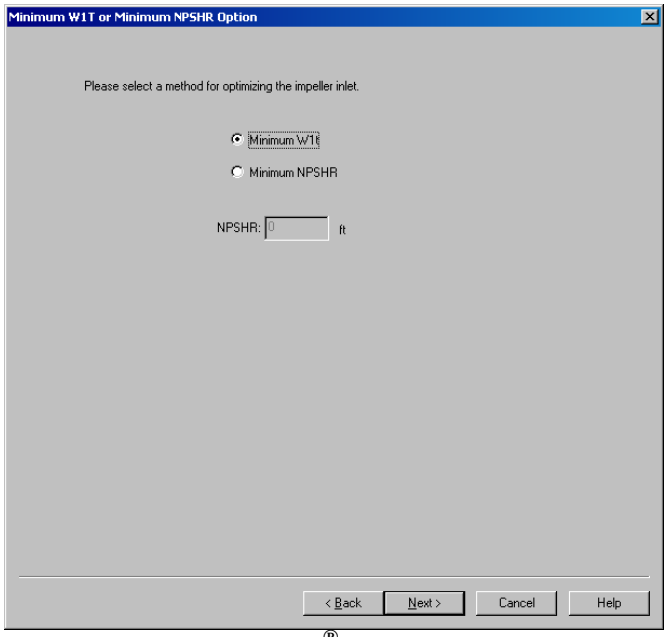

Figure 46 Pumpal® Wizard Step Nine

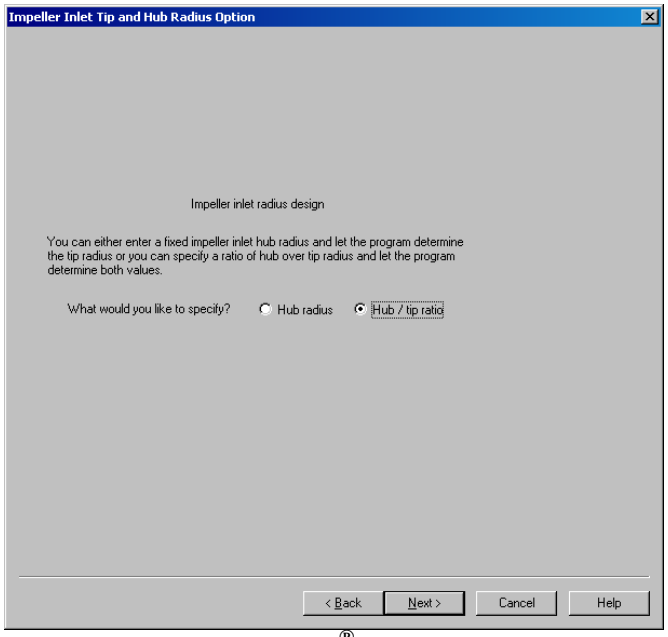

Figure 47 Pumpal® Wizard Step 10

Figure 46 show the ninth step. Here the user selects the method for optimizing the impeller inlet. The minimum W1t method will result in a more efficient design in comparison to minimum NPSHR. The minimum W1t was selected for the DEAN TPH.

Figure 47 shows step ten where the user is asked for the impeller sizing option. The user can specify the inlet radius or have the program calculate the tip radius using the specified hub/tip ratio.

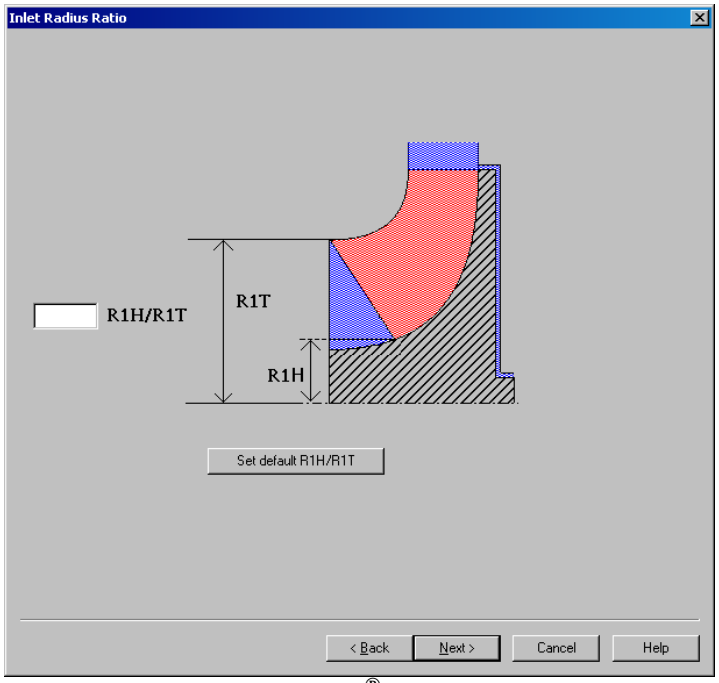

Figure 48 Pumpal® Wizard Step 11

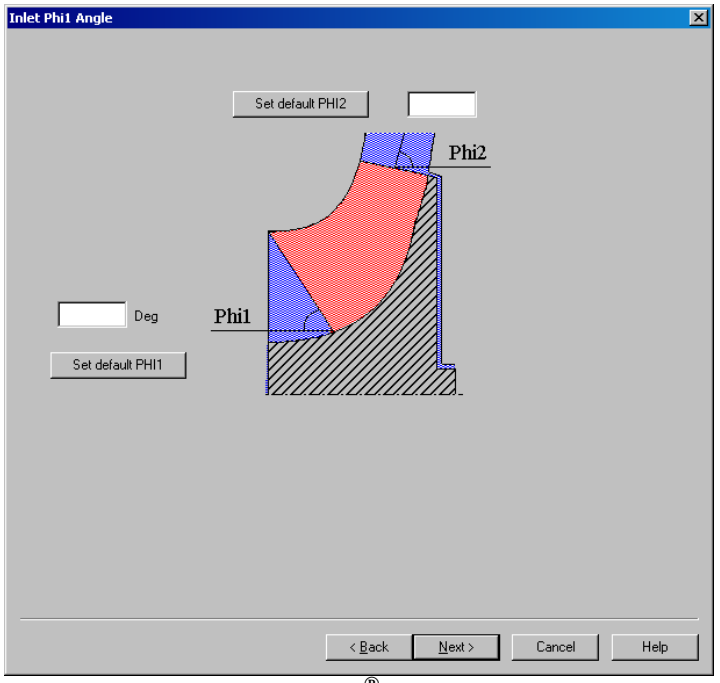

Figure 49 Pumpal® Wizard Step 12

Figure 48 shows the 11th step where the user inputs the hub/tip value. A typical hub/tip ratio is 0.3.[23]

Figure 49 shows the 12th step where the user sets the inlet and exit inclination angle. For axial flow PHI1 should be set to zero. The typical exit inclination angle is 90°, this is the DEAN TPH value.

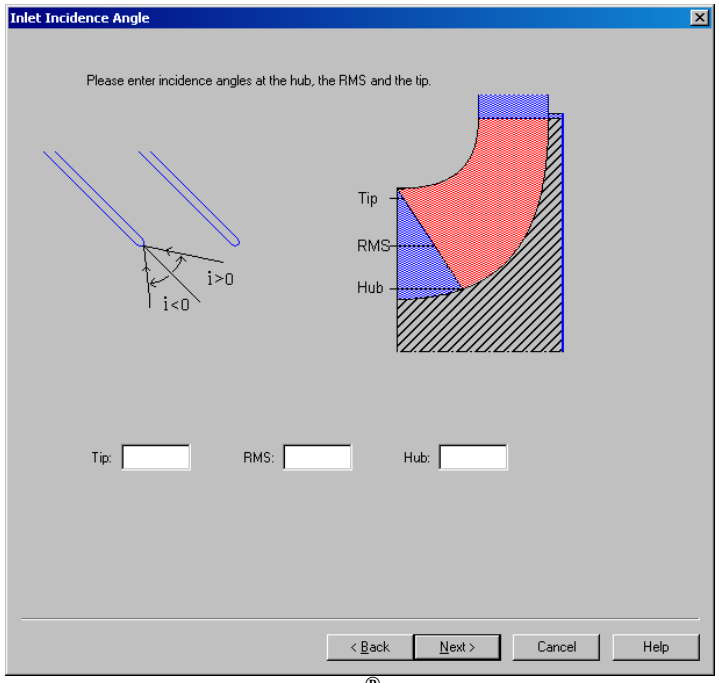

Figure 50 Pumpal® Wizard Step 13

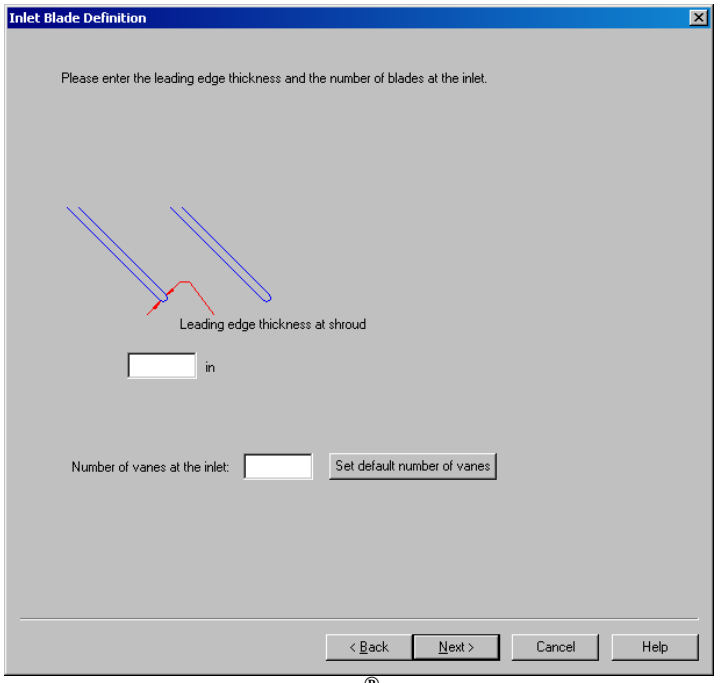

Figure 51 Pumpal® Wizard Step 14

Figure 50 shows the 13th step here the inlet incidence angle is set. The ideal incidence angle is 0^o this value is used for the DEAN TPH design. This is common practice for stages requiring a very wide operating range.[27]

Figure 51 is the 14th step here the leading edge blade thickness is specified along with the number of inlet blades. For stage 1 the blade backsweep angle is set to 65.0^o. The number of inlet blades was set to three with an inlet blade thickness of 0.1 inches. For stage 2

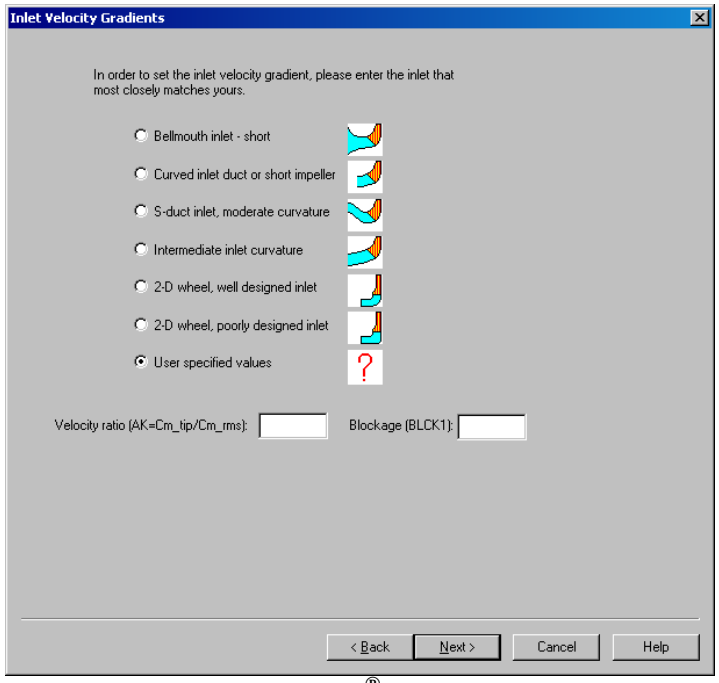

Figure 52 Pumpal® Wizard Step 15

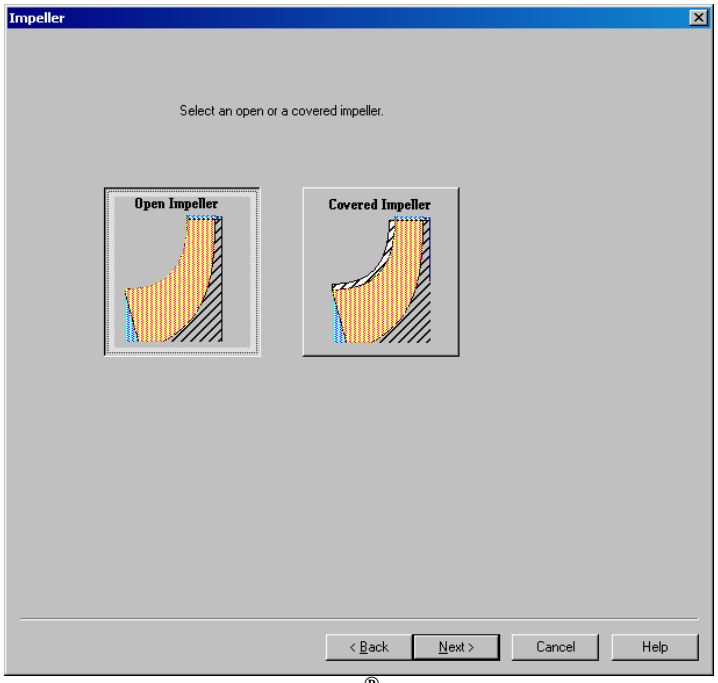

Figure 53 Pumpal® Wizard Step 16

Figure 52 shows the 15th step where the user sets the velocity gradient profile by specificying the inlet the most closely matches the design. The DEAN TPH is designed as the curved inlet duct or short impeller.

Figure 54 shows the 16th step here the impeller is specified as open or covered. The DEAN TPH is designed with open impellers.

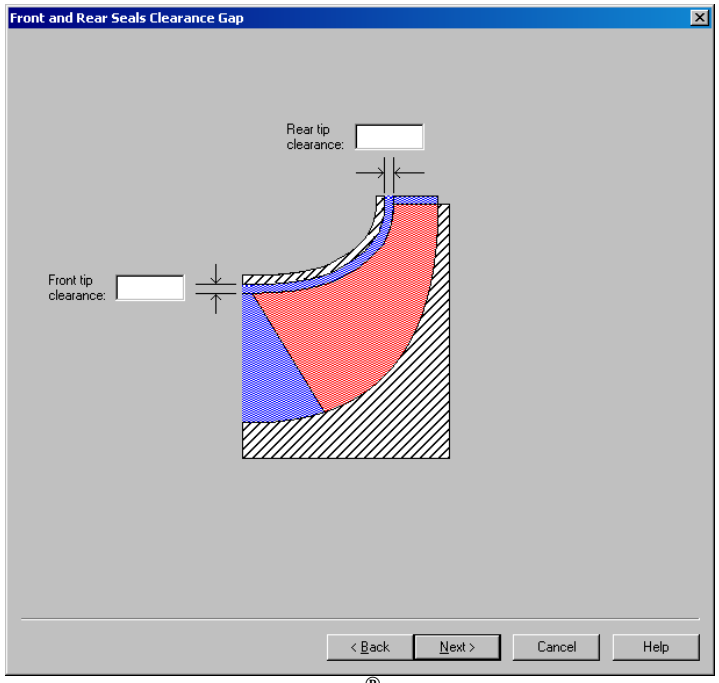

Figure 54 Pumpal® Wizard Step 17

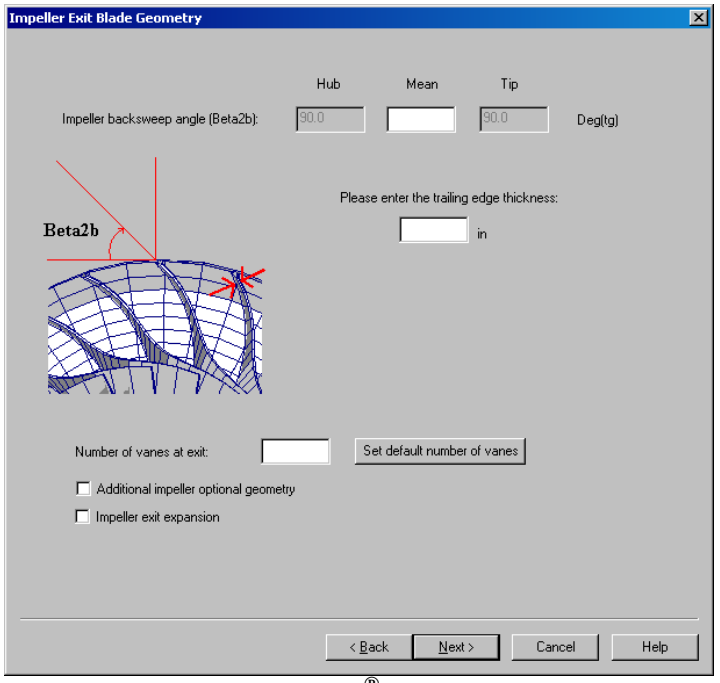

Figure 55 Pumpal® Wizard Step 18

Figure 54 is the 17th step here the front and rear clearance values are set. The type of manufacturing will dictate the clearance levels. The DEAN TPH runs with 0.0039 inch clearance for the all impellers.

Figure 55 shows step 18 where the impeller blade backsweep is set. The useful range is 50-60°. The trailing edge thickness and the number of exit blades are required. For stage 2 the trailing edge thickness is set to 0.1 inches with 15 exit blades.

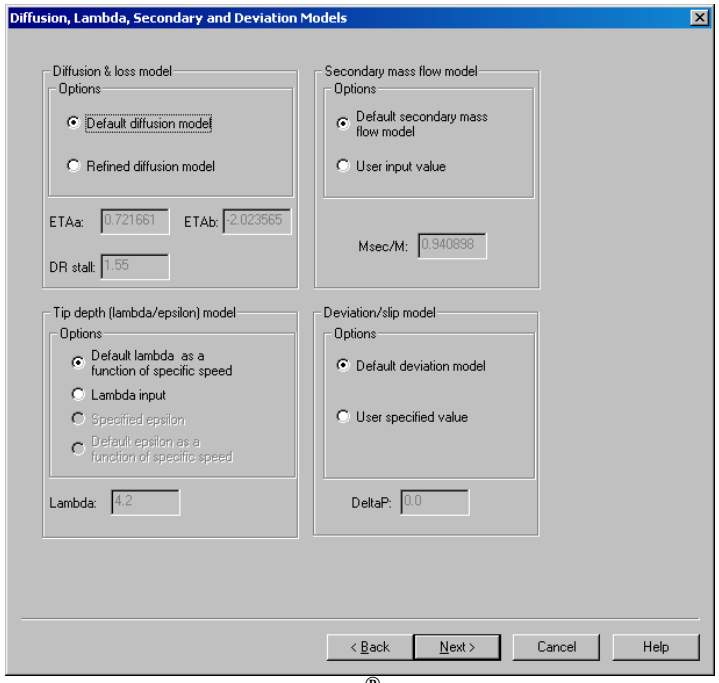

Figure 56 Pumpal® Wizard Step 19

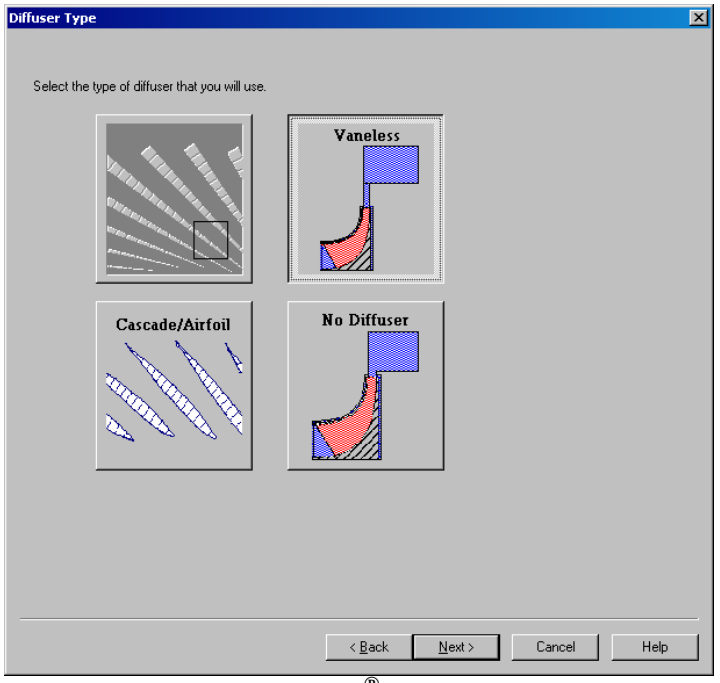

Figure 57 Pumpal® Wizard Step 20

Figure 56 shows step 19 where the user defines the diffusion, lambda and deviation models. The defaults models where used for the DEAN TPH.

Figure 57 shows step 20 where the user specifies the diffuser type. The DEAN TPH is designed with a vaneless diffuser.

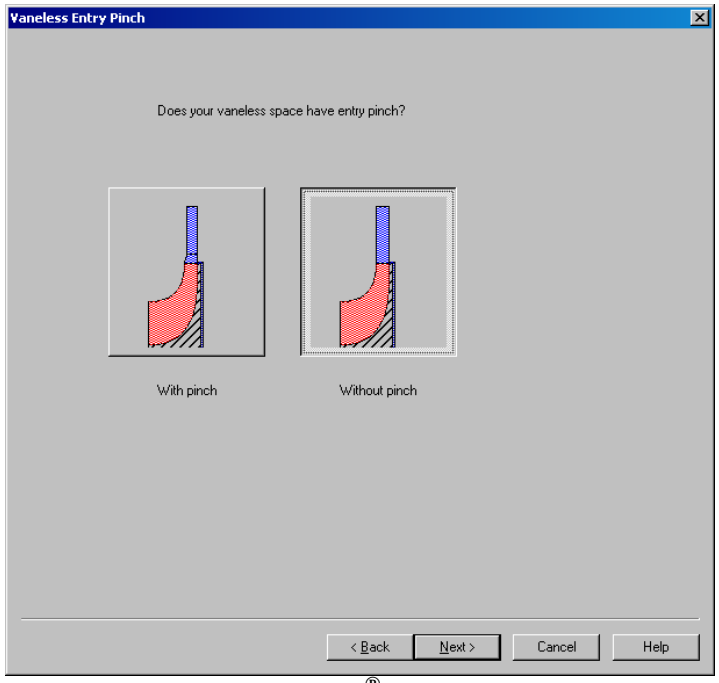

Figure 58 Pumpal® Wizard Step 21

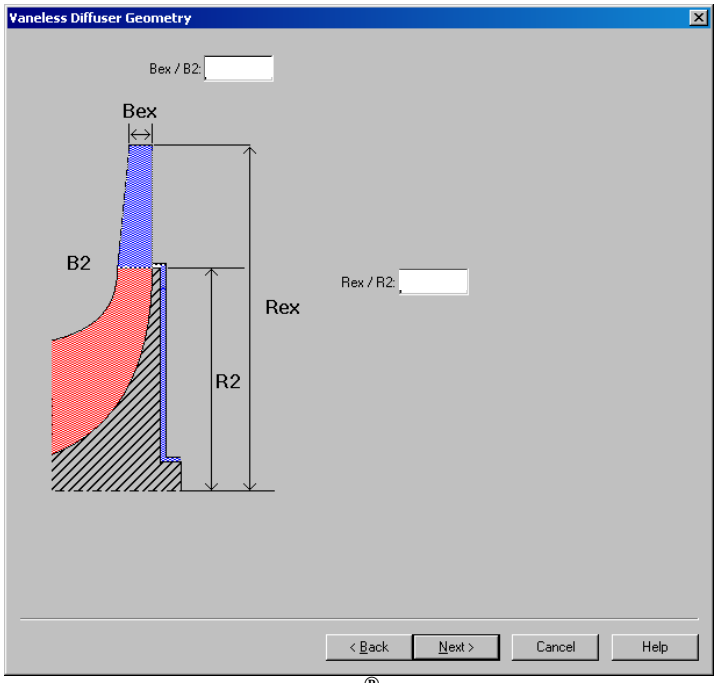

Figure 59 Pumpal® Wizard Step 22

Figure 58 shows step 21 here the user defines whether the diffuser will use an inlet pinch. The DEAN TPH is designed without a pinch.

Figure 59 shows step 22 here the user specifies the vaneless diffuser geometry.

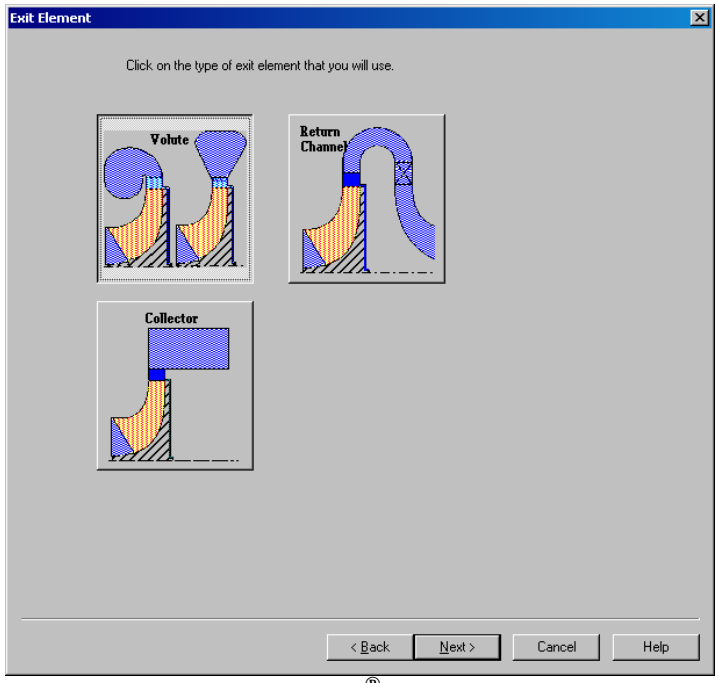

Figure 60 Pumpal® Wizard Step 23

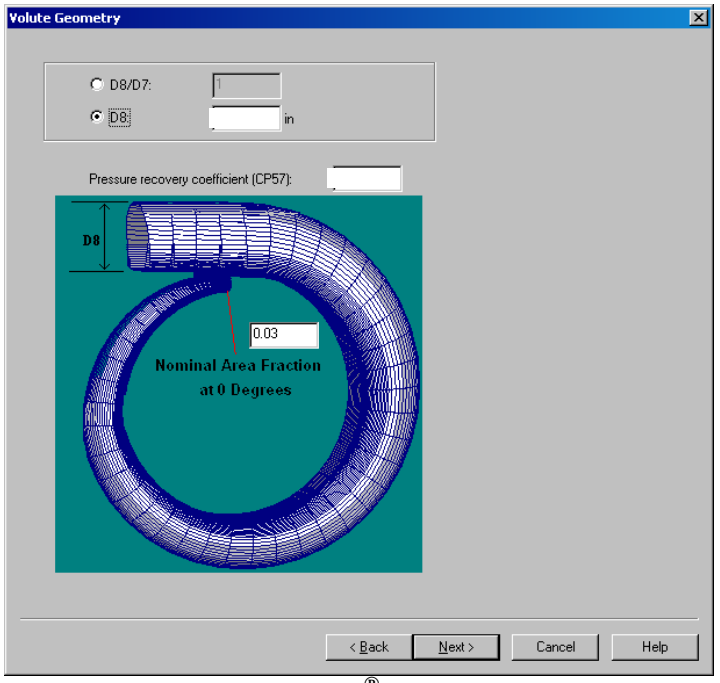

Figure 61 Pumpal® Wizard Step 24

Figure 60 show step 23 here the exit element is chosen by the user. The DEAN TPH uses a volute for both stages.

Figure 61 shows step 24 here the user specifies the volute geometry.

Appendix B RITAL® Wizard Steps

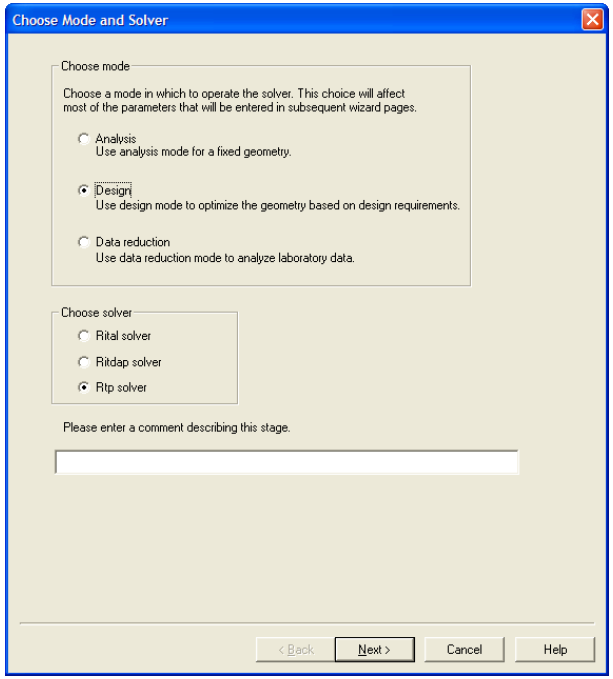

Figure 62 RITAL® Wizard Step One

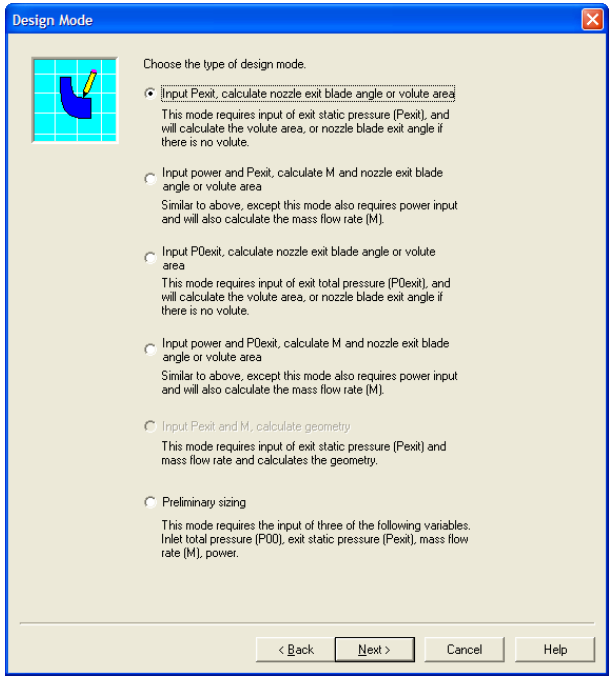

Figure 63 RITAL® Wizard Step Two

Figure 62 shows step one of the design process. There are three modes the user can choose, Design, Analysis and Data Reduction. The initial design was completed in Design Mode. The RTP solver is used in the design of the DEAN TPH.

Figure 63 shows the Design mode options. With the exit total pressure and power know this option was selected.

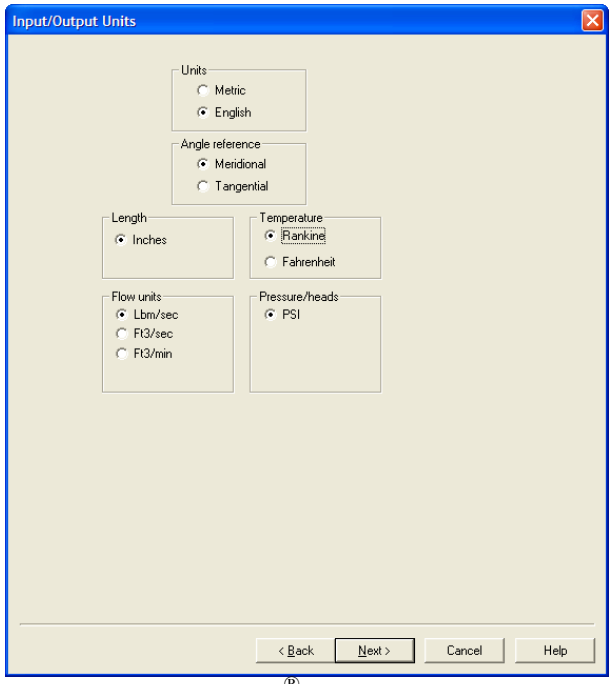

Figure 64 RITAL® Wizard Step Three

Figure 64 shows the input/output units were set to English and the angle reference was set to the tangential.

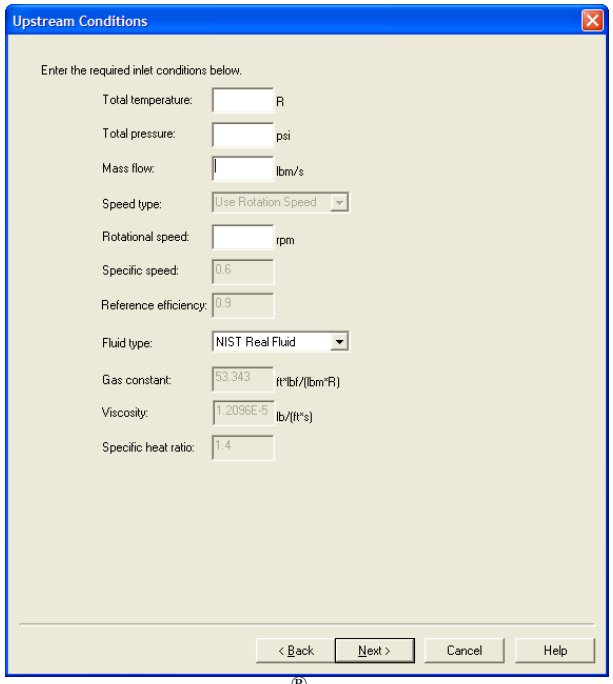

Figure 65 RITAL® Wizard Step Four

Figure 65 shows the upstream condition input options. The NIST Real Fluid was selected from the drop down menu. The calculation method was set to Gas with value of unity.

Table 37 RITAL® Upstream Conditions

Variable	Units	Value
T_o	R	60
P_0	psi	3626
$\dot{m}$	lbm/s	7.55
N	rpm	110,000

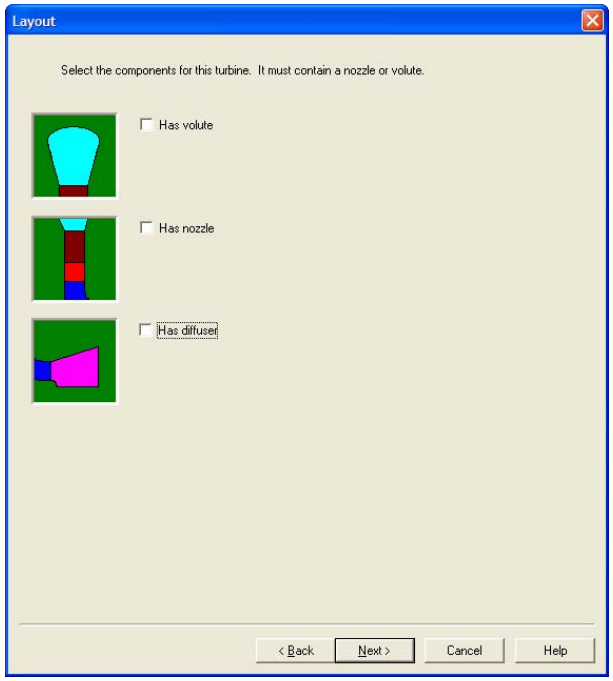

Figure 66 RITAL® Wizard Step Five

Figure 66 shows the component choices available for the turbine layout. The DEAN turbine is designed without a nozzle. A nozzle less turbine provides for a smaller unit and reduced manufacturing cost.[29]

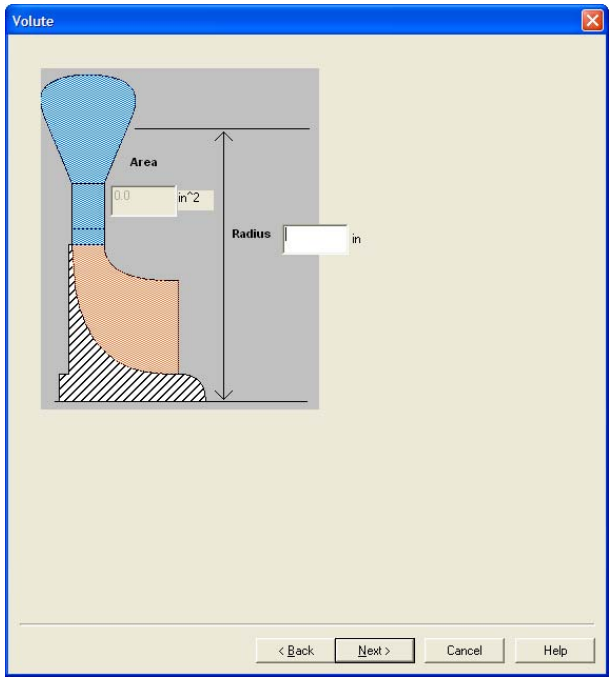

Figure 67 RITAL® Wizard Step Six

Figure 67 shows the required user inputs to define the volute. A right overhung volute design was chosen.

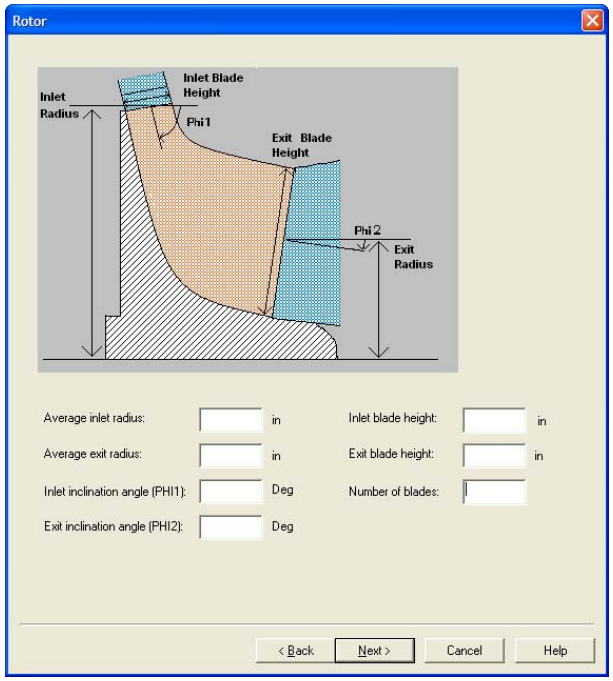

Figure 68 RITAL® Wizard Step Seven

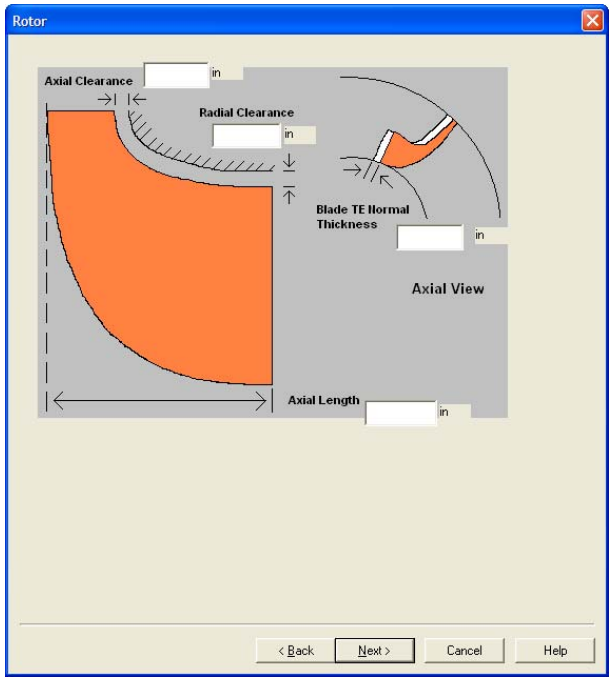

Figure 69 RITAL® Wizard Step Eight

Figure 68 shows step seven where the rotor geometry is defined. The average inlet radius limit is set by the size requirement. The inlet and exit inclination angle where set to 90 and 0 degrees to simulate a radial flow turbine. The inlet and exit blade height are 23 and 25% of the inlet and exit radius.

Figure 69 shows step eight here the clearance, axial length and trailing edge blade thickness are defined. The turbine runs with 0.0039 inches axial and radial clearance. The trailing edge blade thickness is 0.04 inches and an axial length of 1.01 inches.

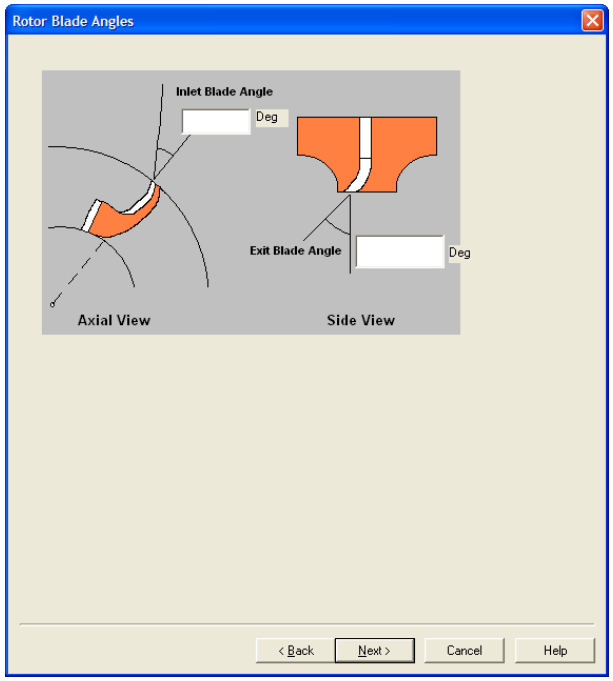

Figure 70 RITAL® Wizard Step Nine

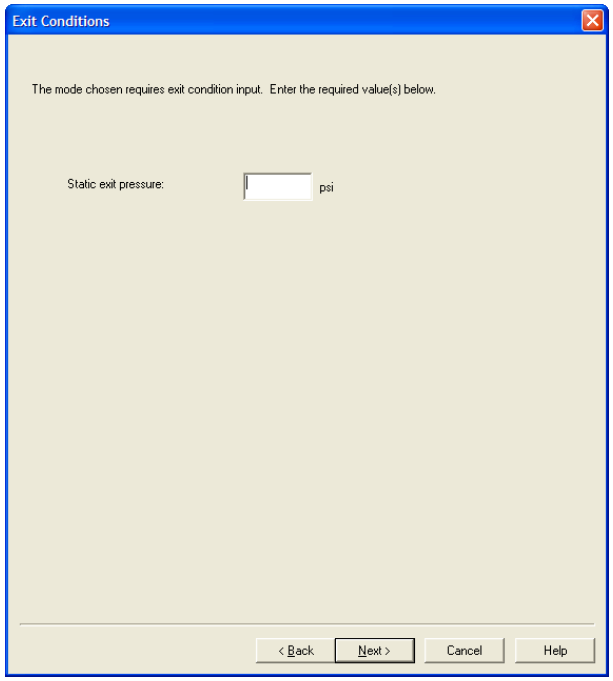

Figure 71 RITAL® Wizard Step 10

Figure 70 shows step nine where the inlet and exit blade angles are defined. The inlet and exit blade angles are set to -90 and 3°.

Figure 71 shows the final step here the static exit pressure is the input. This value is taken from the power balance.

Appendix C DEAN TPH CAD Drawings

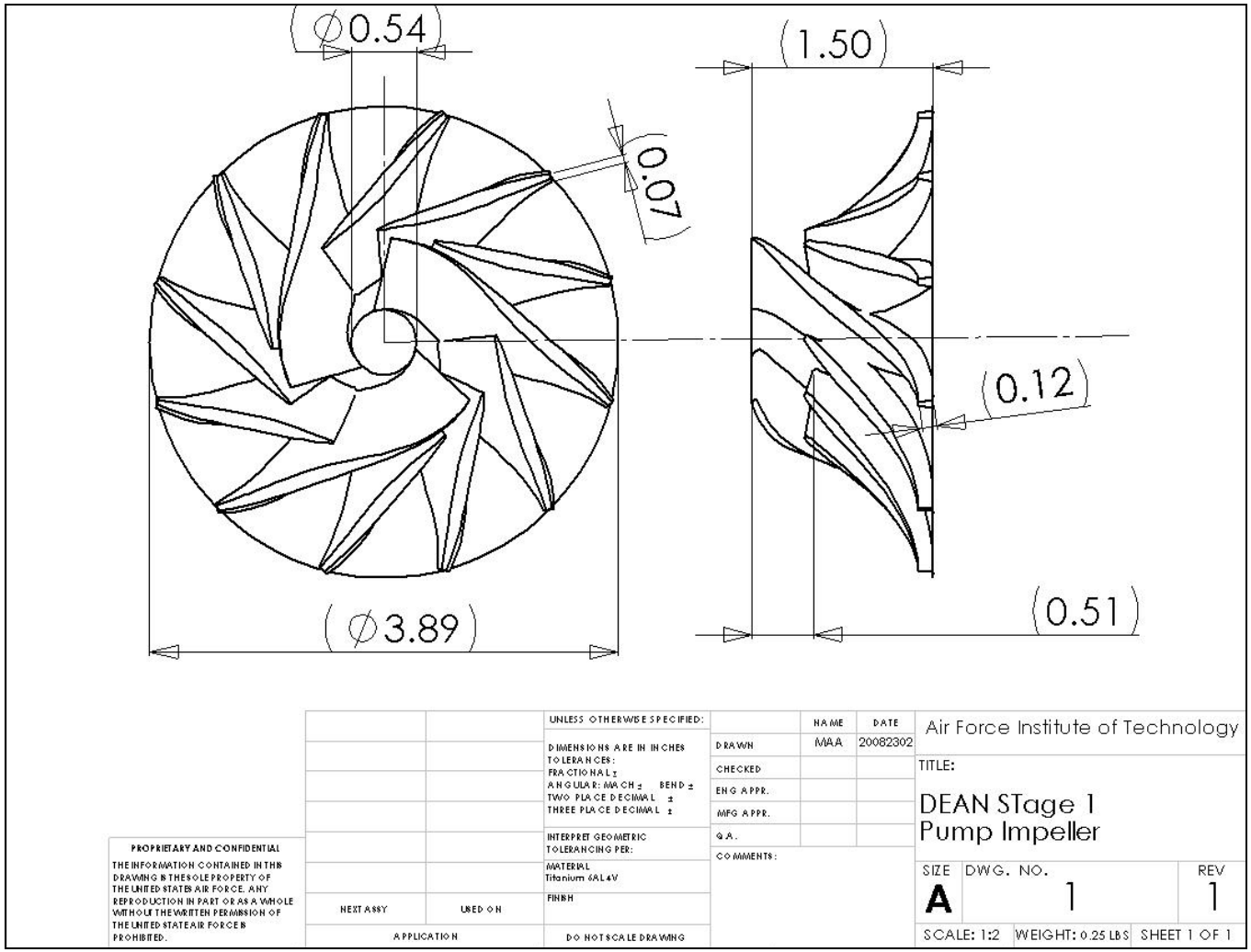

Figure 72 DEAN Stage 1 Impeller

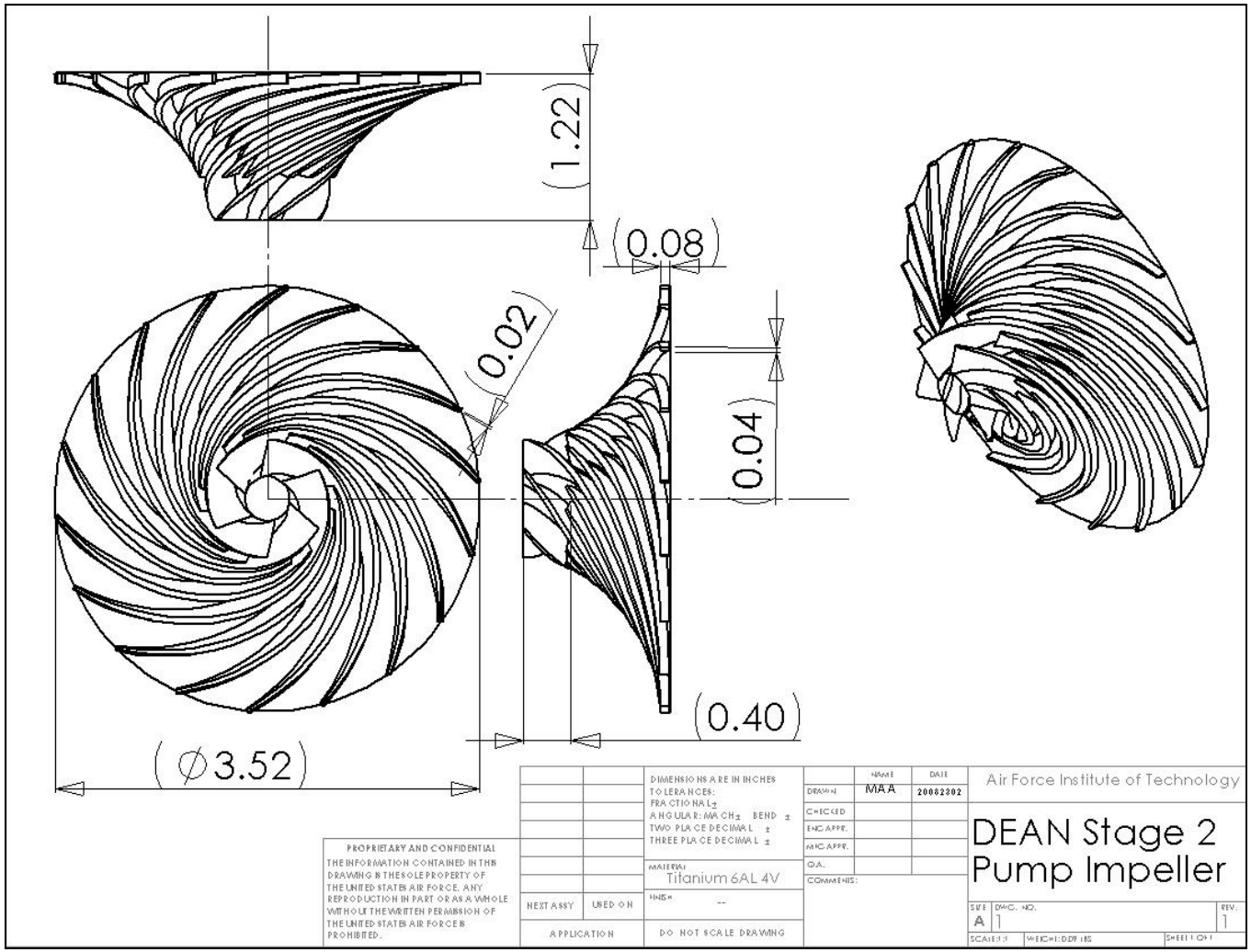

Figure 73 DEAN Stage 2 Impeller

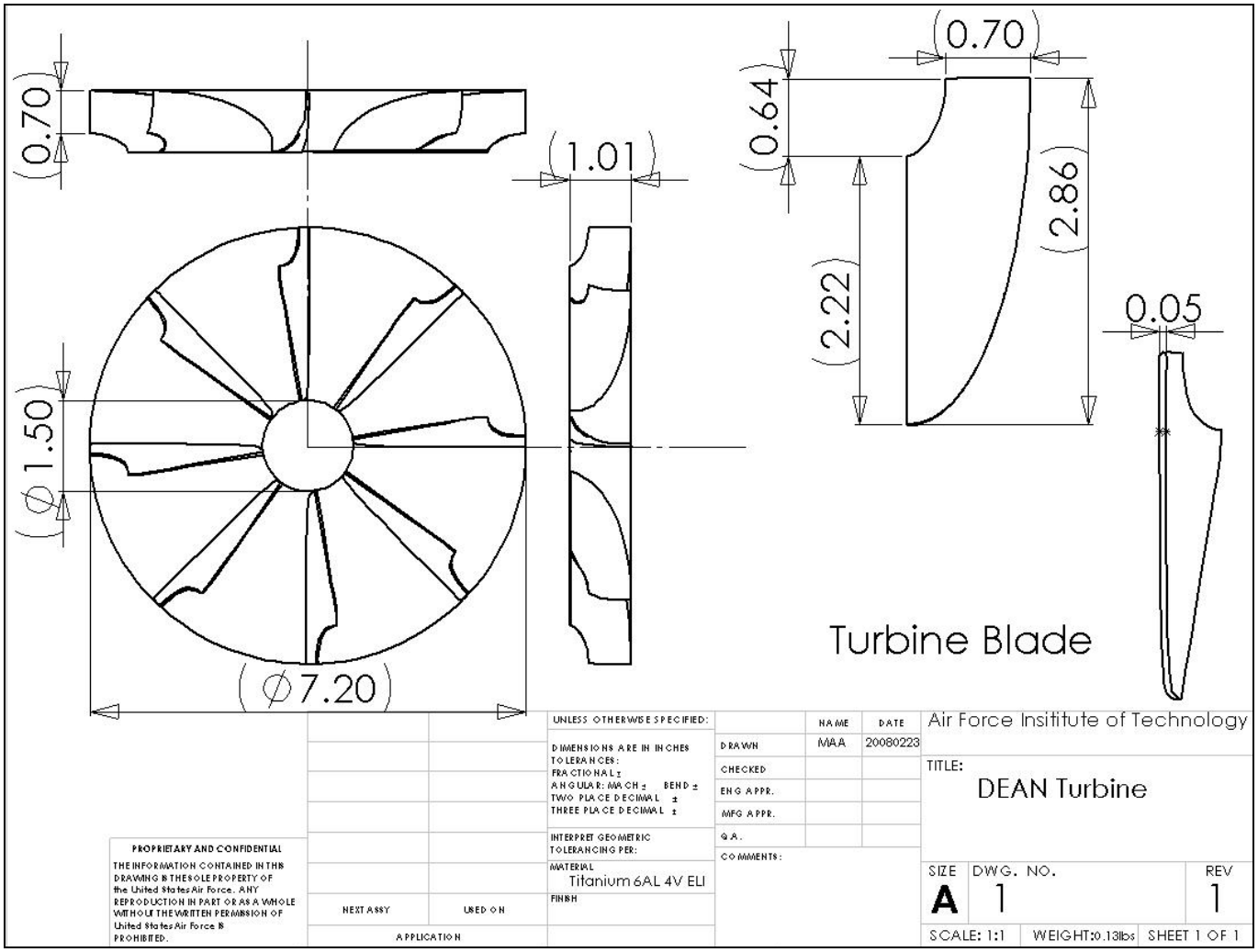

Figure 74 DEAN Turbine

This page intentionally left blank

Bibliography

[1] DeGeorge, D., and Fletcher, S., "The Integrated High Payoff Rocket Propulsion Technology Program and Tactical Missile Propulsion Status," Air Force Research Lab, AFRL-PR-ED-TP-2002-214, Edwards AFB CA Space and Missile Propulsion DIV, 2002.

[2] Butner, M.F., "Liquid Rocket Engine Turbopump Bearings," National Aeronautics and Space Administration, Springfield, Va., 1971.

[3] Nypan, L.J., Hambrock, B.J., Scibbe, H.W., "Predicted Characteristics of an Optimized Series-Hybrid Conical Hydrostatic Ball Bearing," NASA-TN-D-6607;1971.

[4] Gu, A., "Cryogenic Foil Bearing Turbopumps," AIAA Paper 1994-0868, 1994.

[5] Binder, M., Tomsik, T., Veres, J.P., "RL10A-3-3A Rocket Engine Modeling Project," National Aeronautics and Space Administration ; Springfield, Va., 1997,.

[6] Sack, W.F., Watanabe. J., Atsumi, M., "Development Progress of The MB-XX Cryogenic Upper Stage Rocket Engine," *39th AIAA/ASME/SAE/ASEE Joint Propulsion Conference and Exhibit; Huntsville, AL; July 20-23, 2003,* AIAA Paper 2003-4486.

[7] Minick, A., and Peery, S., "Design and Development of an Advanced Liquid Hydrogen Turbopump," AIAA Paper 1998-3681, 1998.

[8] Concepts NREC Inc., "PUMPAL," Version 7.9.30, 2006.

[9] Marcu, B., "Turbo-pump Development and Test for the MB-XX Advanced Upper Stage Engine Demonstrator," AIAA Paper 2006-4380, 2006.

[10] Alliot, P., Lassoudiere, F., Fiorentino, C., "Development Status of the VINCI Engine For The Ariane 5 Upper Stage," *41st AIAA/ASME/SAE/ASEE Joint Propulsion Conference & Exhibit; Tucson, AZ; USA; 10-13 July 2005,* AIAA Paper 2005-3755.

[11] Sutton, A.M., Peery, S.D., and Minick, A.B., "50K Expander Cycle Engine Demonstration," *Space Technology and Applications International Forum (STAIF-98); Proceedings of the 2nd Conference on Applications of Thermophysics in Microgravity and 3rd Conference on Commercial Development of Space, Albuquerque, NM; UNITED STATES; 25-29 Jan. 1998,* Woodbury, NY: American Institute of Physics (AIP Conference Proceedings, No. 420), 1998.

[12] London, J.R., and Air University (U.S.). Press., "LEO on the Cheap Methods for Achieving Drastic Reductions in Space Launch Costs," Air University Press, Maxwell Air Force Base, Ala., 1996.

[13] Anonymous "GDP Deflator," 2008.

[14] Shelley, J.S., LeClaire, R., and Nichols, J., "Metal Matrix Composites for Liquid Rocket Engines," AD-A410056, 2001.

[15] Huzel, D.K., and Huang, D.H., "Design of Liquid Propellant Rocket Engines," Springfield, Va. 1971.

[16] Collongea, L., Edeline, E., Frocot, M., "Development Status of High DN LH2 Bearings in Snecma," *41st AIAA/ASME/SAE/ASEE Joint Propulsion Conference & Exhibit; Tucson, AZ; USA; 10-13 July 2005,* AIAA Paper 2005-3950.

[17] Ohta, T., Kimoto, K., Kawai, T., "Design, Fabrication and Test of the RL60 Fuel Turbopump," *39th AIAA/ASME/SAE/ASEE Joint Propulsion Conference and Exhibit,* 2003.

[18] Pratt and Whitney Aircraft, "RL10A-3-3 Rocket Engine Design Report," NASA-CR-80920, 1966.

[19] Pugh, R.L., "The Many Facets of the RL10 Liquid Rocket Engine - A Continuing Success Story," *AIAA/ASME/SAE/ASEE Joint Propulsion Conference & Exhibit, 34th, Cleveland, OH; United States; 13-15 July 1998,* AIAA Paper 1998-3680, 1998.

[20] Johnsson, R., Brodin, S., Ekedahl, P., "Development of Hydrogen and Oxygen Pump Turbines for Vinci Engine," AIAA Paper 2002-4331, 2002.

[21] Goirand, B., Alliot, P., Barthoulot, J.-., "Testing the First Fuel Turbopump of the VINCI Engine," *39th AIAA/ASME/SAE/ASEE Joint Propulsion Conference and Exhibit; Huntsville, AL; July 20-23, 2003,* AIAA Paper 2003-5069.

[22] Peery, S., Minick, A.,"Design and Development of a 50K LOX/Hydrogen Upper Stage Demonstrator," 1998.

[23] Long, R., Grabowski, R., Minick, A., "Development Status of a 50k LOX/Hydrogen Upper Stage Demonstrator," 1999.

[24] Humble, R.W., Henry, G.N., Larson, W.J., "Space Propulsion Analysis and Design," McGraw-Hill, New York, 1995.

[25] NASA John H. Glenn Research Center at Lewis Field, "NPSS Rockets Supplement," Version. 1.6.4, 2006.

[26] Perry, R.H., Green, D.W., and Maloney, J.O., "Perry's Chemical Engineers' Handbook." McGraw-Hill, New York, 1997.

[27] Japikse, D., Marscher, W.D., and Furst, R.B., "Centrifugal Pump Design and Performance," 1997.

[28] Concepts NREC Inc., "RITAL," Version 7.11.2.0, 2006.

[29] Donachie, M.J., "Titanium a Technical Guide," ASM International, Metals Park, OH, 1988.

[30] Beer, F.P., and Johnston, E.R., "Mechanics of Materials," McGraw-Hill, New York, 1981.

[31] Karassik, I.J., "Pump Handbook," McGraw-Hill, New York, 2001.

Vita

Captain Michael A Arguello was born in San Antonio, TX. He is a 1998 graduate of G.W. Brackenridge H.S. He received a four-year AFROTC scholarship and attended the University of Miami in Coral Gables, FL. During his AFROTC commitment, he was selected as the cadet wing commander of Detachment 155. Upon graduation, he was awarded a Bachelor of Science degree in Mechanical Engineering with an Aerospace emphasis. His first assignment was to the Air Force Flight Test Center (AFFTC) at Edwards AFB. While at the AFFTC, he was an integral member in conducting the first flight of the X37 autonomous vehicle, a future Air Force space launch asset. Upon graduation, he will be assigned to the Air Force Research Lab at Kirtland AFB in Albuquerque, NM.

REPORT DOCUMENTATION PAGE

Form Approved
OMB No. 074-0188

1. REPORT DATE *(DD-MM-YYYY)*	**2. REPORT TYPE**	**3. DATES COVERED** *(From – To)*
01-03-2008	Master's Thesis	March 2002 – March 2008

4. TITLE AND SUBTITLE

THE CONCEPT DESIGN OF A SPLIT FLOW LIQUID HYDROGEN TURBOPUMP

5a. CONTRACT NUMBER

5b. GRANT NUMBER

5c. PROGRAM ELEMENT NUMBER

6. AUTHOR(S)

Arguello, Michael A., Captain, USAF

5d. PROJECT NUMBER

5e. TASK NUMBER

5f. WORK UNIT NUMBER

7. PERFORMING ORGANIZATION NAMES(S) AND ADDRESS(S)

Air Force Institute of Technology
Graduate School of Engineering and Management (AFIT/EN)
2950 Hobson Way, Building 640
WPAFB OH 45433-8865

8. PERFORMING ORGANIZATION REPORT NUMBER

AFIT/GAE/ENY/08-M01

9. SPONSORING/MONITORING AGENCY NAME(S) AND ADDRESS(ES)

Mr. Michael Huggins, AFMC AFRL/RZS
Building: 8353 Room: 216B
5 Pollux Drive, Edwards CA 93524

10. SPONSOR/MONITOR'S ACRONYM(S)

11. SPONSOR/MONITOR'S REPORT NUMBER(S)

12. DISTRIBUTION/AVAILABILITY STATEMENT

APPROVED FOR PUBLIC RELEASE; DISTRIBUTION UNLIMITED.

13. SUPPLEMENTARY NOTES

14. ABSTRACT

An initial design of a split flow liquid hydrogen turbopump for the Dual Expander Aerospike Nozzle (DEAN) upper stage engine was completed. The engine nozzle is an annular aerospike. The engine cycle requires a combustion chamber pressure of 1,740 psia. The DEAN is designed to deliver 57,200 lb_f of thrust and 472 seconds of I_{sp}. The turbopump design was completed using a meanline software tool. The design consists of a single piece rotor, with a two-stage pump and radial inflow turbine. The turbopump flow rates are 15.1 and 7.55 lbm/s into the first and second stage, respectively. The first and second stage pumps use unshrouded impellers. An interstage transfer models the fluid split flow. The fluid for each stage exits through a volute. The first and second stage impeller hub-tip ratios are 0.3 and 0.35, respectively. The turbine is a full admission reaction type. At the design condition, the turbine delivers 3,607 horsepower at a total pressure ratio of 1.84.

15. SUBJECT TERMS

Split flow liquid hydrogen turbopump, Dual expander rocket engine, Integrated High Payoff Rocket Propulsion Technology Program

16. SECURITY CLASSIFICATION OF:			**17. LIMITATION OF ABSTRACT**	**18. NUMBER OF PAGES**	**19a. NAME OF RESPONSIBLE PERSON**
a. REPORT	**b. ABSTRACT**	**c. THIS PAGE**			Branam, Richard D. Maj, USAF
U	**U**	**U**	**UU**	125	**19b. TELEPHONE NUMBER** *(Include area code)* (937) 255-3636, ext 7485 (emailname@afit.edu)

Standard Form 298 (Rev. 8-98)
Prescribed by ANSI Std. Z39-18